In-plane aligned assemblies of 1D-nanoobjects: Recent approaches and applications

Received 00th January 20xx,
Accepted 00th January 20xx

DOI: 10.1039/x0xx00000x

Hebing Hu,[ab] Shancheng Wang,[ab] Xueling Feng,[c] Matthias Pauly,[d]* Gero Decher,[defg]* and Yi Long[abh]*

One-dimensional (1D) nanoobjects have strongly anisotropic physical properties which are averaged out and cannot be exploited in disordered systems. The goal of the present review is to describe the current methods for preparing macroscopic composite films in which the long axis of individual 1D-nanoobjects is more or less parallel to the x,y-plane of the substrate as well as to each other (alignment direction). Such structures are generally described as in-plane anisotropic and many of their physical properties show minima or maxima parallel to the alignment direction. Optical polarizers are a typical class of such materials, but anisotropic materials properties can enhance the performance of devices and materials over many length scales in various disciplines of materials science including electronic devices, environmental sensors, energy saving and energy generation applications, plasmonic devices, Surface-Enhanced Raman Scattering (SERS) and biological applications. The reviewed alignment methods fall into two categories: techniques in which all nanoobjects remain in the x,y-plane and the in-plane densities and alignment are controlled; and techniques allowing building complex architectures in which each stratum of multilayered or stacked films may differ in chemical nature or alignment direction or both. This review serves a purpose to provide a platform to inspire new alignment approaches with improved assembly quality and upscaling potential and new applications with enhanced performance by alignment.

1. Introduction

In the last two decades, inorganic or organic 1D-nanoobjects such as nanotubes (NTs), nanorods (NRs), nanowires (NWs), nanobelts (NBs) and nanofibers (NFs) have attracted wide attention because of their various technological applications, to list a few, in opto-electronic nanodevices,[1-5] energy storage,[6-8] optics,[9, 10] medical diagnosis,[11-13] biosciences,[14-16] mesoscopic physics,[17-19] and many more. Till now, various techniques have been explored and developed to prepare these 1D-nanoobjects, which have been summarized in a number of review articles.[17, 18, 20-22] While significant effort and progress have been made to fabricate these 1D-nanoobjects, they are usually used as disordered macroscopic assemblies with random positions and orientations, leading to the loss of the anisotropic properties of the individual 1D-nanoobject.[23, 24] For example, one typical process of NW device fabrication consists in depositing NWs from a suspension in an organic solvent onto the desired substrate followed by metallization and lift-off.[25, 26] However, this drop-casting technique can only lead to randomly assembled NWs with a low device yield, which is not suitable for cost-effective large-scale production of high-performance nanodevices.

It was demonstrated that 1D-nanoobjects assembled as an aligned array exhibit superior properties compared to those of randomly oriented structures.[27] For instance, as electrons can be transported directly from the end of one nanoobject to the other along the longitude direction, the electronic transport properties along the alignment direction are better than those in a randomly oriented cross-linked network.[28-30] Furthermore, the optical, electrical, catalytic and magnetic properties of 1D-nanoobject assemblies may differ from those of the individual 1D-nanoobject because of coupling effects and synergetic collective properties which could be much enhanced in ordered structures.[31] Furthermore, the controlled assembly of nanoobjects is necessary to fabricate nanoobject-based devices on a large scale as well as to incorporate such objects into complex architectures with novel functionalities. Specifically, the well-defined orientation, interspacing and location are the keys to the next generation of high-performance opto-electronic nanosystems.[31-33]

To date, various assembly strategies have been developed for the alignment of 1D-nanoobjects on various substrates.[34, 35] Generally, these methods can be divided into the following two categories: (1) growing the 1D-nanoobjects in a specific direction starting from a pre-defined position (directed growth method), which involves the directed growth (synthesis) of the nanoobjects, and (2) assembling pre-synthesized 1D-nanoobjects onto the desired substrate (directed assembly method). The directed growth method can align the 1D-nanoobjects with both a controlled position and orientation,[36-39] while only the orientation is controlled in the directed assembly.

[a] School of Materials Science and Engineering, Nanyang Technological University. 50 Nanyang Avenue, Singapore 639798
[b] Singapore-HUJ Alliance for Research and Enterprise (SHARE), Nanomaterials for Energy and Energy-Water Nexus (NEW), Campus for Research Excellence and Technological Enterprise (CREATE), Singapore 138602
[c] Key Laboratory of Science and Technology of Eco-Textile, Ministry of Education, College of Chemistry, Chemical Engineering and Biotechnology, Donghua University, Shanghai 201620, China
[d] Université de Strasbourg, CNRS, Institut Charles Sadron, F-67000 Strasbourg, France
[e] Faculté de Chimie, Université de Strasbourg, 1 rue Blaise Pascal, F-67008 Strasbourg, France
[f] International Center for Frontier Research in Chemistry, 8 allée Gaspard Monge, F-67083 Strasbourg, France
[g] International Center for Materials Nanoarchitectonics, 1-1 Namiki Tsukuba, Ibaraki 305-0044, Japan
[h] Sino-Singapore International Joint Research Institute (SSIJRI), Guangzhou 510000, China

Emails: longyi@ntu.edu.sg; decher@unistra.fr; matthias.pauly@ics-cnrs.unistra.fr

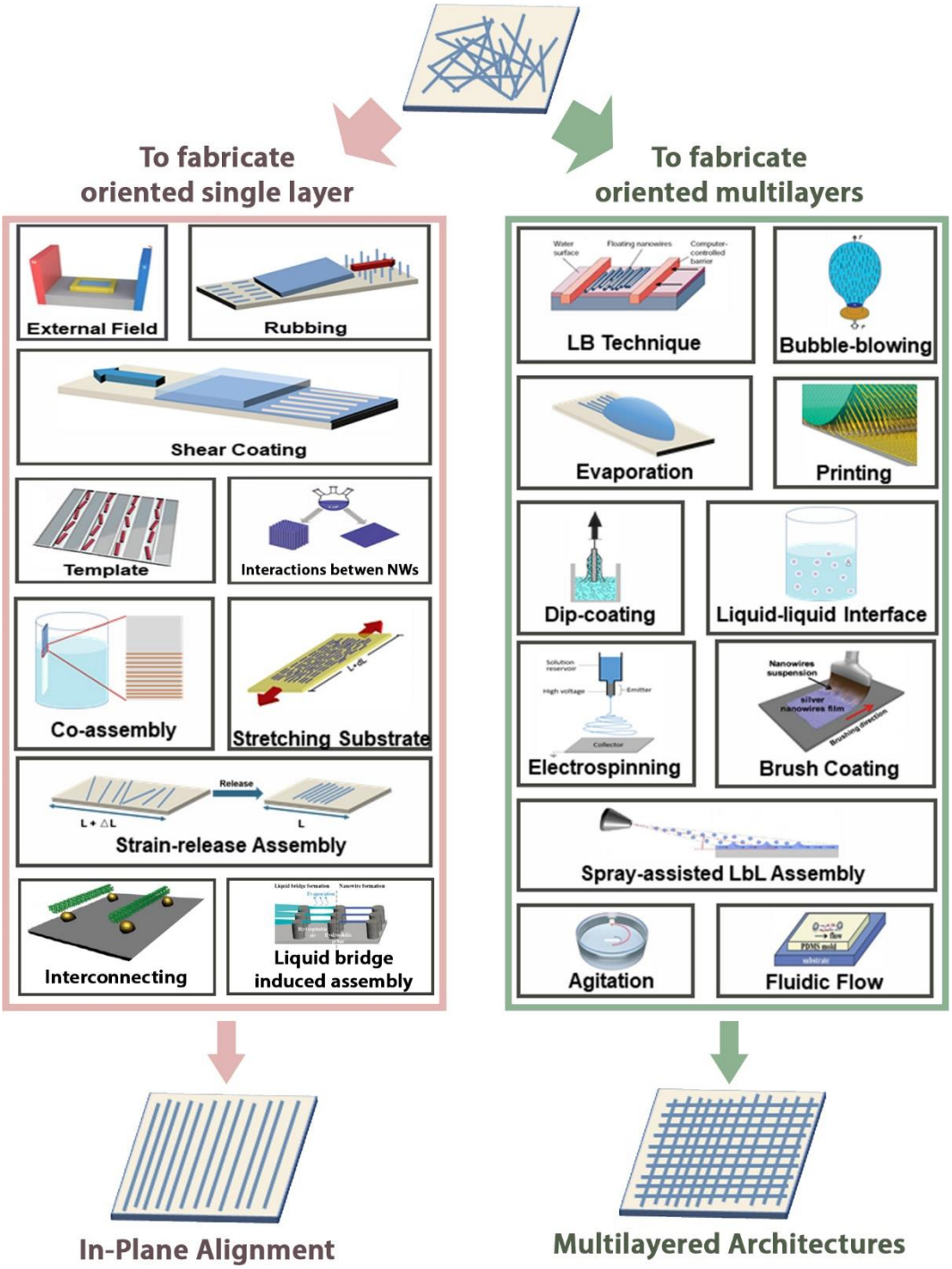

Fig. 1 Schematic illustration of assembling methods that can be applied to fabricate monolayer or multilayer aligned 1D-nanoobjects assemblies.

However, the later approach can be implemented with lower fabrication costs, facile processing procedure and higher production efficiency as well as better flexibility in choosing the nanoscale building blocks, architecture and substrates.

Thus, we mainly focus on the alignment of existing 1D-nanoobjects onto a substrate. Five comprehensive review papers about the orientation of 1D-nanoobjects were published more than five years ago.[31, 34, 35, 40, 41] In this review, we will still briefly present the main techniques that have been introduced some years ago to ensure exhaustiveness, but more focus will be put on novel approaches and emerging applications for the oriented assembly of 1D-nanoobjects developed within last five years. We will first introduce the methods that lead to an oriented monolayer deposition at an interface as shown in Fig. 1**,** including assembly by external fields, rubbing, shear coating, assembly by templated substrates, Interactions between NWs, co-assembly with other nanoobjects, stretching of the substrate, assembly induced by liquid crystals, interconnecting patterned surfaces with 1D-nanoobjects and liquid bridge induced

assembly. Subsequently, we will discuss the methods that can be repeated to form oriented multilayers, including Langmuir-Blodgett technique, bubble blown extrusion, evaporation-induced assembly, contact printing, dip-coating, assembly at liquid-liquid interfaces, electrospinning, brush-coating, spray-assisted Layer-by-Layer assembly, agitation-assisted Layer-by-Layer alignment and fluidic flow (Fig. 1). If the thickness of the final assembly is on the order of the diameter of the 1D-nanoobject, it can be considered as a "monolayered" structure. In contrast, some methods can be repeated to prepare oriented multilayers giving access to much more complex anisotropies as they offer more flexibility in choosing the 1D-nanoobjects, the alignment direction and the position of each individual layer, which is the ultimate goal of 1D-nanoobject assemblies. Some applications of these ordered 1D-nanoobject assemblies will also be reviewed, in particular for electronic devices, environmental sensing, biological applications, plasmonics and Surface-Enhanced Raman Scattering as well as energy saving and energy generation applications. Considering the numerous studies that have been published, great opportunities and growing interest in the field, this review intends to inspire efforts towards the invention of new assembly approaches as well as explore innovations for next-generation high-performance electronic, optoelectronic and electromechanical nanodevices.

2. Methods that lead to a single oriented layer at an interface

Among the numerous approaches that have been developed for the oriented assembly of 1D-nanoobjects into aligned monolayers at an interface, we will present in this section the most prominent ones (Fig. 1) and discuss their intrinsic limits that hinder them from being used for more complicated structures.

2.1 Assembly by an external field.

External fields such as magnetic and electric field have been widely used to align 1D-nanoobjects. Under the effect of an external field, the longitudinal axis of the 1D-nanoobjects usually orients along the field direction.

2.1.1 ***Magnetic-field.*** Magnetic fields can be used to induce the nanoobjects to orient like magnetized bars, and to form patterns that follow the field lines.[42-50] Atkinson and co-workers have investigated the alignment of ferromagnetic NWs within a magnetic field.[49] The angular distribution of the NWs deposited on the substrate from a dilute solution depended on the magnetic field strength. The percentage of NWs aligned along the applied field was found to increase dramatically with increasing the field strength. The proportion of wires oriented within 0-20° using a magnetic field of 1 kOe was ~82% for $Ni_{0.8}Fe_{0.2}$ NWs, 71% for Ni NWs, and dropped down to 53% for CoNWs. The effect of the wire length on the efficiency of magnetic orientation demonstrated that the alignment could be improved with longer NWs.[49] Fu *et al.* reported the controllable preparation of Fe_3O_4-coated AgNWs that can be oriented by a magnetic field.[48] The AgNWs were decorated with magnetite nanoparticles (Fe_3O_4 NPs) in deionized water. The magnetite NPs loading on the AgNWs was controlled by the initial feeding ratio of Fe_3O_4 NPs to AgNWs. The decorated AgNW suspension was cast in a Poly(methyl methacrylate) (PMMA) mold and placed between two magnets, inducing the NW alignment along the magnetic field lines (Fig. 2a). Fig. 2b shows the optical microscopy image of aligned Fe_3O_4-coated AgNWs. The orientation of the NWs depended significantly on the amount of magnetite NPs.[48]

2.1.2 ***Electric-field.*** Dielectrophoresis (DEP) is a phenomenon in which a non-uniform electric field induces a force on a 1D-nanoobject, leading to its alignment.[51-69] An electric field applied on a nanoobject suspension will induce its polarization with the charges being separated at the surface of the 1D-nanoobject. When a NW is subjected to an inhomogeneous electric field (either an AC field or an inhomogeneous DC field), it will be oriented along the electric field gradient lines and will be attracted to the closest electrode. In order to induce the oriented assembly of such 1D-nanoobjects within an electric field, the 1D-nanoobjects suspension is usually deposited on top of a pair of electrodes. The gap between the electrode pair should be comparable to the length of the 1D-nanoobjects so that the 1D-nanoobjects can bridge the gap between the electrodes after alignment and deposition. Generally, the conductivity of the 1D-nanoobjects should be higher than that of the solvent, so that they can be attracted towards the edges of the electrode where the field gradient is the highest, which further allows to place and orient the 1D-nanoobjects precisely at the desired orientation and position.

Stumbo *et al.* reported on the dielectrophoretic assembly of NWs and achieved a 98.5% yield of single NWs assembled over 16,000 patterned electrode sites with submicrometer alignment precision.[59] The process was governed by the balance between hydrodynamics, forces arising from the electrostatic double-layer interaction between the NW and the substrate and dielectrophoretic forces that led to the controllable self-assembly. As the NW suspension was flown through the channel, the NWs were polarized and attracted towards the electrodes by the dielectrophoretic forces. After a single NW was captured at an electrode, a second NW assembling on the same electrode might displace the original NW.[59] Furthermore, the number of NWs occupying each electrode depended strongly on the applied voltage for a given flow rate of the suspension. Above 404.5 mV, two NWs were stable on a single electrode. As the voltage was reduced, one of the two NWs escaped from the electrode. With a further decreased in voltage, more NWs were released until only single NWs were observed on the electrodes. With a further reduction of the voltage at 320 mV, single NWs began to be released from the electrodes. At less than 270 mV, all the electrodes were empty. Thus, single NWs can be assembled on each electrode with high probability by carefully controlling the balance between hydrodynamic and dielectrophoretic forces.[59]

Zheng *et al*. reported the orientation of pn silicon NWs (SiNWs), consisting in two segments with different doping (namely n- and p-

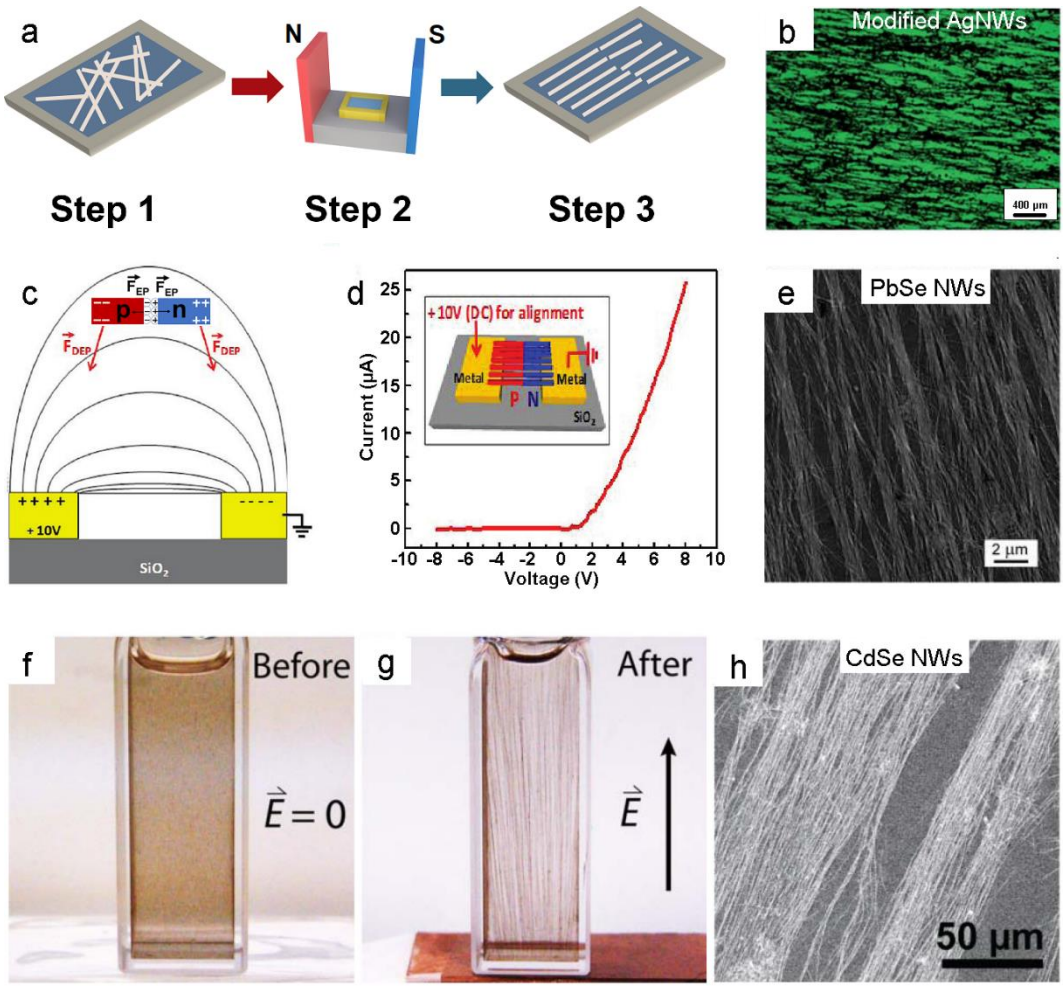

Fig. 2 (a) Schematic representation of the alignment of Fe_3O_4-coated AgNWs assisted by a magnetic field. Adapted from ref. 48 with permission from Royal Society of Chemistry. (b) Optical microscopy image of aligned Fe_3O_4-coated AgNWs with a Fe_3O_4/AgNWs mass ratio of 0.3:1. Reproduced from ref. 48 with permission from Royal Society of Chemistry. (c) Schematic illustration of the orientation of pn-SiNWs using an electric field. (d) I-V curve of the oriented pn-SiNWs showing a forward-biased rectifying behavior when a positive DC voltage was applied on the left electrode. Reproduced with permission from ref. 60. Copyright 2010 American Chemical Society. (e) Arrays of aligned PbSe NWs prepared using a DC electric field. Reproduced with permission from ref. 57. Copyright 2007 American Chemical Society. (f) CdSe NWs suspended in hexane before applying an electric field. (g) CdSe NWs suspended in hexane after applying an electric field. (h) SEM image of CdSe NWs film. Reproduced with permission from ref. 65. Copyright 2013 Wiley-VCH.

segments) under a direct current (DC) electric field (Fig. 2c).[60] The orientation process of the pn-SiNWs showed that they first moved to the nearby region of the electrode edges because of the DEP forces, then rotated to the proper direction and were finally attracted to the electrodes.[60] The oriented pn-SiNWs were parallel to the external electric field with the n-segment contacting the lower potential side of the electrode pair and the I-V curve suggested a forward-biased rectifying behavior when a positive DC voltage was applied on the p-side of the NWs (Fig. 2d). The density of the aligned pn-SiNWs was controllable by changing the NW concentration in the suspension. The orientation direction of the pn-SiNWs can be changed by reversing the potential applied to the electrodes.[60] Talapin *et al.* reported the alignment of Lead Selenide NWs (PbSe NWs) using a DC electric field.[57] The NWs were suspended in an organic solvent mixture at a concentration of ~1 mg/mL. A small amount of the NW suspension was deposited and evaporated between two Au electrodes patterned on a SiO_2 substrate. The unidirectional orientation of PbSe NWs was observed between the two electrodes with a spacing ranging from 0.2 to 40 μm with applied electric field strengths ranging from 10^3 to 10^5 V.cm^{-1} (Fig. 2e).[57] We should note that the electric field strength and the solvent evaporation rate are the two key parameters in the electric-field assisted assembly. For instance, individual NWs can be oriented and deposited from very volatile solvent, but the fast evaporation rate is not suited for fabricating densely packed and well-oriented NW arrays.

Lee *et al.* applied DC and AC electric fields of various frequencies for the alignment of gallium nitride NWs (GaN NWs). They found that the GaN NWs were better oriented with a higher yield of about 80% over the entire array using an AC rather than a DC electric field.[56] This is probably due to the fact that an AC electric field has the advantage of avoiding the interference of electro-osmotic and electrochemical effects that exist when a DC electric field is used.[70]

While the electric-field assisted assembly is efficient for aligning 1D-nanoobjects, it relies on a charge excess that may need to be induced by an additional process. Some semiconductor 1D-

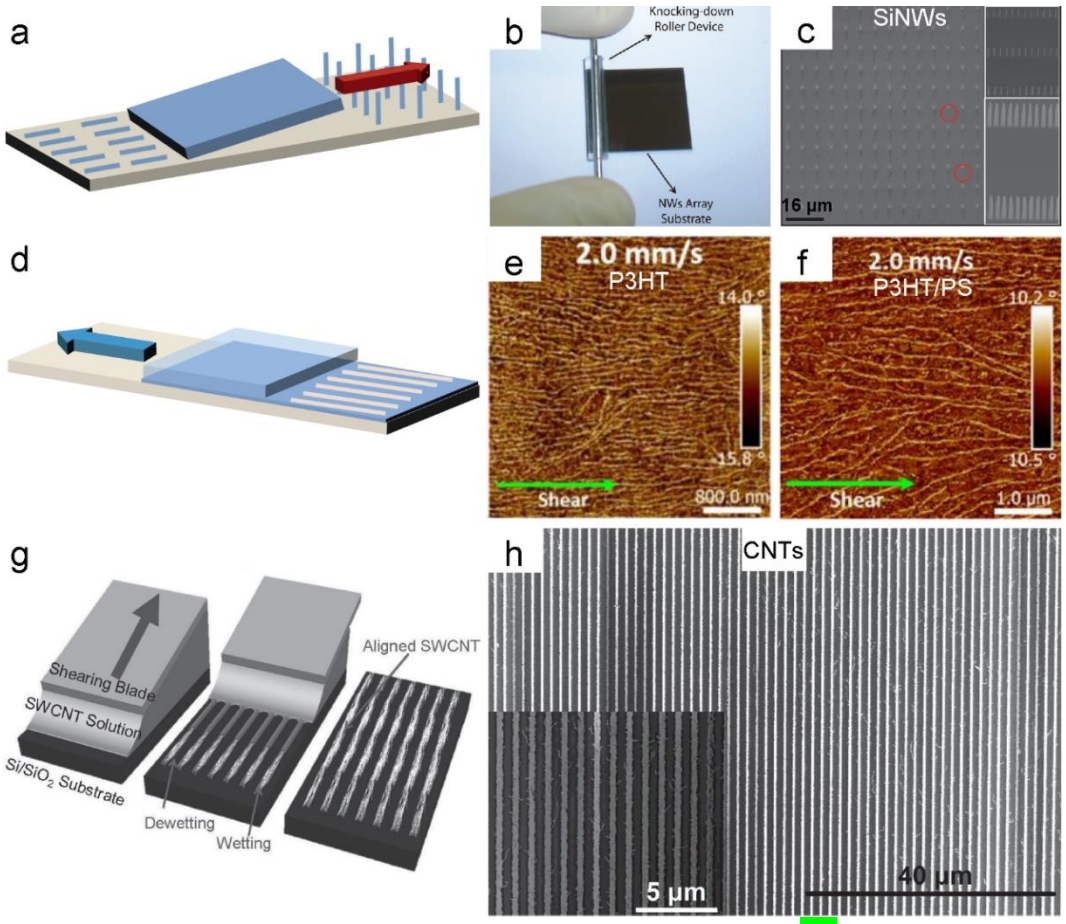

Fig. 3 (a) Schematic illustration of rubbing assembly of NTs. (b) Photography of the knock-down process used for the fabrication of aligned NW arrays with a roller. (c) A 15 × 11 NW array after the knock-down process. Red circles represent defective sites. Insets : (top) Array with an interwire pitch of 400 nm, and (bottom) array with an interwire pitch of 100 nm. Reproduced with permission from ref. 72. Copyright 2010 American Chemical Society. (d) Schematic representation of 1D-nanoobjects aligned on a substrate by a solution shear coating technique. (e) AFM image of a P3HT film obtained from a pristine solution shear coated at 2.0 mm/s. Reproduced with permission from ref. 73. Copyright 2016 American Chemical Society. (f) AFM image of a P3HT/PS (20/80) composite film shear-coated at 2.0 mm/s. Reproduced with permission from ref. 74. Copyright 2016 American Chemical Society. (g) Schematic depiction of SWCNT alignment using shear coating. (h) Large-area SEM image of the shear-aligned SWCNTs on 500 nm wide solvent-wetting regions. The inset is a zoomed-in image of the same area. Reproduced with permission from ref. 75. Copyright 2015 Wiley-VCH.

nanoobjects can be charged when exposed to light of a given wavelength, and the number of photogenerated charges within such semiconductors can be orders of magnitude larger than residual excess charges. These photoexcited 1D-nanoobjects will be oriented upon application of an electric field. Recently, Petchsang *et al.* reported the orientation of semiconductor NWs by combining light and electric field.[65] The assembly was triggered by illumination at various wavelengths under an electric field. For visible and near-infrared (NIR) absorbing semiconductors such as CdSe and PbSe, the ambient room light illumination is strong enough to induce their assembly. However, materials that only adsorb higher energy wavelengths such as ZnSe NWs can only be oriented under near-ultra-violet (UV) illumination.[65] Since only the excited NWs can be oriented, different types of NWs in a complex mixture can be selectively aligned by exciting at specific wavelengths. For example, under ambient light illumination, before applying an external electric field, a high aspect ratio CdSe NW suspension in a low dielectric constant solvent such as toluene or hexane formed a random colloidal suspension (Fig. 2f). When the suspension was subjected to an electric field, the NW bundles were aligned along the direction of the electric field (Fig. 2g). This method can also be used to align NWs on various substrates by using the same approach while the solvent was evaporated (Fig. 2h). By combining light illumination with external electric fields, various NWs can be oriented.[65]

Manners and co-workers also reported the electric field assisted assembly of organic cylindrical block copolymer micelles.[68, 69] The alignment of this polyferrocenylsilane (PFS)-containing cylindrical micelles were highly dependent on the concentration and length of the micelle. The cylindrical micelles were aligned parallel to the electric field and perpendicular to the walls of the capillary tube. The alignment is reversible by applying or removing the electric field.[68]

2.2 Rubbing

Rubbing alignment of 1D-nanoobjects was reported by de Heer and co-workers.[71] In this seminal work, an aligned CNT array was fabricated by drawing the nanotube suspension through a ceramic filter with 0.2 μm pore size. This resulted in a CNT forest aligned perpendicularly to the filter which was transferred onto a plastic

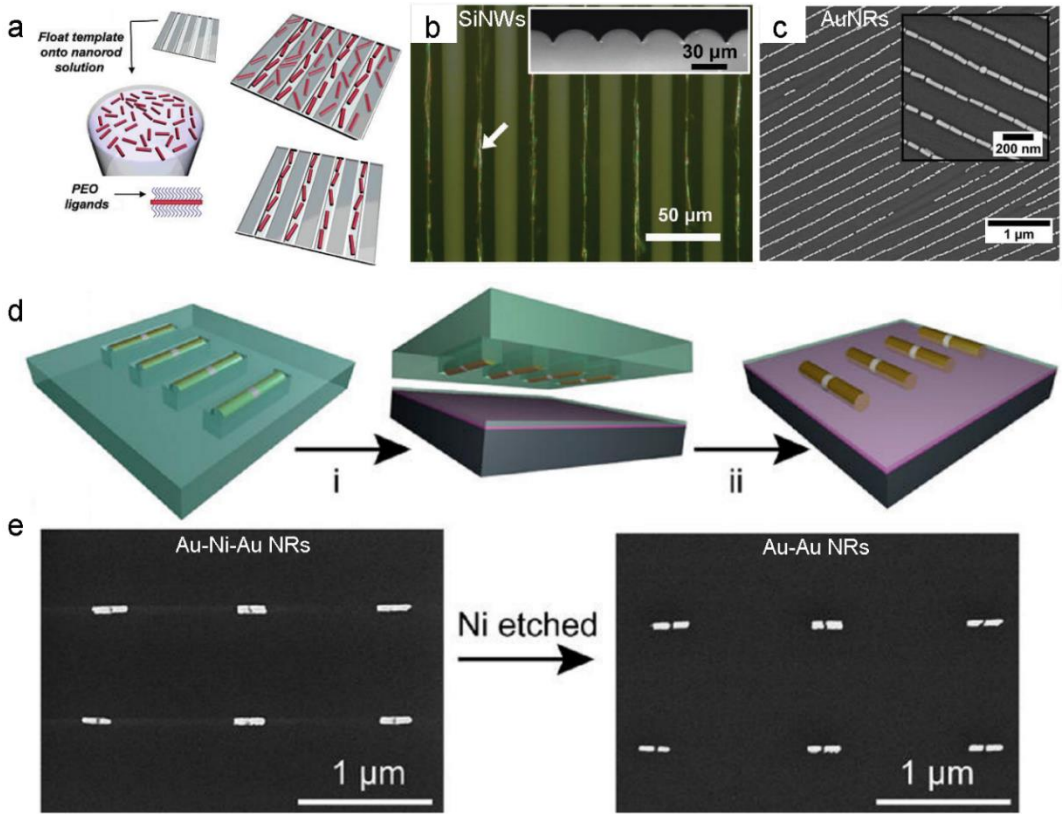

Fig. 4 (a) Schematic representation of the template-assisted aligning process. Reproduced with permission from ref. 89. Copyright 2006 American Chemical Society. (b) Polarized optical microscopy image of oriented SiNWs on a wrinkled template. Reproduced with permission from ref. 93. Copyright 2013 Wiley-VCH. (c) SEM image of oriented functionalized AuNRs in wrinkles. Reproduced from ref. 91 with permission from the Royal Society of Chemistry. (d) Schematic illustration of the deposition of multi-segmented NR arrays into a trenched PDMS followed by the transfer of the NRs to a desired substrate (i), leaving behind an aligned arrays (ii). (e) SEM images of transferred NRs, before and after Ni etching. Reproduced with permission from ref. 94. Copyright 2014 American Chemical Society.

surface by pressing the CNT-coated side of the filter onto the polymer followed by lifting off the filter.[71] A remarkable transformation occurred when the surface was gently rubbed with a Teflon sheet or aluminum foil giving a silvery appearance and an oriented CNT along the direction in which the film was rubbed as illustrated in Fig. 3a.[71] Another knocking-down assembly technique was reported by Patolsky and co-workers.[72] In this work, NW forests were fabricated on a large scale by the formation of ordered metal nano-island arrays that serve as templates for either the top-down sculpting of NWs or as seeds for the bottom-up growth of NWs. The in-place planarization of the vertical NWs was obtained by "knocking down" with an elastomer-based roller made for example of poly(dimethylsiloxane) (PDMS) or Teflon (Fig. 3b). Fig. 3c shows the SEM image of the NW arrays after the knock-down process, with red circles marking defective sites. The insets in Fig. 3c show an array with an interwire pitch of 400 nm (top) and an array with an interwire pitch of 100 nm (bottom).[72] In these methods, the in-plane oriented 1D nanoobjects were obtained by directly knocking down vertically aligned ones. This approach is thus restricted to nanoobjects that can first be aligned vertically and the quality of the final in-plane alignment is strongly related to the quality of the original vertical alignment.

2.3 Shear coating

Solution shear coating rely on the uniaxial shearing of a suspension, for example between two flat substrates moved at a controlled speed (Fig. 3d).[73, 74] Such an approach can be easily scaled up to an industrial manufacturing process and it has been extensively applied to the oriented crystallization of small molecules,[76] the alignment of semi-crystalline semiconducting polymers in thin films,[77-86] and more recently to the preparation of ordered 1D polymer NFs.[73] The alignment of 1D-nanoobjects strongly depends on the shearing speed, the viscosity of the solvent and the aspect ratio of the 1D-nanoobjects. The shear coating of a poly(3-hexylthiophene) (P3HT) NF suspension led to the extension or coplanarization of the polymer backbone in highly aligned network films, which resulted in an enhanced intra- and intermolecular ordering and reduced grain boundaries (Fig. 3e).[73] In a following work, the P3HT-NFs were oriented and embedded within an insulating polystyrene (PS) matrix (Fig. 3f). It was shown that the orientation of the P3HT-NF/PS blend depended on the shearing parameters and the composition. In particular, the concentration of PS played an important role in the alignment of the NFs. P3HT-NF/PS blend films with ~80 wt% of PS showed a better orientation than pure P3HT-NFs as the viscosity played a vital role in the alignment quality.[74]

Bao and co-workers aligned single-walled carbon nanotubes (SWCNTs) by shear coating.[75] An SWCNT suspension was sandwiched between a shearing blade and a wafer patterned with alternating solvent-wetting and dewetting regions (Fig. 3g). The solution

meniscus dried while the shearing blade was moved, leading to the dense alignment of SWCNTs on the solvent wetting regions (Fig. 3h). A small volume of liquid was required to coat a large area (≈ 200 µL to coat a 4-in. wafer), which resulted in a high density of SWCNT (150-200 SWCNTs per micrometer). The aligned SWCNTs thin films obtained by this technique showed a better performance than randomly oriented SWCNTs, with the on-current density and mobility improved by a factor of 45 and 20 respectively.[75]

Recently, shear coating was also reported for AgNWs, in which the AgNW suspension was swept by a glass rod.[87] The alignment and density of AgNWs can be tuned by the sweeping rate.[87]

2.4 Assembly by templated substrates

Templates are widely used to assemble 1D-nanoobjects.[88-99] These templates are usually solid substrates which were previously patterned, for example with channels or wrinkles used to selectively constrain the deposition of 1D-nanoobjects to a specific area and/or orientation. The substrate templates are placed into the suspension of the 1D-nanoobjects attracting the 1D-nanoobjects to the trenches while the remaining 1D-nanoobjects outside the channels can be removed easily. Consequently, the size of the channels or wrinkles plays a vital role in this process and non-oriented films are obtained if the size of the channels are not matched to the size of the 1D-nanoobjects.[88]

Russell and co-workers prepared templates made of a copolymer thin film on a silicon wafer resulting in 30 nm wide channels used to assemble pre-modified CdSe NRs.[89] The template was floated onto a CdSe NR aqueous suspension for 10-12 h followed by rinsing with water, leaving NRs confined in the channels with a local ordering (Fig. 4a).[89]

Wrinkled patterns can be used to align 1D-nanoobjects. Such wrinkles are usually fabricated by exposure of a pre-stretched elastomeric substrate to UV-ozone or plasma followed by strain release. The periodicity and amplitude of the wrinkles is controlled by the applied strain.[90-92] Cho's group used such wrinkled substrates not only as a template to assemble SiNWs on various grooved substrates by evaporation of the solvent but also as a stamp to transfer the aligned NWs to targeted substrates (Fig. 4b).[93] Fery and co-workers aligned monodisperse gold nanorods (AuNRs) by dip-coating on wrinkled surfaces and transferred these assemblies to indium tin oxide (ITO) substrates.[91] The order parameter can be as high as 0.97, which is close to perfect uni-axial alignment. The mean inter-NR gap along the NR longitudinal direction is about 7 nm (Fig. 4c).[91] This low inter-NR distance translates into a high filling factor of 88%. On the contrary, Mirkin *et al.* used designed templated substrates that allow the large-area orientation of pre-treated multi-segmented NRs of different sizes, lengths and aspect ratios with controlled NR position and distance.[94] The template (shown in Fig. 4d) was obtained with a Si master made by e-beam lithography stamped into a PDMS substrate. The NRs containing Au and Ni segments were first functionalized with Cetyltrimethylammonium Bromide (CTAB) to obtain a positively charged NR coating and then deposited onto the patterned PDMS. The aligned segmented NRs can be transferred to a desired substrate through microcontact printing (Fig. 4d). After transfer, Ni segments can be etched in a HCl aqueous solution and gapped NR arrays were obtained (Fig. 4e).[94] Brugger *et al.* also demonstrated that templated substrates comprising funneled traps and auxiliary sidewalls can be used for the assembly of AuNRs with simultaneous control on the position, orientation and interparticle distance at the nanometer level.[96] Up to 100% assembly yield over centimeter-scale substrates was achieved by optimizing the three sequential stages of nanoobject assembly: insertion of nanorods into the traps, resilience against the receding suspension front and drying of the residual solvent.[96]

Moreover, some organic 1D-nanoobjects can also be aligned within microchannels.[97-99] For example, Schroeder and co-workers aligned π-conjugated oligopeptides using colloidal microchannels. These latter were fabricated on a solid surface by drying a film of PS latex NPs on a solid substrate, which formed highly ordered channels due to capillary forces during film drying. The π-conjugated oligopeptides solution was then drop-casted near the center of the channel pattern, which allowed the solution to spread into the channels via capillary forces.[97] After evaporation of the solvent, the microchannels were removed by toluene that selectively dissolves PS, leaving a millimeter-sized solid surface loaded with oriented oligopeptides fibers.[97] Keller *et al.* fabricated topographically patterned silicon surfaces for assembly of DNA origami.[98] Self-organized nanoscale rippled patterns with periodicities ranging from 20 nm to 50 nm were fabricated by low-energy ion irradiation and served as template for DNA origami adsorption and alignment. A high alignment yield of up to ~70% can be obtained by optimizing the pattern dimensions.[98] In a following work, these rippled patterning surfaces were also applied for the alignment of AuNP decorated DNA origami.[99]

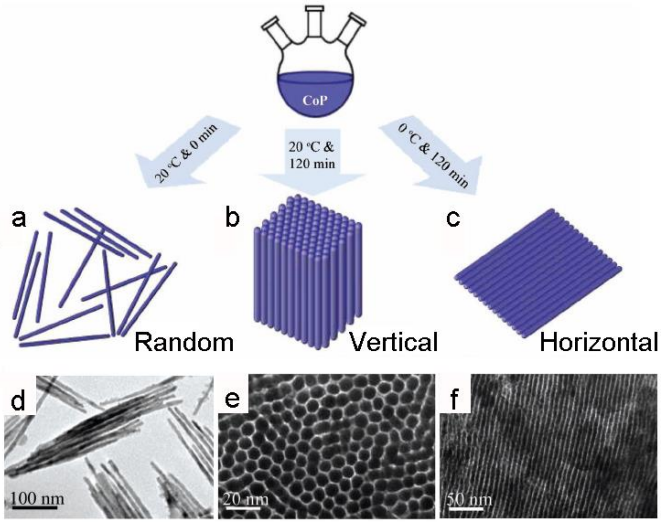

Fig. 5 (a-c) Schematic representation of aging temperature-dependent self-assembly of CoP NWs. (d-f) TEM images of randomly oriented NWs, vertically oriented NWs and horizontally oriented NWs. Reproduced with permission from ref. 100. Copyright 2012 Wiley-VCH.

2.5 Interactions between NWs

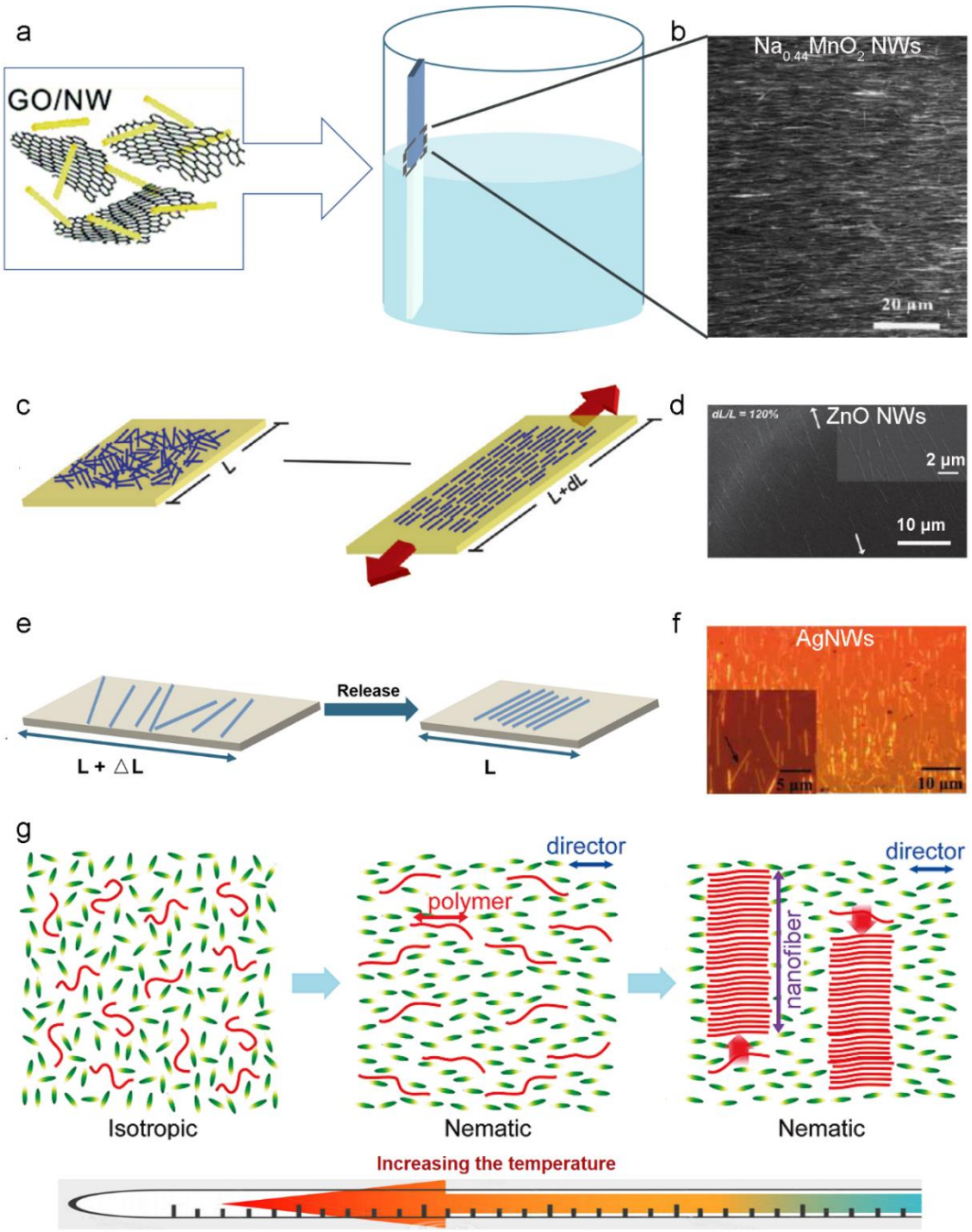

Fig. 6 (a) Schematic representation of co-assembly of graphene oxide (GO) nanosheets with $Na_{0.44}MnO_2$ NWs. Adapted with permission from ref. 101. Copyright 2009 American Chemical Society. (b) SEM image of aligned $Na_{0.44}MnO_2$ NWs. Reproduced with permission from ref. 101. Copyright 2009 American Chemical Society. (c) Schematic illustration of the alignment through stretching of a substrate. (d) SEM image of ZnO NWs aligned by stretching the substrate for 120%. Reproduced with permission from ref. 104. Copyright 2012 American Chemical Society. (e) Schematic illustration of the strain-release assembly. Adapted with permission from ref. 106. Copyright 2011 American Chemical Society. (f) Optical image AgNWs aligned after the strain applied on a substrate was released (Inset is the SEM picture at higher magnification). Reproduced with permission from ref. 106. Copyright 2011 American Chemical Society. (g) Schematic illustration of the assembly of NFs in a nematic liquid crystal with the change of temperature. Reproduced with permission from ref. 109. Copyright 2009 American Chemical Society.

The approaches discussed above make use of directional forces (external field, mechanical or capillary forces) to induce the assembly, and to the substrate-nanoobject attractive interaction to immobilize the nanoobjects on a surface. The inter-nanoobject interaction had a minor influence in those processes. However, interactions between the nanoobjects can also be used to induce a mutual alignment between the nanoobjects as such interactions can lead to the formation of bundles. Zhang *et al.* reported the first example of aligned cobalt phosphide (CoP) NWs with high aspect ratio into vertical or horizontal assemblies directly from the synthesis medium.[100] CoP NWs were prepared at 120°C, followed by cooling of the reaction medium to room temperature leading to random

orientation (Fig. 5a and d). Interestingly, when the reaction solution was kept at ambient temperature for ~2h, very large amounts of vertically oriented CoP NWs were observed, in which the CoP NWs formed a hexagonal array (Fig. 5b and e). In contrast, when the reaction solution was stored at 0°C for ~2 h, the CoP NWs were assembled horizontally into layered arrays composed of parallel NWs (Fig. 5c and f). The distance between neighboring NWs in horizontally or vertically assembled arrays were constant once the self-assembly process was completed, i.e. when the solution was kept for 2 h or longer.[100] These vertical or horizontal assemblies were very stable under ultrasonication, thermal treatment and organic solvents due to the strong attractive interaction between neighboring CoP NWs. This temperature/duration dependent assembly was mainly controlled by the nucleation and subsequent growth of ordered arrays and depended on the viscosity or diffusion rate of the NWs.[100] However, this process is not universal and cannot be applied to any NW system as it relies on inter-NW interactions that depend on numerous parameters, making the growth mechanism difficult to control.

2.6 Co-assembly with other nanoobjects.

The previous example used the interactions between similar NWs in a suspension to induce mutual alignment. Two different nanoobjects in suspension may also assemble side-by-side if there is an attractive interaction between them, and this effect can be used to co-assemble 1D-nanoobjects with other nanomaterials.[101-103] Li *et al.* investigated the co-assembly of graphene oxide (GO) nanosheets and $Na_{0.44}MnO_2$ NWs.[101] When GO nanosheets were added to the NW aqueous suspension, the NWs aggregated and accumulated at the air-liquid interface because of hydrogen bonding and ion-dipole interactions between GO nanosheets and the $Na_{0.44}MnO_2$ NWs (Fig. 6a). Due to the high concentration of NWs at the air-liquid interface, the NWs tend to be parallel to each other. These assemblies can be further transferred to hydrophilic substrates with their orientation parallel to the air-liquid-substrate contact line upon evaporation of the solvent (Fig. 6b).[101] Hwang *et al.* followed the assembly of collagen on muscovite mica using Atomic Force Microscopy (AFM).[102] They suggested that the assembly occurred in 3 steps: i) surface adsorption of collagen, ii) diffusion, iii) nucleation of NWs and growth. The potassium ions were used to bind the negatively charged mica surface and neutralized it, thus reducing the binding affinity of collagen and enhancing surface diffusion.[102] The co-assembly of AuNWs with multiwalled CNT (MWCNTs) was also reported.[103] Strong van der Waals and hydrophobic interactions between the side chains of oleylamine-coated AuNWs and the sidewalls of MWCNTs induced the assembly of NWs along the longitudinal axis of CNT. Interestingly, the assembly was found to be independent of the aspect ratio of the AuNWs.[103]

2.7 Mechanical stretching of substrate

One approach to align NWs is to linearly stretch an elastomeric substrate on which the NWs have been deposited.[104, 105] Randomly arranged Zinc oxide (ZnO) NWs were for instance deposited on a PDMS substrate, and the alignment occurred when the substrate was stretched (Fig. 6c).[104] Up to 90% of the ZnO NWs can be aligned within ± 15° of the stretching direction (Fig. 6d).[104] Xu *et al.* introduced a facile yet effective method for the alignment of NWs on a stretchable substrate. The so-called strain-release assembly consists in depositing the NWs to a pre-strained substrate, followed by releasing the substrate (Fig. 6e).[106, 107] AgNWs aligned by this approach are shown in Fig. 6f. The process can be repeated several times by transferring the NWs to another pre-strained substrate to improve the ordering of NWs in the transverse direction. For example, the alignment on PDMS after two assembly steps increased

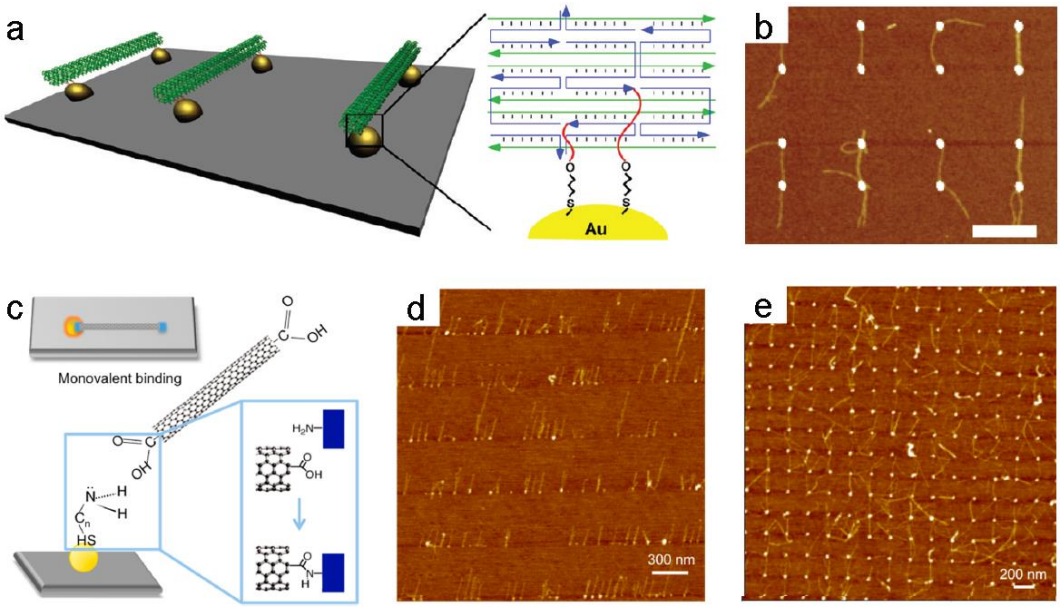

Fig. 7 (a) Schematic representation of Au islands connected by DNA origami tubes on a substrate. (b) AFM images of Au islands connected by DNA origami tubes (scale bar: 500 nm). Reproduced with permission from ref. 111. Copyright 2010 American Chemical Society. (c) Schematics of the monovalent binding of a SWCNT functionalized with carboxyl groups at its tips with a nanodot functionalized with amines on a surface. (d-e) AFM image of an array of SWCNTs attached to amine functionalized nanodots through monovalent (d) or divalent (e) bonding. Reproduced with permission from ref. 113. Copyright 2010 American Chemical Society.

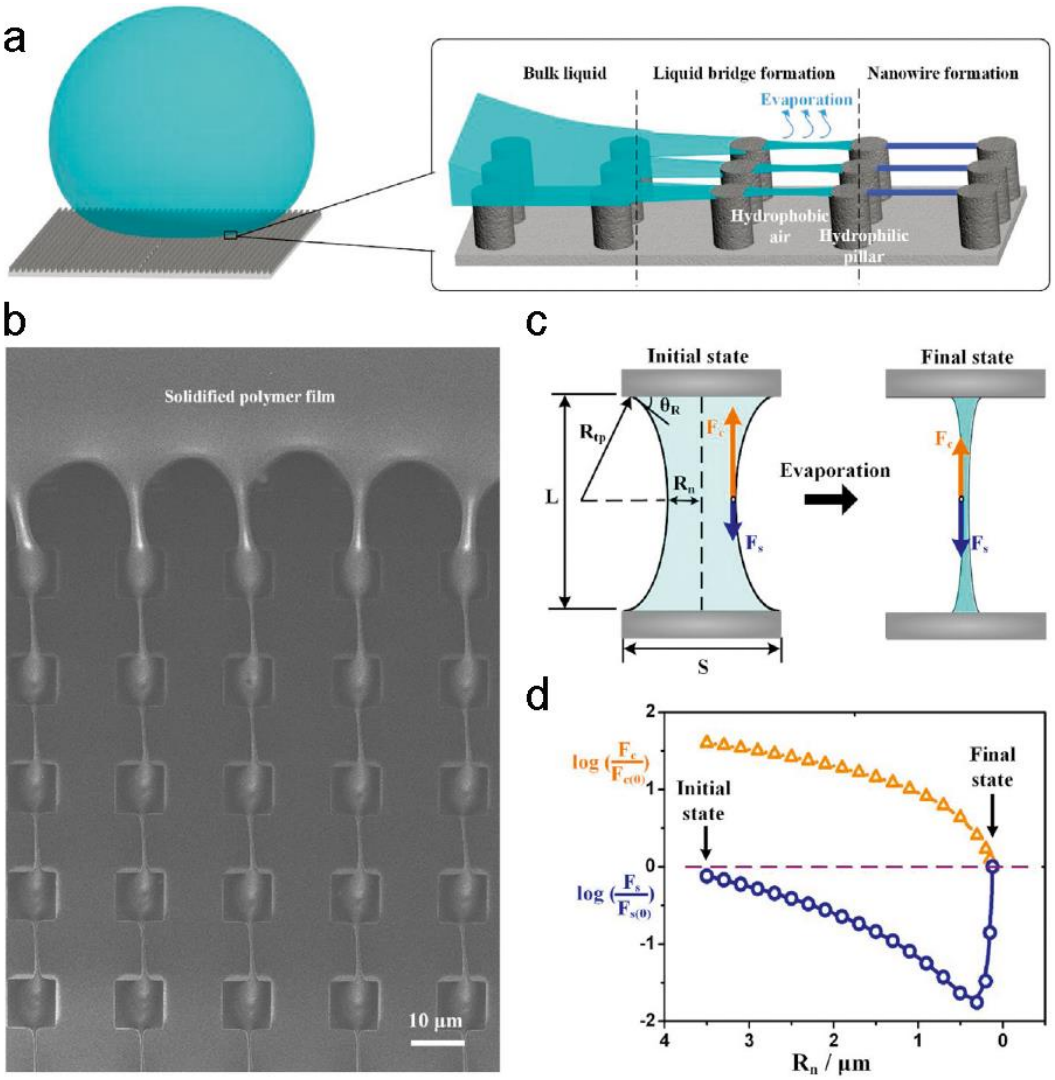

Fig. 8 (a) Schematic illustration and (b) SEM image of the formation process of oriented NWs during the regular liquid rupture upon a superhydrophobic pillar-structured substrate. (c) Schematic illustration of F_c and F_s inside one liquid bridge. (d) Dependence of F_c and F_s on the radius of the liquid bridge neck (R_n). The two forces get equal to each other as water is evaporated. Reproduced with permission from ref. 115. Copyright 2019 Elsevier Inc.

from 29% to 90% for AgNWs and from 25% to 88% for SiNWs. The density of AgNWs and SiNWs increased by 60% and 75% respectively.[106] The success of this method depended on the large-strain elasticity of the substrates and the static friction between the NWs and the substrate.[106] It must be noted that the orientation of NWs in the former technique[104, 105] happened along the stretching direction while the substrate was stretched, while the alignment of NWs in the latter approach [106, 107] occurred perpendicularly to the stretching direction when the substrate was released to its original state. Interestingly, such a mechanism to align 1D-nanoobjects can be used not only with mechanically stretched substrates but also with other stimuli such as temperature or pH which induce the shrinkage of a substrate.[108]

2.8 Assembly induced by the liquid crystals

Liquid crystals are intrinsically ordered. In particular, elongated molecules forming a nematic phase have no positional order but tend to align to have a long-range directional order with their long axes more or less parallel to each other. It can be used as a molecular template to induce the orientation of inorganic or polymer 1D-nanoobjects.[109, 110] For instance, Samitsu *et al.* reported the alignment of conducting polymer NFs using anisotropic crystallization in a nematic liquid crystal.[109] Poly(3,3'''-didodecylquarterthiophene) (PQT12) was chosen as a model polymer because of the excellent miscibility in liquid crystals. In an isotropic liquid phase (T > 102°C), polymer chains showed a random orientation (Fig. 6g left). At lower temperature (60-102 °C), the nematic phase induces the alignment of the individual polymer chains along the director (Fig. 6g middle).[109] The increase in liquid crystalline order during further cooling made the polymer chains more extended along the director (Fig. 6g right). The polymer chains crystallized in a nearly one-dimensional structure and self-assembled into aligned NFs consisting of stacked polymer chains.[109] Recently, Pal *et al.* reported the use of supramolecular hydrogen liquid crystals to assist the orientation of cadmium selenide (CdS) NWs.[110] The supramolecular hydrogen liquid crystals were combined with CdS

NWs to obtain composites in which the NWs were unidirectionally dispersed within the hydrogen-bonded liquid crystals.[110]

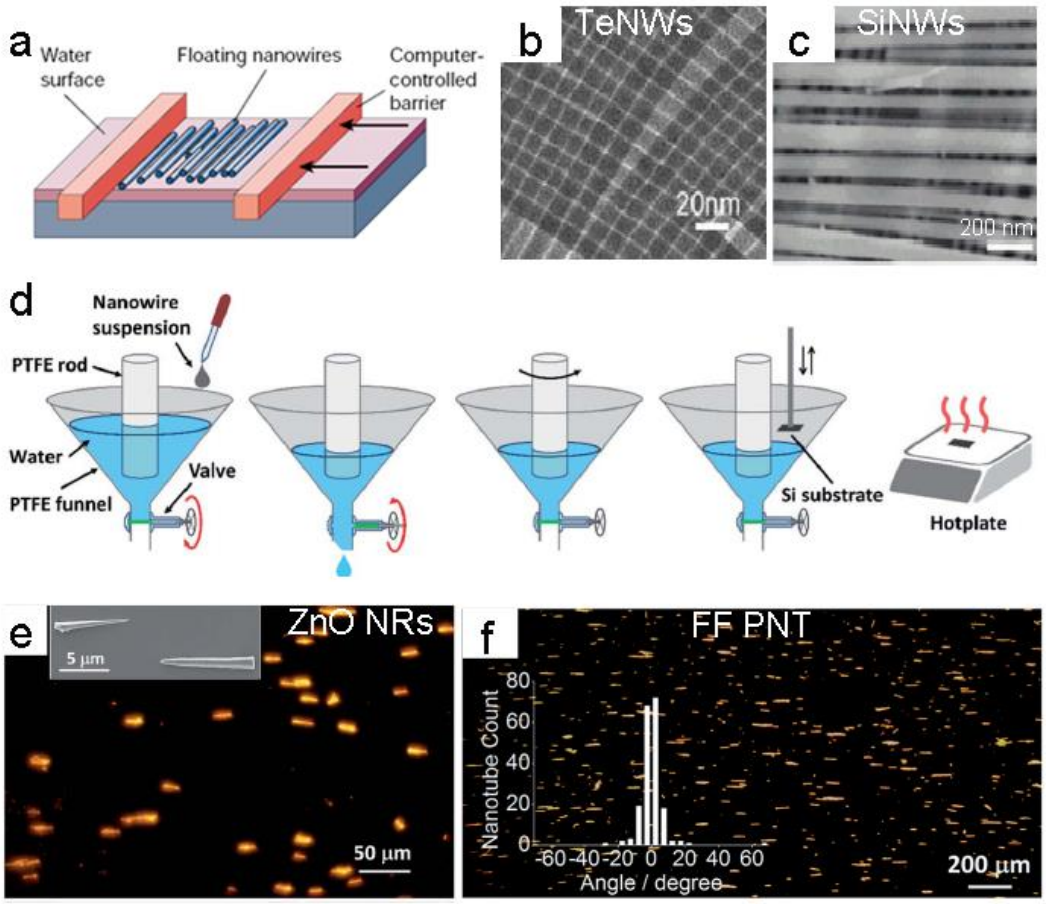

Fig. 9 (a) Schematic representation of the LB technique. Reproduced with permission from ref. 133. Copyright 2003 Nature. (b) TEM image of a two-layered cross-oriented TeNWs thin film oriented by the LB technique. Reproduced with permission from ref. 124. Copyright 2010 American Chemical Society. (c) SEM image of a cross-oriented SiNWs array. Reproduced with permission from ref. 128. Copyright 2003 American Chemical Society. (d) Schematic illustration of the shear-assisted-Langmuir technique: NW spread, compression, shear by spinning, NW transfer, and surfactant removal. (e-f) Optical microscope image of an oriented ZnO NR array (e) and an oriented FF PNT array (f). Inset: angular distribution of the NTs. Reproduced from ref. 134 with permission from the Royal Society of Chemistry.

2.9 Interconnecting patterned surface with 1D-nanoobjects

This approach involves the chemical bonding of an ordered pattern on a surface with the tips of 1D-nanoobjects. Depending on their chemical nature, the tips of 1D-nanoobjects can be different from the core surface, enabling them to selectively interact or chemically bind to specific sites of a patterned surface. The alignment of 1D-nanoobjects is highly dependent on the binding mechanism and the geometry of the binding sites. Weak chemical interactions allow enough mobility for the 1D-nanoobjects to align with the binding sites, and the distances between neighboring binding sites should be slightly smaller than the length of the 1D-nanoobjects to maximize the possibility of bridging two binding site by a single 1D-nanoobject. Many different 1D-nanoobjects including DNA origami,[111, 112] CNT[113] and inorganic nanorods[114] have been assembled by this technique. Yan *et al.* reported the assembly of thiolated DNA origami nanotubes by directly attaching the tubes to gold islands on the substrate through thiol-Au bonds (Fig. 7a-b).[111] The efficiency of DNA nanotube attachment to the patterned surface is affected by the incubation time of the patterned substrate in the DNA origami nanotube solution, the number of thiol groups at each end of the DNA nanotube, the size of the gold islands and the DNA origami nanotube concentration. Complex DNA tube patterns can be fabricated by optimizing incubation conditions and modifying the gold island pattern.[111] Wind and co-workers also aligned end-functionalized SWCNT by binding to lithographically defined nanoscale anchors with controlled position (Fig. 7c). Orientation of the SWCNTs was higher in case of a monovalent bonding compared to a divalent bonding because of the higher mobility of the SWCNTs (Fig. 7d-e).[113] Schvartzman *et al.* also reported the assembly of 1D nanodumbbells (Au-tipped CdS NRs) into arbitrary 2D arrays through their chemical docking to nanopatterned functionalities. The metallic nanodots were functionalized with an organic monolayer whose terminal thiol groups could bind the nanodumbbell tips.[114]

2.10 Liquid bridge induced assembly

When a volatile liquid droplet is placed onto a solid surface, its three-phase contact line (TCL) will shrink towards the geometric center driven by evaporation. The dewetting process of a liquid droplet on a homogeneous surface is continuous, but it will be interrupted by wettability-heterogeneous domains.[115, 116] Jiang *et al.* use this effect

in the so-called liquid-bridge induced assembly method to prepare NW arrays on superhydrophobic pillar-structured Si substrates.[116] The basic mechanism relies on the discrepancy between the hydrophilic pillar tops and the hydrophobic gap between the pillars (Fig. 8a). Oriented NW arrays can be prepared by simply driving a polymer-containing droplet "slipping" through an anti-wetting pillar-structured surface (Fig. 8b). The dynamics of narrowing and formation of NWs are mainly dominated by two competitive forces. One is the capillary force, F_c; the other is a structural cohesive force, F_s. Both F_c and F_s change as the liquid bridge is narrowed by the evaporation of water (Fig. 8c). The NWs form when F_c and F_s are well balanced (Fig. 8d).[116] The direction of the liquid bridge is always parallel to the TCL shrinkage direction. Furthermore, the position of each NW and the distance between neighboring NWs can be precisely controlled by well-designed micropillars.[116]

3. Methods that can be repeated to form multilayered architectures

As presented in Section 2, very diverse approaches that rely on different forces (mechanical stress, capillarity, chemical interactions, external electric or magnetic fields) can be implemented to align 1D-nanoobjects on a substrate in a monolayered architecture. Each of the presented approaches has its intrinsic strength and limitations. One major challenge in order to design functional nanodevices is to be able to fabricate arrays of nanoobjects that have a complex anisotropy and/or consist of different nanomaterials ordered in a controlled architecture. To this end, we review in the following section approaches that can form multilayered architectures of oriented 1D-nanoobjects.

3.1 Langmuir-Blodgett technique

The Langmuir-Blodgett (LB) assembly technique is one of the most classical methods to align 1D-nanoobjects.[117] The technique was initially used to transfer molecular monolayers from a liquid-air interface onto a solid substrate. In recent years, the approach has been extended to effectively assemble nanoobjects, including NPs,[118-120] NRs,[121, 122] NWs,[123-130] NTs,[131] and even 2D nanosheets.[132] The schematic representation of the LB technique for alignment of 1D-nanoobjects is shown in Fig. 9a.[133] 1D-nanoobjects are usually dispersed in a volatile organic solvent and then spread onto a subphase (usually water). When the solvent is evaporated, the nanoobject layer floating at the air-liquid interface is slowly compressed with a barrier with a controlled surface pressure and moving speed. The 1D-nanoobjects are close-packed with their longitudinal axis aligned perpendicular to the compression direction to achieve one Langmuir monolayer that can be transferred to a substrate. Dai and his co-workers prepared chemically functionalized Germanium NWs (GeNWs) soluble in organic solvents and assembled them into close-packed films.[127] The LB assembly of vanadium dioxide NWs (VO_2 NWs),[125] AgNWs,[126, 130] and gold microwires[129] were also reported.

If these LB assembled monolayers are transferred onto a solid substrate repeatedly, it results in the formation of complex nanostructures with a defined thickness. For instance, Yu *et al.* aligned high aspect ratio flexible tellurium NWs (TeNWs) by LB. Nanomesh-like nanostructures or more complex architectures could be fabricated very easily by changing the orientation of the substrate (Fig. 9b).[124] Lieber and his co-workers used this method to successfully align mono- or multi- layered SiNWs and the spacing of the transferred NWs was controlled from the micrometer scale to close packing by the compression step (Fig. 9c).[128]

Recently, Yang's group developed a novel shear-assisted-Langmuir technique to align inorganic and organic NWs.[134] The NWs were first dispersed at the air-water interface, and compression was obtained by draining the water through a funnel outlet (Fig. 9d). Spinning of the liquid by a Poly(tetra fluoroethylene) (PTFE) rod induced a shear force which led to the orientation of the 1D-nanoobjects. The aligned NWs could be further transferred on a substrate which was heated to remove the surfactant molecules added in the suspension to adjust the surface tension (Fig. 9d). This modified technique can be applied to orient zinc oxide (ZnO) NRs (Fig. 9e) and diphenylalanine peptide nanotubes (FF PNTs) (Fig. 9f). A functional device comprising these surfactant-enhanced shear flow aligned NWs can be made within 20 mins. The density of the aligned NW can be tuned by controlling the height of water in the funnel and amount of NWs.[134] The presence of surfactant molecules was crucial for the quality of alignment as it controlled the viscosity to avoid aggregation. It is worth mentioning that a minimum threshold concentration is necessary to orient the NWs.[134]

3.2 Bubble blowing extrusion

Bubble Blown film (BBF) extrusion is a well-established technique to produce polymer thin films, especially when large amounts of plastic films are demanded. In this method, the molten polymer is usually extruded out and inflated to form a balloon, and then collapsed to form homogeneous flat films. Lieber and coauthors applied this general idea to fabricate nanocomposite thin films in which the density and alignment of NWs and NTs were well controlled.[135] The basic three steps in this method consisted in (1) the preparation of a stable and homogeneous suspension of NWs or NTs in a polymer solution, (2) expansion of the NW- or nanotube-containing polymer suspension using a stainless steel die with a gas inlet at the bottom, an outlet at the top and a ring centered over the gas outlet, which was moved upward while introducing N_2 gas, and (3) transfer of the bubble film to a substrate (Fig. 10a).[135] The bubble expansion setup is shown in Fig. 10b. The shear force generated when the NW-containing polymer suspension passed through the die oriented the NWs along the strain direction, and these oriented NW thin films can then be transferred to various substrates (Fig. 10c-d).[135] Cao and co-workers applied this method for large-area assembly of TeNWs into

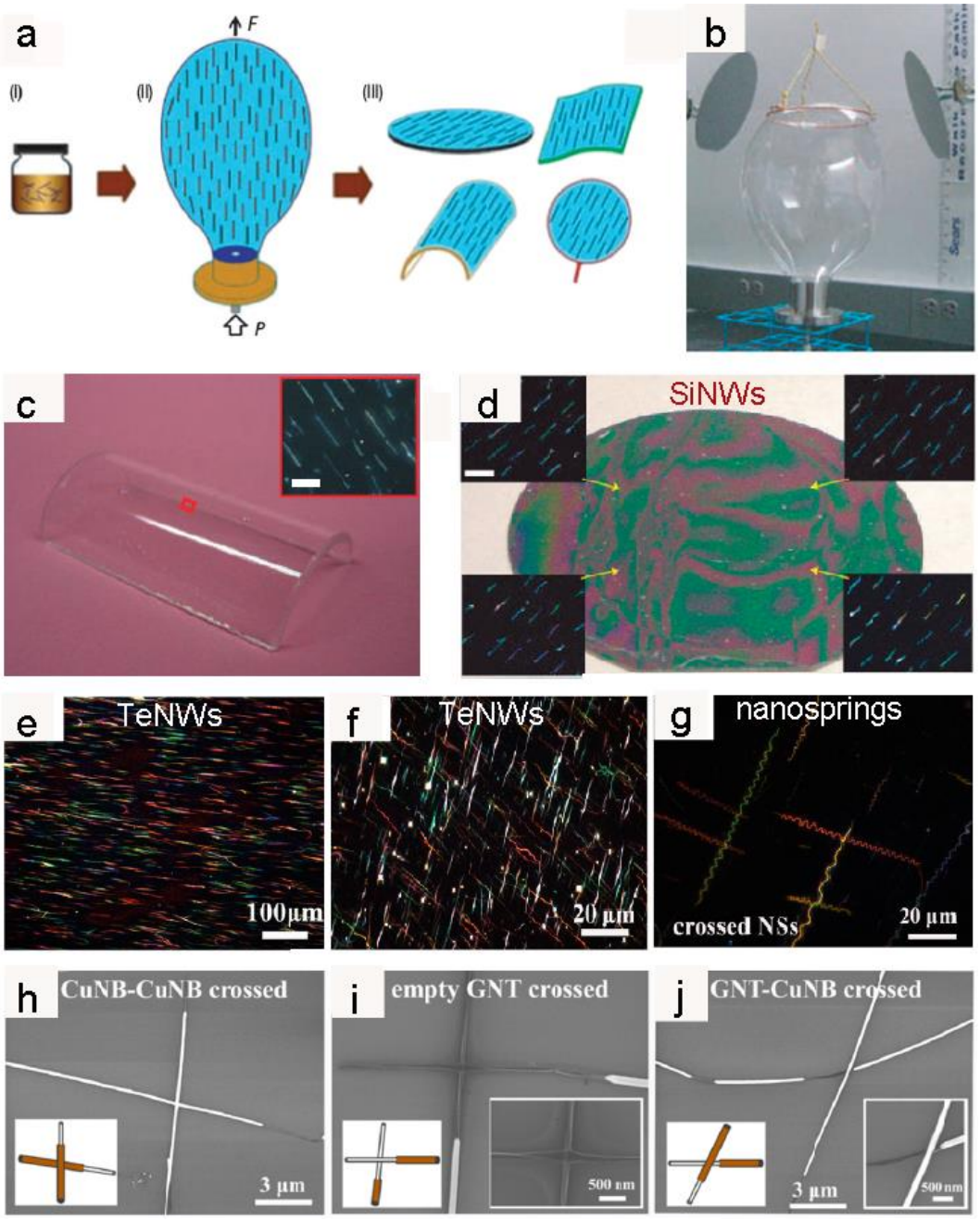

Fig. 10 (a) Schematic illustration of the blown bubble expansion process. (b) Photographs of the directed bubble expansion. (c) Image of oriented SiNWs transferred onto a curved surface (scale bar: 10 μm). (d) Image of oriented SiNWs transferred onto a silicon wafer (scale bar: 10 μm). Reproduced with permission from ref. 135. Copyright 2007 Nature. (e) Optical microscopy image of well-aligned TeNWs. (f) Optical microscopy image of a double-layer array of NWs crossed at an angle of 60°. (g) Optical microscopy image of crossed nanosprings. Reproduced with permission from ref. 136. Copyright 2014 American Chemical Society. (h-j) SEM images of three junctions crossed at different regions (Insets are the enlarged images of the junctions and corresponding models). Reproduced with permission from ref. 137. Copyright 2016 American Chemical Society.

aligned and crossed NW arrays as well as buckled nanosprings (NSs) arrays (Fig. 10e-g).[136] Following this work, they employed the same technique to assemble copper nanoblocks (CuNBs) followed by graphene deposition to form graphene nanotubes (GNTs). Such GNT@CuNB nanostructures were transferred to Si wafer with crossed orientations giving different junction structures (i.e. CuNB-CuNB crossed, GNT-GNT crossed and GNT-CuNB crossed) on the wafer (Fig. 10h-j).[137] Recently, alignment of 1D bismuth sulfide nanoobjects was also reported by the same group.[138]

3.3 Evaporation-Induced assembly

1D-nanoobjects can be aligned at the solid-liquid-gas interface of a drying droplet of the nanoobject suspension spread on a substrate. The dynamics and mechanism of the evaporation are very complicated and involve many challenging problems in physics.

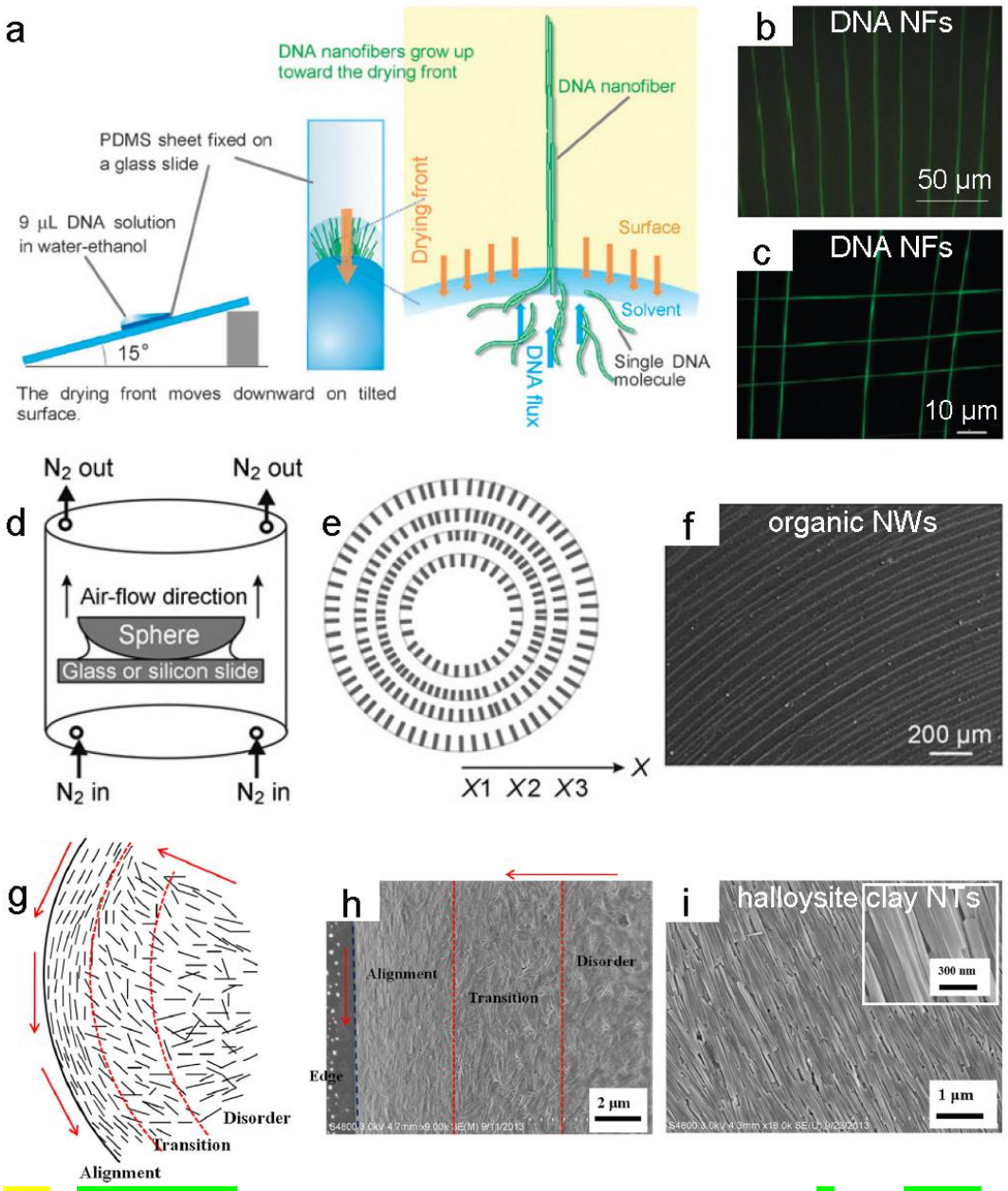

Fig. 11 (a) Scheme of the solvent vapor-induced process for aligning DNA NFs. (b-c) Fluorescent optical images of an oriented monolayer (b) and of a 2D array of DNA NFs (c). Reproduced from ref. 144 with permission from the Royal Society of Chemistry. (d) Illustration of the sphere-on-flat evaporation setup. (e) Representation of as-prepared concentric rings of organic NWs. (f) SEM image of the concentric rings of DMQA NWs. Reproduced with permission from ref. 149. Copyright 2011 Wiley-VCH. (g) Sketch of the flow for halloysite NTs. (h) SEM image of the different sections of the dried dispersion droplet. (i) SEM image of oriented halloysite clay NTs on Si substrate. Reproduced with permission from ref. 152. Copyright 2015 Elsevier Inc.

However, alignment induced by evaporation is common and the solvent evaporation rate is believed to be a critical factor to align nanoobjects with well-controlled orientations.[139-156] When a drop of liquid is placed on a substrate, it spreads on the surface until an equilibrium governed by the balanced interfacial forces is reached, followed by the evaporation of the solvent in a controlled manner. This evaporation induces a convective flow towards the solid-liquid-gas interface, and the reduction of the volume of the droplet leads to an increase in the concentration of the nanoobjects. The relatively weak interactions such as van der Waals forces or dipole-dipole interactions between the dispersed nanoobjects become dominant, driving the nanoobjects to assemble. As early as 1994, Bensimon *et al.* introduced the molecular combing method to extend DNA molecules and align them perpendicular to the receding interface. This is the earliest report on the alignment of 1D-nanoobjects by evaporation.[139]

Here we introduce some recently reported examples using evaporation for precisely organizing 1D-nanoobjects on a substrate. Miki *et al.* reported the growth and alignment of 1D DNA NFs by solvent evaporation on a tilted PDMS substrate.[144] The DNA solution was deposited on a PDMS substrate that was tilted at 15° while the solvent was evaporated to move the drying front downwards (Fig. 11a).[144] DNA molecules suspended in the solution were pulled

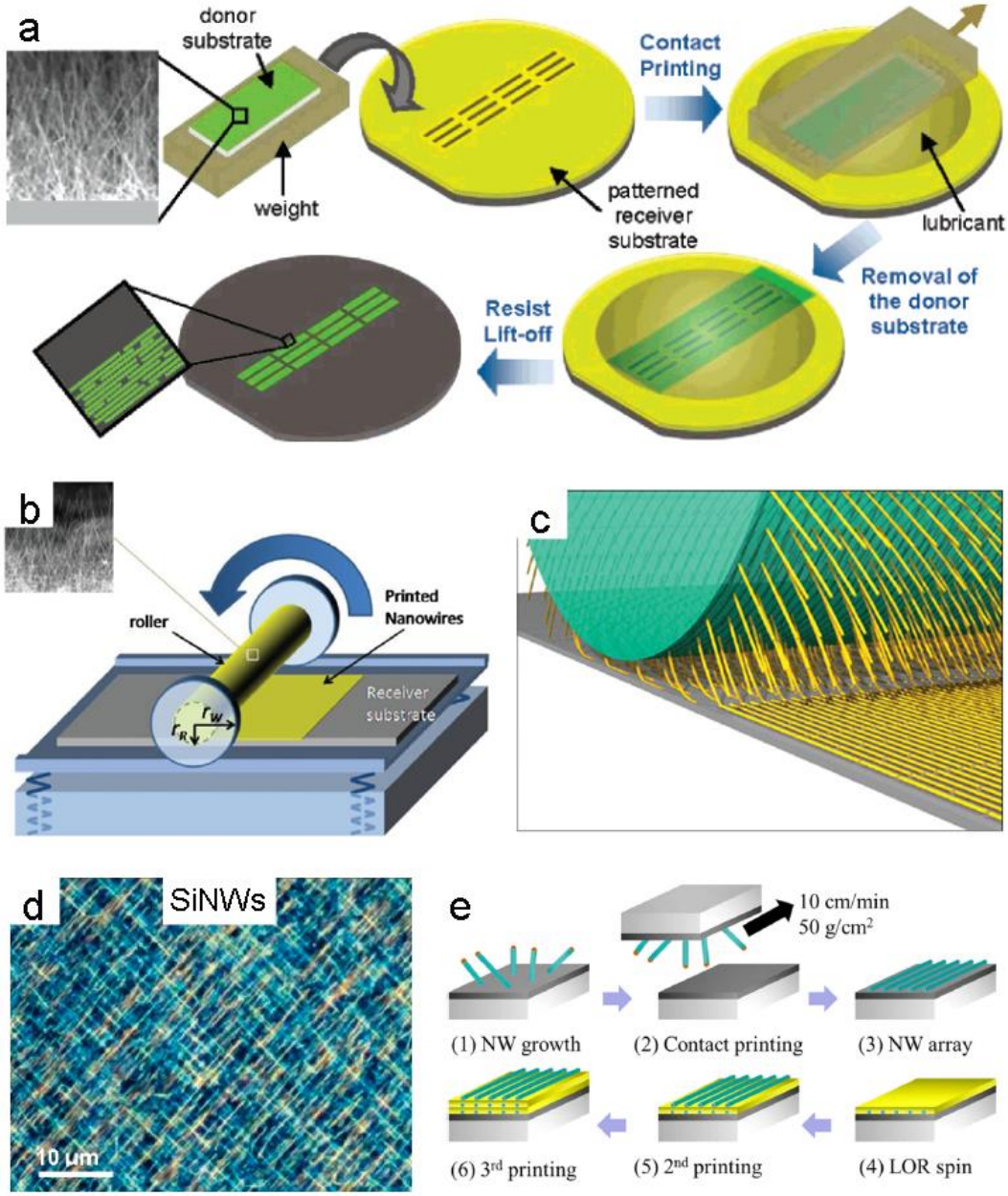

Fig. 12 Schematic representation of the contact printing of NW arrays involving (a) planar and (b-c) cylindrical growth (donor) substrates. The SEM images in the insets of (a) and (b) show that the grown GeNWs are perpendicular to the growth substrate, resembling a forest. The NWs are oriented and transferred to the receiving substrate by applying a directional shear force, resulting in the printing of sub-monolayer parallel NW arrays on the receiving substrate. (d) Optical image of a double layer of cross-aligned SiNWs. Reproduced with permission from ref. 158. Copyright 2008 American Chemical Society, ref. 159. Copyright 2009 Wiley-VCH. (e) Schematics of the successive printing steps to obtain GaAs multilayer NW arrays. Reproduced with permission from ref. 173. Copyright 2016 American Chemical Society.

towards the drying front by convection and aligned at the moving interface (Fig. 11a). The surface tension at the drying front induced the DNA molecules alignment as shown in Fig. 11b and crossed 2D patterns of DNA NFs can be further obtained with this method by simply changing the drying front direction (Fig. 11c).[144] Instead of tilting the substrate, Zhang *et al.* introduced a pulling process for forming parallel stripes of aligned organic NWs.[147] When a substrate was slowly pulled out of the organic NW solution, the CH_2Cl_2 solvent evaporated, and the organic NWs aggregated on the substrate with the alignment direction parallel to the moving direction because of the strong intermolecular interactions.[147] The surface morphology of the substrate, temperature, evaporation rate and the substrate pulling speed played a key role in the dimension of the NWs and the stripes.[147] However, the contact line was not easy to control using this simple approach, and the same group improved the method by evaporating droplets within a confined geometry consisting of a glass slide and a spherical lens. The two surfaces were brought into contact, and the *N,N'*-Dimethylquinacridone (DMQA) solution was dropped into the gap between slide and lens. A steady upstream of nitrogen gas was blown nearby the setup to help evaporate the solvent (Fig. 11d). After the solution was dried on the substrate, a number of ordered rings of NWs were left which aligned and formed concentric rings on both surfaces (Fig. 11e-f).[149]

The evaporation-induced orientation of halloysite clay NTs was reported by Lvov and co-workers.[152] The surface charge of the halloysite NTs was enhanced to stabilize the colloids and the assembly of NTs started after dropping the colloidal halloysite aqueous suspension on a heated substrate. The alignment was tuned by changing the length and surface charge of the NTs as well as the ionic strength and pH of the solvent.[152] When the local concentration at the periphery increased up to a critical value, the NTs evolve to a liquid crystalline phase and stabilized into an aligned structure parallel to the edge. This interesting parallel orientation at the edge was mostly due to the development of a flow-induced torque on the NTs. The outmost end of the NTs was pinned by the contact line and flow direction changed to parallel to the edge because of the geometrical constraints (Fig. 11g).[152] The coupled effect from the frictional force between the substrate and the NTs in suspension and the accelerated evaporation at the contact line produced a torque rotation, which aligned the first NTs that reached the edge. Once the first NTs were aligned parallel to the droplet edge, other NTs from the suspension can accumulate upon evaporation of the liquid, ordering from the periphery towards the less ordered inner region (Fig. 11h-i).[152]

3.4 Contact printing

A variety of inorganic semiconducting NWs with the desired composition can be vertically grown on a substrate by chemical vapor deposition (CVD). These vertically oriented NWs can be transferred from the growth substrate (which can be flat or cylindrical) to a flat receiving substrate through contact printing.[157-176] Compared with the rubbing method (section 2.2), NWs are grown on a "donor" substrate and can be printed repeatedly onto a "receiving" substrate, in contrast to knocking down NWs on the growth substrate itself. Contact printing thus allows much more complicated multilayered architectures to be prepared by repeated deposition cycles. However, similarly to the rubbing method, the alignment of the NWs on the "receiving" substrate strongly depend on the vertical alignment quality on the "donor" substrate.

Javey *et al.* reported a germanium/silicon (Ge/Si) core/shell NW array that can be grown on a Si substrate.[158] As shown in Fig. 12a, Ge/Si NWs were grown vertically on the donor substrate followed by transferring to a photolithographically patterned receiving substrate. Gentle pressure was applied from the top to slide the growth substrate and to ensure the deposition of NWs on the receiving structures. After removing the growth substrate, well-oriented NW arrays were left on the receiving substrate (Fig. 12a).[158] During this NW transfer process, chemical treatment of the receiving substrate can improve the printed NW density, the orientation degree and the uniformity of the transferred array.[158] For instance, GeNWs have been transferred with a high density (~ 8 NW/μm) on a receiving substrate functionalized with $-NH_2$ or $-N(Me)_3^+$ terminated monolayers, while there was almost no transfer of NWs on a $-CF_3$ terminated monolayers with the same printing process, which meant that the contact printing process required strong chemical interactions between the NWs and the receiving substrate. The use of a lubricant can also increase the density of transferred NWs.[158] Following this work, the same group prepared aligned NW arrays on patterned receiving substrates by selectively interacting with NWs in different regions.[160] The $-CF_3$ terminated receiving substrate (which is non-sticky to the Si or Ge NWs) can be transformed to a sticky -COOH terminated one by exposure to vacuum ultraviolet light (VUV) in an oxygen-rich environment through a mask. The patterned surfaces were defined in a single step which enabled the highly specific transfer of the NWs to -COOH terminated regions without the need of a subsequent lift-off process.[160]

Recently, Shen *et al.* reported the contact printing of semiconductor NWs such as Zn_2GeO_4, $In_2Ge_2O_7$ and Zn_3P_2 NWs.[164, 165] Strehle *et al.* reported a surface-controlled contact printing,[166] which is based on dry friction between NWs and the receiving surface. The surface morphology of a patterned substrate altered the local friction force in different regions and allowed the assembly and positioning of single NWs at specific predefined positions on the receiving substrate.[166]

Differential roll printing (DRP) of NWs from a cylindrical growth substrate was also reported.[159, 170] This technique required the direct growth of crystalline NWs on a cylindrical substrate using the vapor-liquid-solid process (Fig. 12b). These NWs were then transferred from the donor roller to the receiving substrate (Fig. 12c). It was found that the printing was independent of the rolling velocity if it was less than 20 mm/min. At higher velocities, nonuniform printing was observed. The pressure applied on the roller played an important role as the NWs could not be aligned at low pressure while mechanical damages to the NWs which broke down into shorter NWs (< 1 μm length) were observed at higher pressure. Compared to the previously mentioned contact printing approaches, DRP can minimize the contact area between the donor and receiving substrates since the cylindrical donor substrate rolled over the receiving substrate with only a small tangent contact area, which was highly beneficial for printing NWs on large areas.[159, 170]

Multilayered NW arrays with controlled stacking of NWs can also be fabricated by multistep printing, which usually needs a polymer thin film to serve as a buffer layer between adjacent layers of printed NWs. For example, Javey and co-workers aligned SiNWs with the contact printing technique. Cross-assembled arrays can be fabricated by multistep printing of the SiNWs (Fig. 12d).[158] Moreover, multilayer printing of parallel GaAs NW arrays were printed, and a buffer layer needed to be spin-coated between each array to ensure the integrity of the thin film (Fig. 12e).[173] The contact printing alignment quality

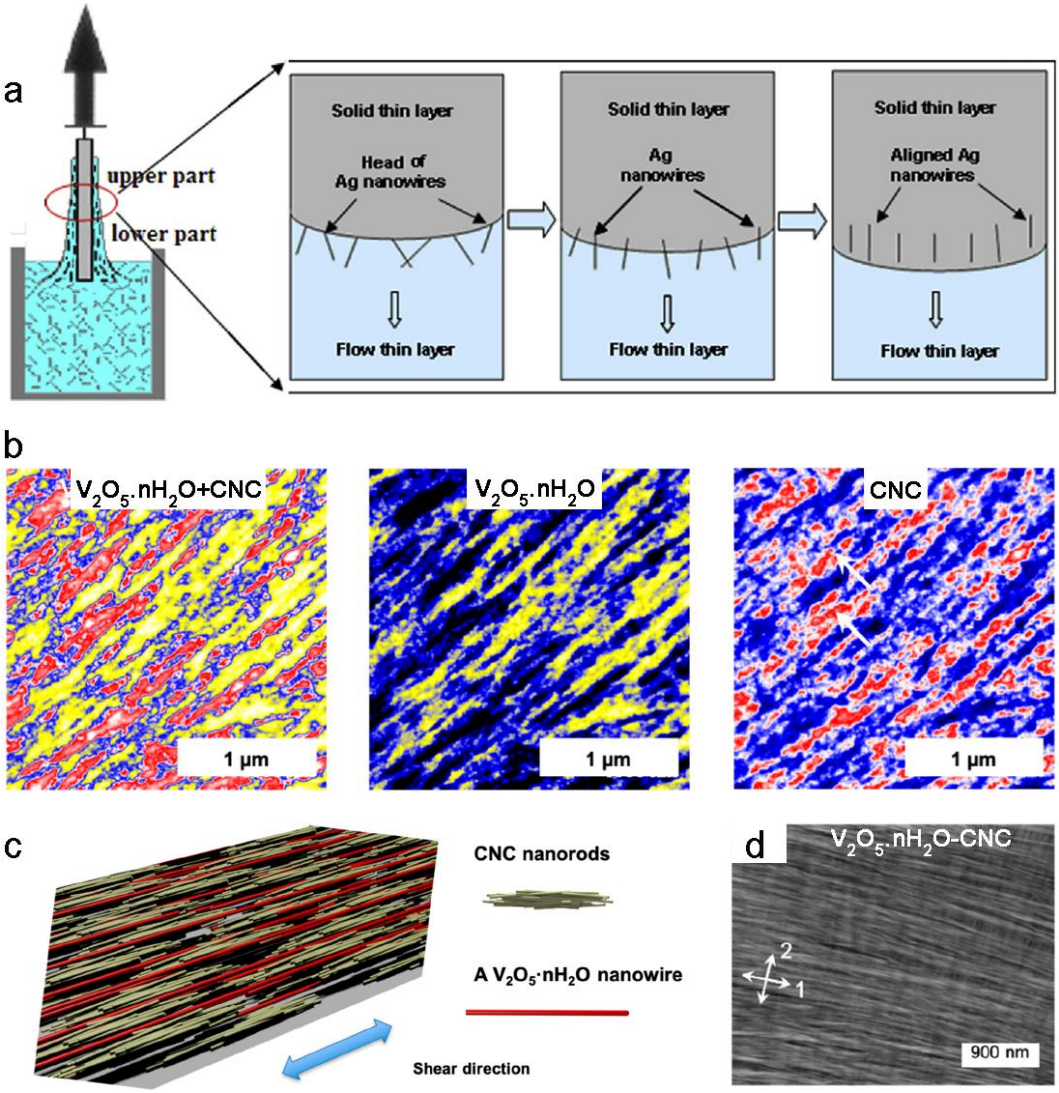

Fig. 13 (a) Schematic representation of the orientation mechanism of AgNWs by dip-coating (left). The upper end of AgNWs adheres to the solid thin layer, while the lower end of AgNWs still remains in the downward flowing thin liquid layer, which will orient the NWs along the flow direction. Reproduced with permission from ref. 178. Copyright 2018 Elsevier Inc. (b) s-SNOM maps of oriented $V_2O_5.nH_2O$ NW and CNC NR binary thin films, showing both $V_2O_5.nH_2O$ and CNC constituents in yellow and red, respectively. (c) Cartoon depicting the planar spatial distribution of both nanoobjects in the binary thin film. (d) SEM image of biaxial $V_2O_5.nH_2O$-CNC binary thin film after two-round dip-coating process, where the two lifting directions were perpendicular to each other. Reproduced with permission from ref. 179. Copyright 2018 American Chemical Society.

was further improved in the form of a "nanocombing" technique by Lieber and co-workers.[176] The NWs were anchored to defined areas of a surface and then drawn out over chemically distinct regions of the surface. Such technique yielded arrays with more than 98.5% of the NWs aligned within ± 1° of the combing (pulling) direction. Crossed NW arrays can also be defined by two consecutive combing steps.[176]

3.5 Dip-coating

Another simple and efficient technique for the alignment of 1D-nanoobjects at the solid-liquid interface is dip-coating. The substrate is directly pulled out from the 1D-nanooject suspension and the oriented assembly occurs at the solid-liquid-gas interface. The substrate moving speed, evaporation speed and viscosity of the solvent are thus the main parameters that control the alignment of 1D-nanoobjects. This technique offers the advantage of being suited for various 1D-nanoobjects and requires minimal material consumption.

Yang and co-workers reported for the first time this simple method for the alignment of various NWs on Si wafers with predefined spacing and tunable wire density.[177] Controlling the alignment of AgNWs on glass slides via this route was also recently reported.[178] When a glass substrate is pulled out from a AgNW suspension, the solution layer adhering to the glass substrate will undergo a transition from a directional flow regime to a stagnant condition during evaporation and the solution layer on the glass substrate can be separated as a lower and upper part (Fig. 13a). In the lower part the liquid is flowing downward along the glass substrate due to its own gravity, while the liquid is not moving anymore in the upper part because of the evaporation of the solvent to form a solid thin film.[178]

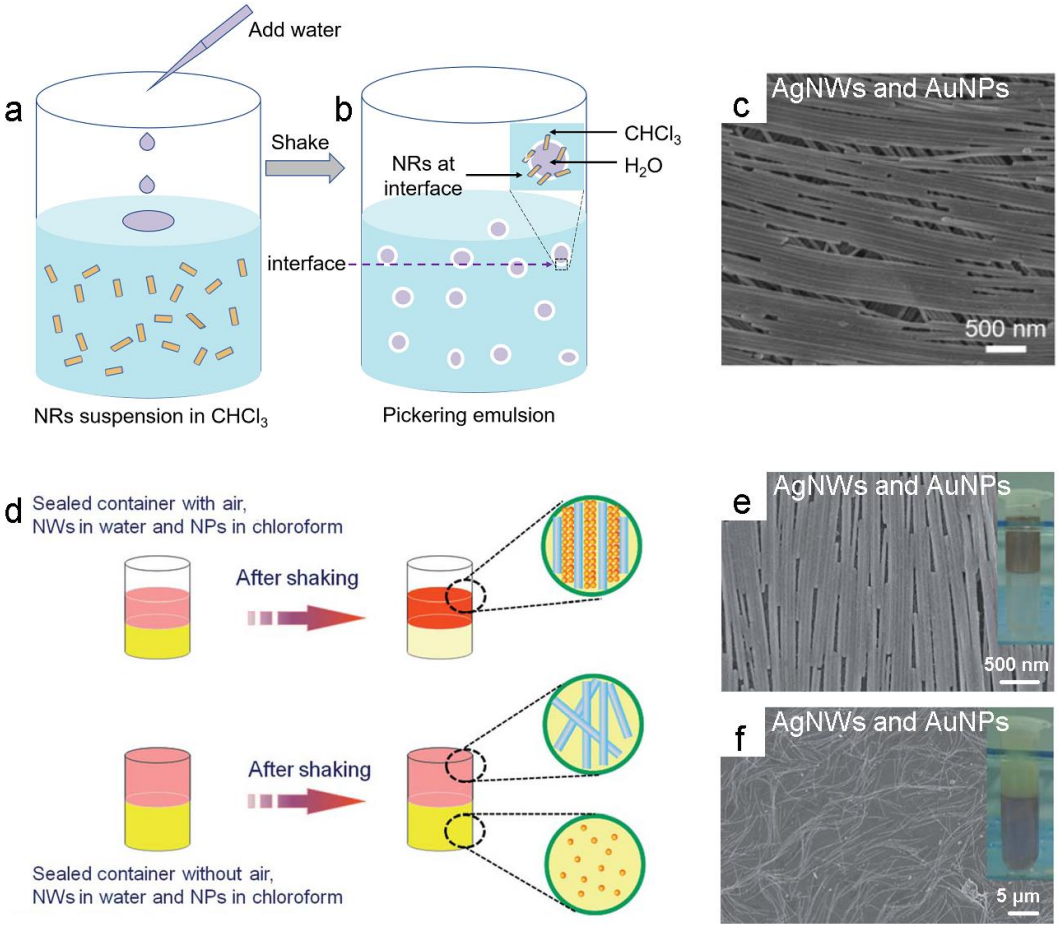

Fig. 14 (a-b) Schematic representation of the assembly at a liquid-liquid interface. Water is added to a NR suspension in chloroform (a), which forms a Pickering emulsion after vigorous shaking (b). (c) SEM image of co-assembled thin films with three layers of AgNWs and AuNPs. (d) Schematic illustration of the role of air in the liquid-liquid assembly process. (e) SEM image of co-assembled film formed by shaking 3 mL of a AgNW suspension (3 mM) and 3 mL of a AuNP suspension (0.8 mM) with 1 mL of air left in the centrifuge tube (Inset: photograph of the assembly results). (f) SEM image of the AgNW suspension: there was no film formed in the system of 3.5 mL of AgNW suspension (3 mM) and 3.5 mL of AuNP suspension (0.8 mM) without air left in the container (Inset: photograph of the assembly results). Reproduced from ref. 184 with permission from Royal Society of Chemistry.

The orientation of AgNWs occurs in the transition region, and the mechanism of alignment is quite similar to the one in the evaporation-induced assembly of a drying droplet on a flat substrate (section 3.3).[152] The upper end of AgNWs adheres to the solid thin layer, while the lower end of the AgNWs still remains in the flowing thin layer. Because of the weak friction between AgNWs and the glass substrate in the flowing thin layer, AgNWs will align along the liquid flow during dipping (Fig. 13a middle and right).[178]

Recently, Bai *et al.* also reported the coalignment of $V_2O_5.nH_2O$ NWs and cellulose nanocrystals (CNCs) by dip-coating.[179] Figure 13b shows scattering-type scanning near-field optical microscopy (s-SNOM) maps of the $V_2O_5.nH_2O$/CNC binary system (left), $V_2O_5.nH_2O$ system (middle, the wires appear in yellow) and CNC (right, the wires appear in red), respectively. It can be observed that the CNC nanorods were organized into ordered shuttle-shaped assemblies along the shearing direction instead of being spatially distributed as oriented individual particles. Furthermore, multiple CNCs are imbedded between adjacent $V_2O_5.nH_2O$ NWs in the binary $V_2O_5.nH_2O$-CNC thin film, and the alignment quality can be enhanced by CNCs as it served as effective, colloidal additives for the alignment of $V_2O_5.nH_2O$ NWs. This cooperative assembly of $V_2O_5.nH_2O$ NWs and CNCs, both cationic, on the other hand, occurred in far-from-equilibrium conditions. Fig. 13c shows the cartoon depicting the cooperative assembly of these two nanoobjects. Multilayered binary thin films with different orientations of the NWs in each layer can be readily fabricated by repeating this process (Fig. 13d).[179]

3.6 Assembly at liquid-liquid interfaces

Immiscible polar and apolar liquids tend to phase-separate, eventually forming an emulsion if droplets of one liquid are dispersed in the other one. Some nanoobjects can spontaneously assemble at this liquid-liquid interface and stabilize the small droplets, forming a so-called Pickering emulsion. This process is governed by minimization of the interfacial energy and may induce anisotropic nanoobjects to orient at the interface. Emrick and co-workers investigated the assembly of functionalized CdSe NRs at the oil (chloroform or toluene)/water interface.[180] The suspension of CdSe NRs in toluene or chloroform was violently shaken with water to yield a Pickering emulsion (Fig. 14a-b). By drawing such solution on a pre-patterned substrate, the aligned NR can be assembled on the solid

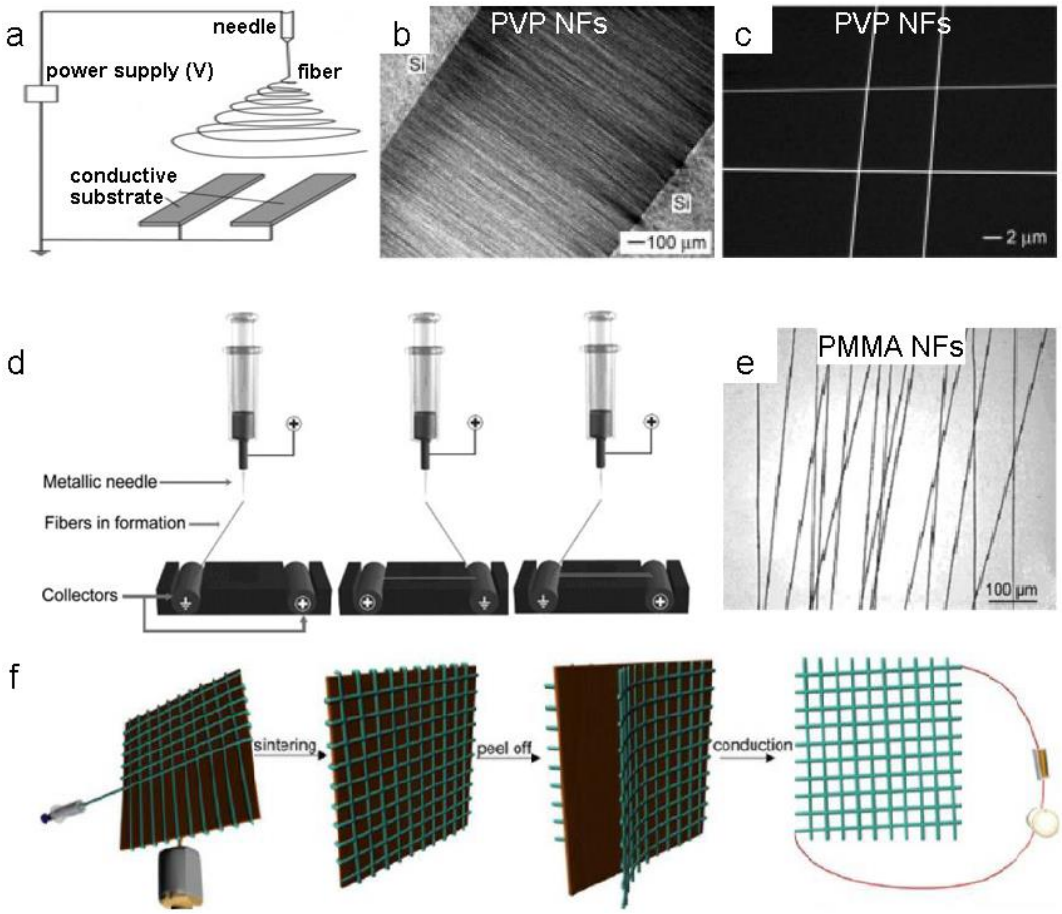

Fig. 15 (a) Schematic representation of the set-up used to electrospin nanofibers as uniaxially aligned arrays. The collector was composed of two conductive substrates separated by a void gap. (b) Optical micrograph of PVP NFs collected across a void gap between two Si strips. (c) SEM image of cross-aligned PVP NFs. Reproduced with permission from ref. 194. Copyright 2004 Wiley-VCH. (d) Schematic illustration of the alternating electric-field assisted electrospinning setup. (e) Optical image of oriented PMMA NFs. Reproduced with permission from ref. 209. Copyright 2008 Wiley-VCH. (f) Schematic of the continuous draw spinning of silver nanofiber arrays. Reproduced with permission from ref. 212. Copyright 2017 American Chemical Society.

surface.[181] The assembled droplets containing NRs were rinsed with toluene to remove excess NRs. The fluorescence confocal microscopy image of CdSe NRs stabilized droplets showed fluorescent circles at the toluene/water interface because of the intrinsic photoluminescence of CdSe NRs that accumulated at the interface.[180]

Yu and co-workers explored the influence of the nature of the oil phase to provide effective platforms for the rapid fabrication of large-area self-assembled nanofilms composed of various nanosized building blocks such as NPs, NWs, nanocubes and nanosheets. Various organic solvents can be used as the oil phase in the liquid/liquid interfacial systems.[182] In a previous study, the same group reported the alignment of AgNWs at an oil-water-air interface.[183]

This assembly method can also be used to fabricate multilayered architectures composed of nanoobjects with different shapes and sizes. Yu *et al.* fabricated co-assembled thin films composed of AgNWs and NPs at the liquid-liquid interface.[184] The AgNWs were suspended in water, and NPs including AuNPs, Ag_2S NPs and Fe_3O_4 NPs were suspended in $CHCl_3$. The obtained films can be deposited onto substrates by placing the substrate under the floating film and quickly lifting up. Multilayered films can be formed by a layer-by-layer transfer and the SEM image of co-assembled AgNWs and AuNPs multilayer thin films are shown in Fig. 14c.[184] It was found that air was a factor for this co-assembly process as illustrated in Fig. 14d. When the volume of AuNP solution, AgNW solution, and air was 3 mL, 3 mL and 1 mL, respectively, well defined co-assembled thin films can be obtained (Fig. 14e). If the air was evacuated from the container, no ordered film can be formed after shaking for a long time (Fig. 14f).[184]

3.7 Electrospinning

Electrospinning is a low-cost and effective method for preparing very fine polymer fibers from a solution.[185-193] The standard electrospinning setup usually consists of three parts: a syringe pump, a spinneret connected to high-voltage and a collector. Sol-gel mixtures, particulate suspensions, polymer solutions or melts are loaded into the syringe and pushed out from a needle by the syringe pump at a constant speed, with a high voltage applied between the needle and the collector. Fibers prepared by conventional electrospinning are randomly oriented, which limits the range of potential applications, especially in the fields of nanoelectronics and

nanophotonics where uniform structures as well as direct and fast charge transfers are needed. To solve this problem, various strategies have been developed, such as separating the collection electrodes,[194-198] using electric field assisted collection[188, 199-202] or magnetic field assisted collection,[203-208] alternating electric state between collectors[209] and rotating the collector.[210-212]

Xia *et al.* modified the conventional electrospinning procedure to align poly(vinyl pyrrolidone) NFs (PVP NFs) into uniaxially oriented arrays over large areas. An insulating gap with various width was used to separate conductive strips on the collector (Fig. 15a).[194] To fabricate this kind of collector, two parallel gold electrodes were placed on the insulator surface by thermal evaporation. It was found that the NFs were oriented and bridged the gap between the two electrodes (Fig.15b).[194] The conductivity of the supporting insulating substrate was the key factor for the orientation and it is worth mentioning that multilayered patterns can be formed by changing the orientation of the substrate (Fig. 15c).[194] Recently, Demir and co-workers electrospun aligned polyurethane fibers containing $CsPbBr_3$ NWs between the separating electrodes.[195] These oriented $CsPbBr_3$ NWs embedded in the electrospun fibers showed a high degree of polarization of the emitted light.[195]

Electric fields or magnetic fields can also be used to prepare oriented fibers. Wang *et al.* have deposited oriented TiO_2 NWs by electrospinning a titanium precursor and PVP solution and incorporating a laminar flow field with AC electric fields. The density of assembled TiO_2 NWs could be controlled by adjusting AC frequencies and flow rates.[202] Yu and co-workers oriented AgNWs with very high aspect ratio within PVP NFs by magnetic-field-assisted electrospinning.[203] The polymer NFs containing the AgNWs produced at the needle exit were influenced by the magnetic field of two magnets. In addition, more complex hierarchical architectures could be prepared by controlling the direction of the AgNWs loaded electrospun polymer fibers.[203]

Attout *et al.* formed aligned polyaniline (PANi) NFs by electrospinning polymer blends like PANi/PMMA (PMMA: polymethyl methacrylate) and PANi/PEO (PEO: polyethylene oxide) on two collectors, one of which was grounded while the other one was maintained at a high voltage. This electric state was alternated

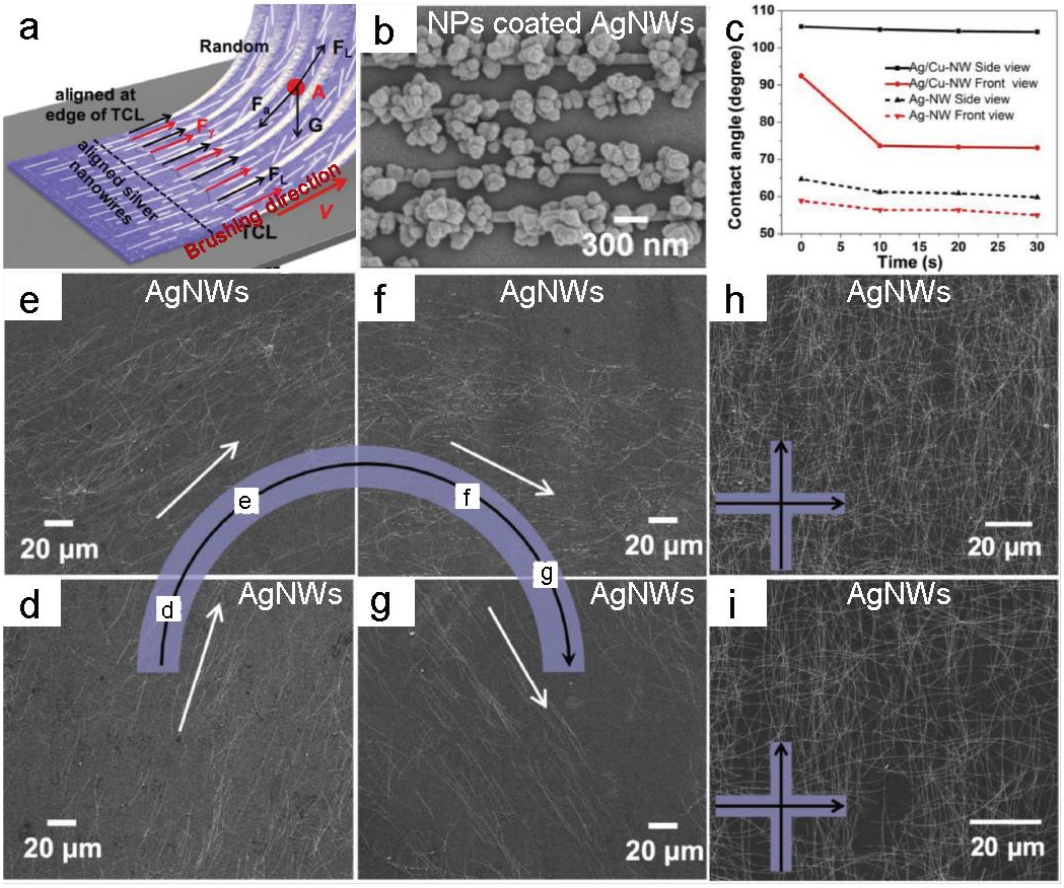

Fig. 16 (a) Schematic representation of the controllable transfer of AgNWs from a solution to the substrate by brush coating, where multiple TCL were formed. (b) SEM image of CuNPs electrodeposited on an oriented AgNW film serving as a template. (c) Contact angle as function of time after a drop of water is deposited on the aligned AgNW thin films (dashed line) and anisotropic Ag/Cu-NWs composite surfaces (solid line). The difference in the contact angle measured from side and front views proves the anisotropic wetting properties of the oriented thin films (d-g) AgNWs aligned in multiple directions in a single brushing step. Here, a semicircular pattern is painted on the substrate by brush coating, and the orientation of AgNWs varies at different locations along the single stroke when the brushing direction changes, as indicated by the black arrows. The SEM images at the locations d, e, f and g are shown in Figure 16d–g, respectively. (h-i) Cross-aligned AgNWs fabricated by repeating the brushing steps. Reproduced with permission from ref. 218. Copyright 2018 Wiley-VCH.

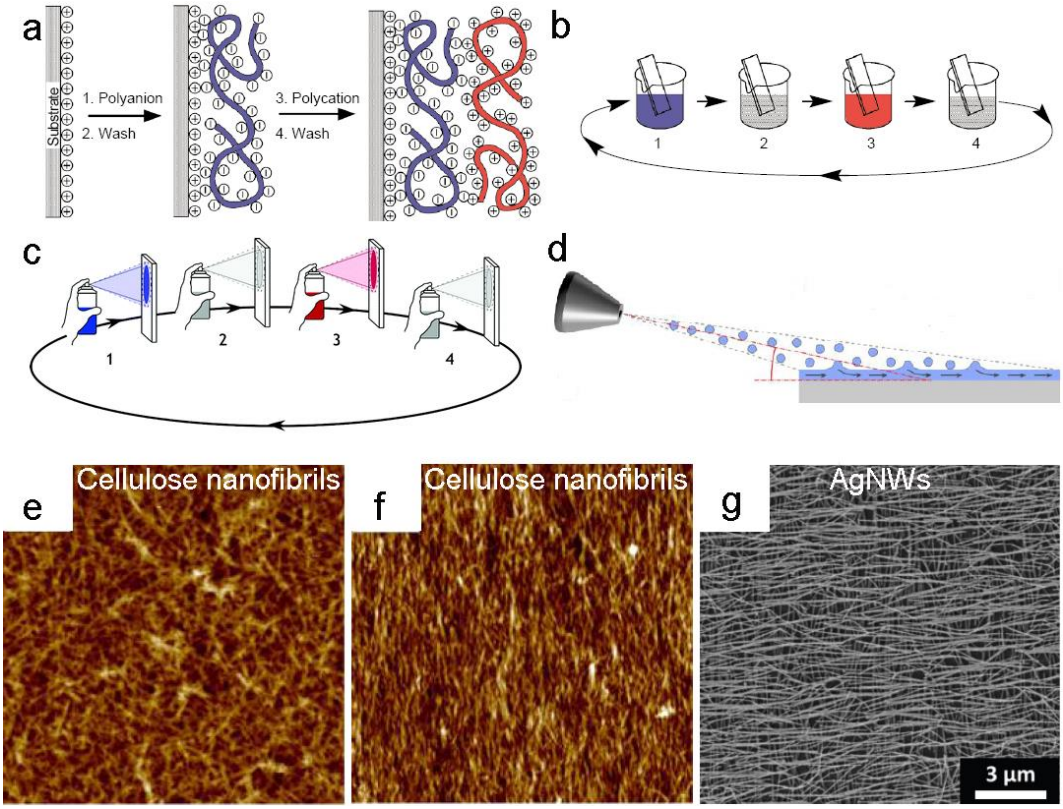

Fig. 17 (a) Simplified molecular picture of the first two deposition steps. (b) Schematic representation of Layer-by-Layer assembly by dipping. Steps 1 and 3 represent the adsorption of polyanion and polycation; steps 2 and 4 are rinsing steps. Reproduced with permission from ref. 219. Copyright 1997 The American Association for the Advancement of Science (AAAS). (c) Schematic representation of Layer-by-Layer assembly by orthogonal spraying. Reproduced with permission from ref. 225. Copyright 2005 American Chemical Society. (d) Schematic of Grazing-Incidence Spraying (GIS). (e) AFM image (2 × 2 µm^2) of cellulose nanofibrils deposited by orthogonal spraying. (f) AFM image (2 × 2 µm^2) of cellulose nanofibrils deposited by GIS. Reproduced with permission from ref. 230. Copyright 2017 American Chemical Society. (g) SEM image of a two-layered AgNW thin film in which the second layer is oriented perpendicularly to the first one. Reproduced from ref. 231 with permission from the Royal Society of Chemistry.

between the two collectors, which caused the charged polymer fiber leaving the needle to bounce from one collector to the other, leaving oriented fibers on the substrate (Fig. 15d). Figure 15e shows the oriented PMMA fibers obtained by this assembly process. PMMA and PEO were used to improve the viscosity and surface tension of PANi so that it can be turned into aligned NFs by electrospinning.[209]

Cross-aligned fibrous scaffolds can be prepared by electrospinning with a rotating collecting substrate. Recently, Wu and co-workers reported a continuous draw electrospinning process of extra-long silver submicron fibers from aqueous solution onto a rotating substrate with a maximum speed of 8 m/s. The fibers can be as long as several kilometers. Fig. 15f shows how the substrate is rotated for fabricating continuous oriented fibers. A small amount of the well-mixed silver nitrate-containing polymer solution was squeezed from the syringe. Oriented fibers could be continuously produced by regulating the rotation speed of the substrate and the flow rate of the solution. A cross-aligned fiber mesh can be obtained by changing the direction of the rotating substrate.[212] This spinning technique is used to fabricate scalable, flexible, ultralow-cost and large transparent conductive metal electrodes.[212]

3.8 Brush coating

Recently, Chinese brush (C-brush) has been introduced by Jiang's group to align polymer and AgNWs.[213-218] Unlike the western brush, C-brush is uniquely made of freshly emergent hairs (FE-hair) of animals which not only possess an anisotropic multiscale structure but also a unique tapered morphology which confines the liquid within the brush without leakage, resulting in a controlled unidirectional flow of the solution during deposition.[215-217] Highly oriented polymer or metal NW films can be fabricated due to the controlled wetting and dewetting under directional stress, where the advancing and receding of the liquid-gas-solid three-phase contact line (TCL) at the front edge of the liquid thin film is well controlled (Fig. 16a).[217, 218] AgNWs have been aligned with this coating technique on a soft poly(ethylene terephthalate) (PET) substrate, where the AgNWs were guided and aligned by the directional stress.[218] The oriented AgNW films showed a better conductivity along the brushing direction compared to that in the orthogonal direction. Copper NPs (CuNPs) were selectively deposited on the oriented AgNWs (Fig. 16b), resulting in a surface with an anisotropic wetting behavior (Fig. 16c). It is worth highlighting that this technique is the only approach able to align AgNWs in different directions in a single brushing step (Fig. 16d-g). Cross-aligned AgNWs can be fabricated by repeating the brushing steps (Fig. 16h-i).[218] This coating technique offers unique advantages to prepare highly

oriented organic and inorganic NWs using a small amount of solution with a simple setup.

3.9 Spray-assisted Layer-by-Layer assembly

Layer-by-Layer (LbL) assembly technique developed by Decher is an easy and versatile tool for fabricating complex architectures.[219-224] A simple description of the build-up of polyelectrolyte multilayers requires two oppositely charged polyelectrolytes (a polycation and a polyanion) and a charged substrate (Fig. 17a).[219] When a positively charged substrate is dipped into a polyanion solution, the polyanion chains adsorb on the substrate due to electrostatic interactions. The substrate is then rinsed with pure water to remove the weakly interacting polymer chains and dried. This process can be repeated in the polycation solution. After rinsing, one layer-pair of polyelectrolyte complex thin film is obtained. The process of alternate deposition of positively and negatively charged layers can be repeated to form multilayer thin film with controlled chemical composition and physical properties (Fig. 17b).[219] However, it takes a few minutes to build a single layer by dipping, and thus the preparation of thin films composed of a large number of layers can be long, and a spraying method was developed to facilitate the process (Fig. 17c).[225] Multifunctional thin films can easily be prepared by Layer-by-Layer assembly technique and can integrate a large range of organic and inorganic nanoobjects . To name a few, LbL films of spherical NPs,[226, 227] NRs[228] and NWs[229] have been reported. The components in each Layer and the sequence of layers can be controlled very straightforwardly with the LbL technique, and controlling the orientation of 1D-nanoobjects in each layer has been recently achieved.[230]

Indeed, Decher *et al.* recently introduced the Grazing-Incidence Spraying (GIS) approach for the orientation of 1D-nanoobjects (Fig. 17d) in which the 1D-nanoobject suspension was sprayed at a low angle (5-20°) on a receiving substrate.[230] Cellulose nanofibrils were randomly oriented if the spraying was done orthogonal to the substrate (Fig. 17e), but GIS resulted in nanofibril thin films with substantial in-plane orientation (Fig. 17f).[230] The orientational order depended on the spraying conditions such as spraying direction, inclination angle of the spray jet, speed and density of the spray droplets, flowing distance and location on the receiving surface.[230] AgNWs were oriented by this GIS technique, and the in-plane orientation of each AgNW layer can be varied by simply changing the spraying direction, resulting in three-dimensional (3D) architectures with complex and tunable anisotropies (Fig. 17g).[231]

As the 1D-nanoobjects were oriented mainly due to the shear force of the flowing liquid in GIS, the aspect ratio of the nanoobject played a very important role, and it was found that longer AuNRs gave better alignment than shorter nanorods (Fig. 18a).[232] The GIS orientation of AgNWs on a wrinkled substrate was also reported by the same group. The in-plane spraying angle φ between the wrinkle and spraying directions was varied (Fig. 18b), and it was shown that wrinkled substrates could enhance the degree of orientation and coverage when the spraying direction was parallel to the wrinkles (Fig. 18c).[233] On the contrary, when the suspension was sprayed perpendicular to the wrinkles, the opposing effects of the substrate-induced alignment along the wrinkles and the spray-induced shear forces perpendicular to the wrinkles led to films with different orientations as function of the distance from the nozzle. AgNWs deposited near the impact point of the spray jet were mainly

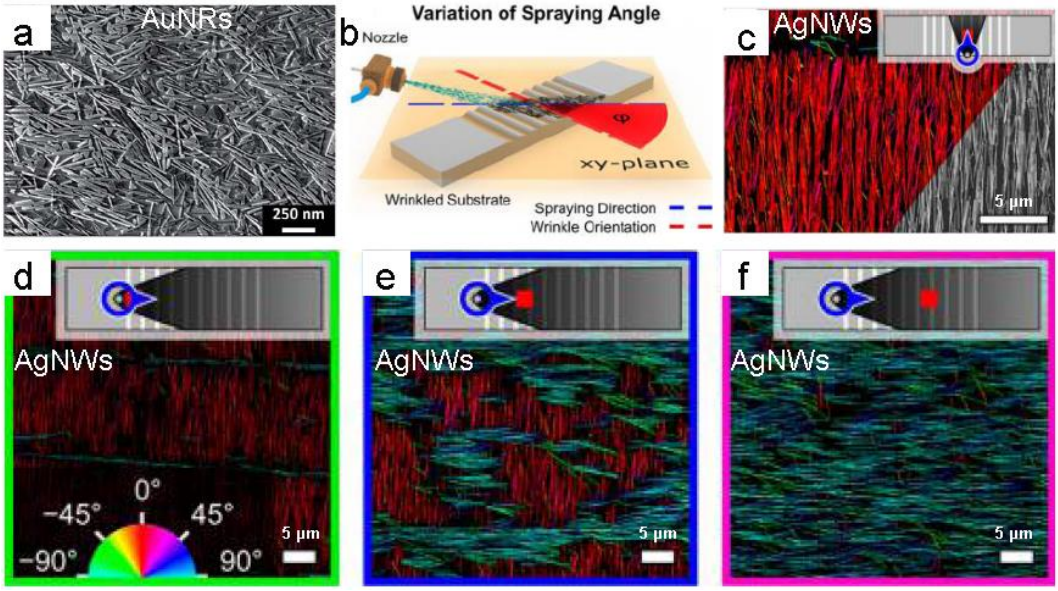

Fig. 18 (a) SEM picture of oriented long AuNRs. Reproduced from ref. 232 with permission from the Royal Society of Chemistry. (b) Schematic illustration of wrinkle-assisted GIS build-up. (c) SEM image of an oriented AgNW film sprayed on a wrinkled substrate. (d-f) Position-dependent SEM images of a AgNW film sprayed at $\varphi = 90^{o}$: (d): impact point; (e): 5 mm away from the impact point; (f): 10 mm away from the impact point. The images are color-coded according to the NW orientation (the color scale is given as an inset in panel (d). Reproduced with permission from ref. 233. Copyright 2018 American Chemical Society.

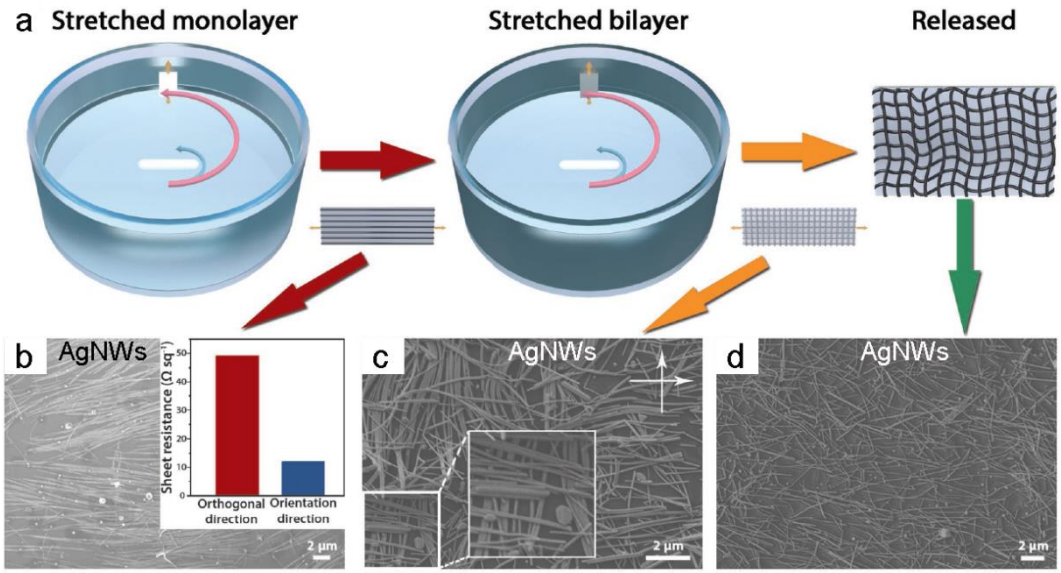

Fig. 19 (a) Schematic illustration of the layer-by-layer agitation-assisted alignment. The AgNW thin films show a cross-aligned nanostructure in the stretched state and an entangled oriented structure in the released state. (b) SEM image of the AgNWs assembled in a monolayer (Inset: sheet resistance measured in the orientation direction and in the orthogonal direction). (c) SEM image of the cross-aligned structure in the stretched state. (d) SEM image of the sample in the released state. Reproduced with permission from ref. 235. Copyright 2019 Wiley-VCH.

oriented along the wrinkles, at intermediate positions on the substrate approximately half of the AgNWs aligned along the wrinkles and the rest aligned along the spraying direction, while 10 mm away from the impact point, almost all the AgNWs were oriented along the spraying direction (Fig. 18d-f).[233]

3.10 Agitation-assisted Layer-by-Layer alignment

1D-nanoobjects can also be aligned by agitation-assisted alignment.[234, 235] Long and co-workers for the first time applied this approach to layer-by-layer deposit AgNWs onto pre-strained flexible substrates to fabricate highly stretchable electrodes based on oriented NWs.[235] In this report, the substrate was placed in the NW suspension, and a magnetic stirrer was used to generate a liquid flow (Fig. 19a left). The alignment mainly depended on the viscosity of the solvent, agitation speed and the coating time and under optimal conditions the majority of the AgNWs were oriented along the same direction as the liquid flow due to its shear force (Fig. 19b). The monolayer aligned AgNW thin film showed anisotropic sheet resistance (Fig. 19b insert). By simply rotating the pre-strained substrate and repeating the assembly process (Fig. 19a middle), a "mesh-like" nanostructure can be fabricated (Fig. 19c), and a released mesh (Fig. 19a right) can give a final more entangled structure (Fig. 19d). This approach has the advantages of facile fabrication set up, large-area ordered nanostructures and no restrictions on substrates.

3.11 Fluidic flow

In the 19th century, logs were flown from forests to sawmills downstream using the current of rivers. As the floating logs did orient along the river flow, this old technique for transporting timbers is an inspiration for developing flow-based methods to orient 1D-nanoobjects.[133] If a suspension of 1D-nanoobjects flows along designed geometrical channels, the shear force and the constrained movement of the 1D-nanoobjects within the channels will make the 1D-nanoobjects to orient along the flow direction.[236, 237] The earliest work in this domain was reported by Lieber and co-workers.[236] Gallium phosphide (GaP), indium phosphide (InP), and SiNW suspensions were passed through fluidic channels with various widths and lengths and aligned along the flow direction (Fig. 20a-b). The flow rate played an important role in the orientation degree and the NW density could be tuned by changing the flow duration. Complex crossed NW arrays can be obtained by layer-by-layer assembly of NWs with different flow directions (Fig. 20c).

Capillary tubes offer a confined space and curved surface which can be applied to direct the assembly of 1D-nanoobjects.[238-240] Wang and co-workers reported the fabrication of assembled structures that resulted from drying a solution of tobacco mosaic virus (TMV) rods in a capillary tube.[239] The TMV concentration, salt concentration in aqueous solution, and property of the capillary inner surface were the three key factors that govern the self-assembly process.[239] Following the same principle, they used a capillary flow to align various 1D-nanoobjects through a glass tube (Fig. 20d) by feeding different solutions, including AuNRs, bacteriophage M13 and TMV. The AFM image and illustration of TMV are shown in Fig. 20e and f respectively.[240] The alignment and coverage of the nanoobjects can be adjusted by changing the flow rate and nanoobjects concentration. In general, better ordering can be achieved when 1D-nanoobjects with higher aspect ratio were used under higher flow rate and higher

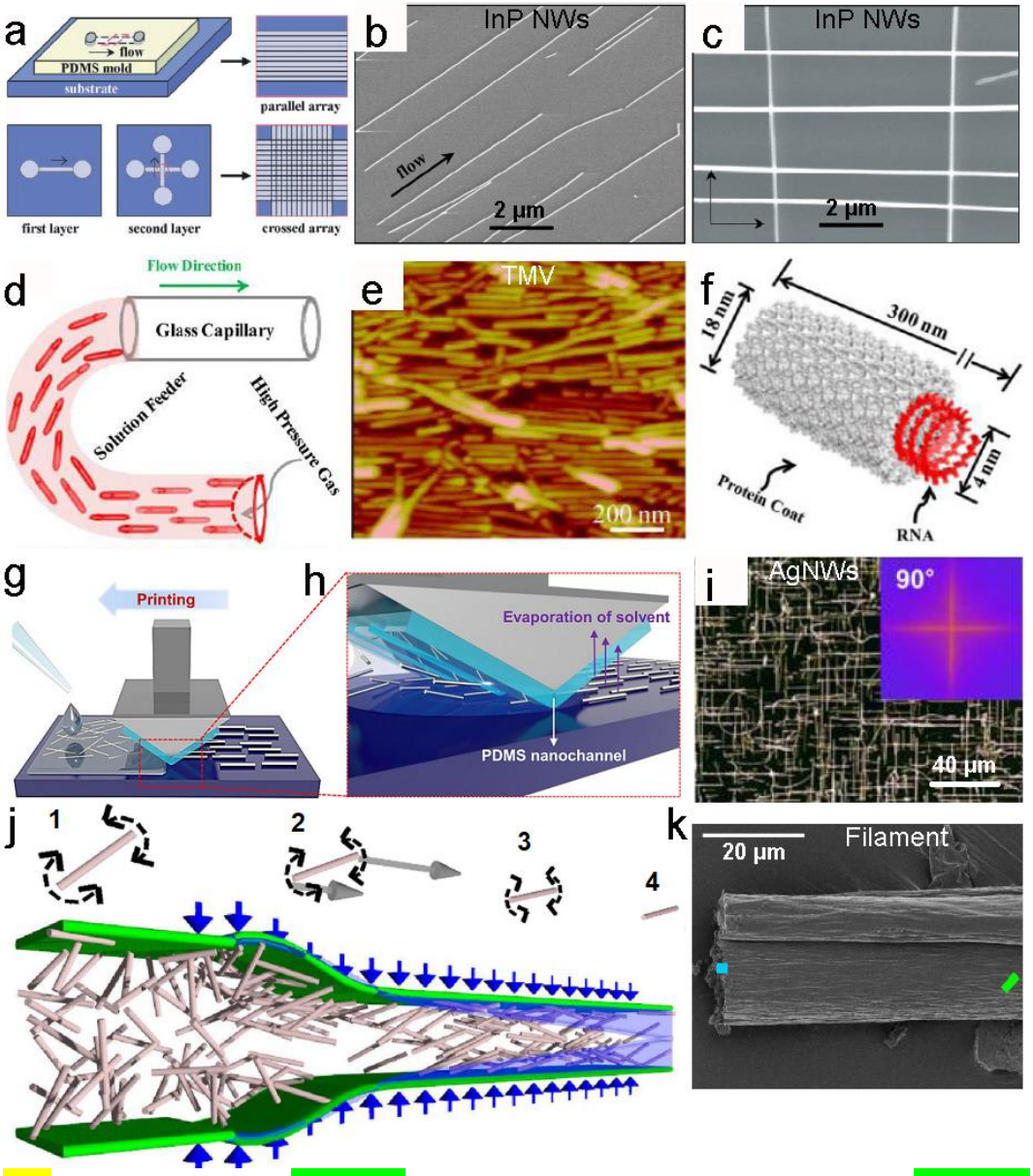

Fig. 20 (a) Schematic representation of fluidic channels used for the orientation of NWs. (b) SEM image of oriented InP NWs using the fluidic channels. (c) SEM image of crossed arrays of InP NWs aligned by the fluidic flow. Reproduced with permission from ref. 236. Copyright 2001 The American Association for the Advancement of Science (AAAS). (d) Schematic of the experimental setup for capillary flowing. (e) AFM image of TMV oriented by capillary flow. (f) Structure illustration of TMV, which has a shape of a hollow cylinder (18 nm in diameter, 300 nm in length, and 4 nm cavity). Reproduced with permission from ref. 240. Copyright 2013 American Chemical Society. (g-h) Schematic representation of the capillary printing process using a nanopatterned PDMS stamp to produce highly aligned NW arrays. (i) Dark-field optical images of crossed oriented AgNW structures fabricated by multistep capillary printing. Reproduced with permission from ref. 241. Copyright 2015 American Chemical Society. (j) Illustration of the hydrodynamically-induced assembly process. (k) SEM image of a filament prepared from assembled nanofibrils. Reproduced with permission from ref. 242. Copyright 2014 Nature.

concentration. These ordered structures can further guide the cell growth and control the cell orientation and morphology,[240] which will be elaborated in section 4.3.

Recently, Kang *et al.* reported the orientation of AgNWs by capillary printing.[241] This technique involved dragging nanopatterned PDMS stamps on a NW suspension under constant velocity and pressure (Fig. 20g-h). A nanopatterned PDMS stamp with 400 nm nanochannels was attached to a trigonal prismatic frame, and the sharp peak of the PDMS stamp was contacted with the substrate during the dragging of AgNW solutions. This technique not only generated unidirectionally oriented NWs but also enabled the fabrication of crossed oriented AgNW arrays with different angles by repeating the printing process without interference of the prealigned layer of AgNW (Fig. 20i).[241]

Lundell et al. developed a process combining mechanical fluidic flow alignment with an electrochemical dispersion–gel transition to fabricate homogeneous filaments from a low-concentration of cellulose nanofibrils in water.[242] The fibrils were aligned in the dispersion followed by inducing a controlled gel transition (Fig. 20j). In the liquid dispersion, due to strong electrostatic repulsion, fibrils

were free to rotate (1). An added accelerating flow (2) aligned the fibrils in the flow direction (3). By diffusing an electrolyre in the suspension, the electrostatic repulsion between the fibrils was reduced before the alignment was lost due to Brownian diffusion, which freezed the aligned structures and formed a smooth gel (4) (Fig. 20k).[242]

The orienting power of fluidic flow has been further exploited to align a large variety of nanoobjects, e.g., the capillary separation of colloidal nanoobjects,[243] capillary flow orientation of AgNWs,[244, 245] CdS NWs[246] and DNA molecules,[247] the flow alignment of AgNWs,[248, 249] or of V_2O_5 NWs,[250] the hydro-tweezers flow orientation of AgNWs[251] and the horizontal-dip flow orientation of AgNWs.[252]

To summarize, a large variety of approaches, often based on the use of directional flow-induced shear forces, have been described for the oriented assembly of diverse 1D building blocks. The density of deposited nano-objects and the quality of alignment usually strongly depend on the processing parameters. The methods presented in this section can all be repeated to build multilayer architectures with complex morphologies, in particular multilayer thin films in which each layer can be oriented in a different direction. Such complex thin films can be further integrated in nanodevices with advanced functional properties, which will be the topic of the following section.

4. Applications of films composed of oriented 1D-nanoobjects

More and more applications require materials in which the physical properties vary in different directions of space or in which the materials properties are enhanced by a specific alignment in comparison to an isotropic system. A great example for the latter case arises from the criss-cross alignment of long conducting nanowires which allows to maintain a strongly conducting percolation network at reduced densities of nanowires which allows for increased translucency of transparent electrodes. Consequently, in-plane anisotropic layers containing 1D-nanoobjects are used for example in electronic devices, environmental sensors, biological and plasmonic applications, Surface-Enhanced Ramon Scattering (SERS) and some energy saving and generation applications.

4.1 Fabrication of electronic devices

Various electronic devices can be prepared from the well-assembled NWs structures.[124, 176, 197, 235, 253-265] Yu and his co-workers have summarized the recent progress about the NW assemblies for electronic devices.[266] Based on this review, we extend some more published in recent years to cover the most emerging applications in flexible and stretchable transparent conductors,[235, 260, 261] field-effect transistors (FETs),[176, 197] electronic skin (E-skin) and strain sensors,[262-264] and touch screens.[265]

4.1.1 Flexible and stretchable transparent electrodes. Metal NWs are candidates for integration in new generation electronic devices because of their high electrical conductivity and the anisotropy of the conductive properties which can be almost one order of magnitude higher in the NW alignment direction as compared to the direction perpendicular to the axis of orientation (Fig. 19b).[235]

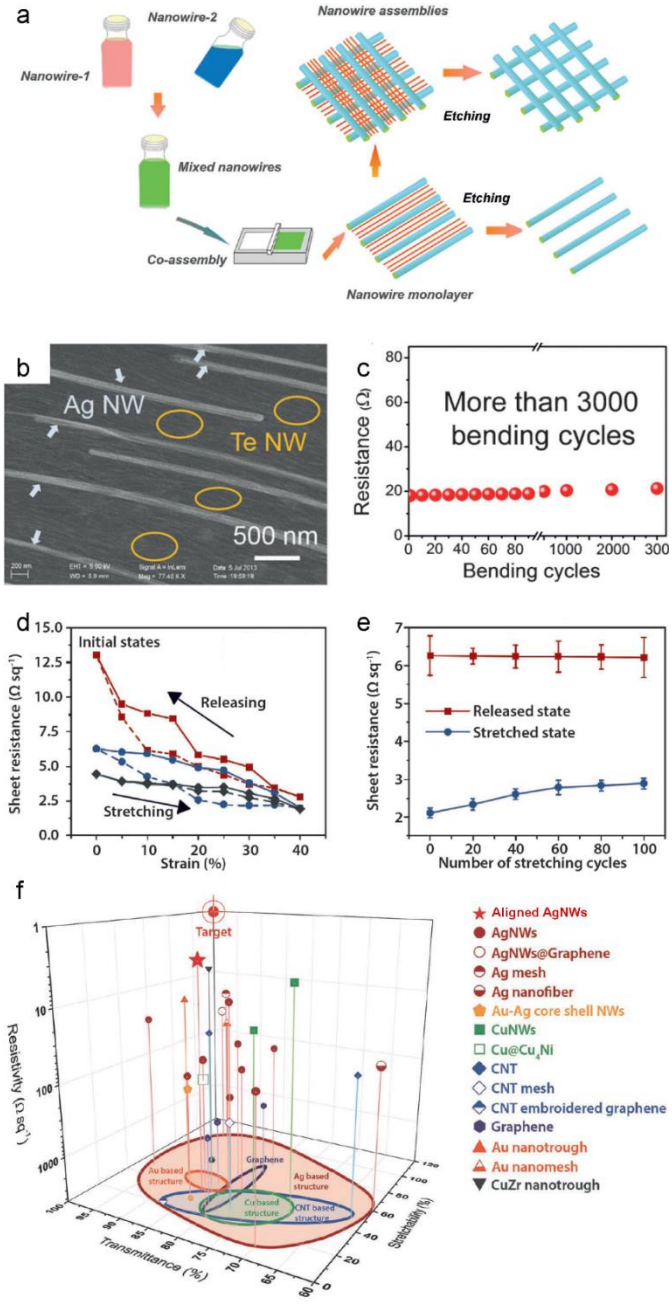

Fig. 21 (a) Schematic illustration of NW co-assembly for making flexible transparent electrodes. (b) SEM image of co-assembled monolayers of Ag and Te NWs. (c) Electrical resistance as a function of the bending cycles at a maximum bending radius of 2.0 mm. Reproduced with permission from ref. 261. Copyright 2014 Wiley-VCH. (d) The conductivity of the highly stretchable electrodes based on aligned AgNWs at different strains. (e) Sheet resistance of the electrode at the released state and stretched state as a function of the number of cycles of stretching for 40%. (f) Comparison of sheet resistance, stretchability and optical transmittance at 550 nm of aligned AgNWs electrodes with other reported electrodes. Reproduced with permission from ref. 235. Copyright 2019 Wiley-VCH.

When the metal NWs are aligned in criss-cross superstructures, they can be used to make transparent electrodes with excellent transparency and conductivity. Yu *et al.* co-assembled two kinds of NWs (Te and Ag NWs) for the fabrication of flexible electrodes (Fig. 21a).[261] Fig. 21b shows the SEM image of monolayer of AgNWs and TeNWs co-assemblies. The TeNWs were applied as sacrificial component to keep special distance between every adjacent AgNWs,

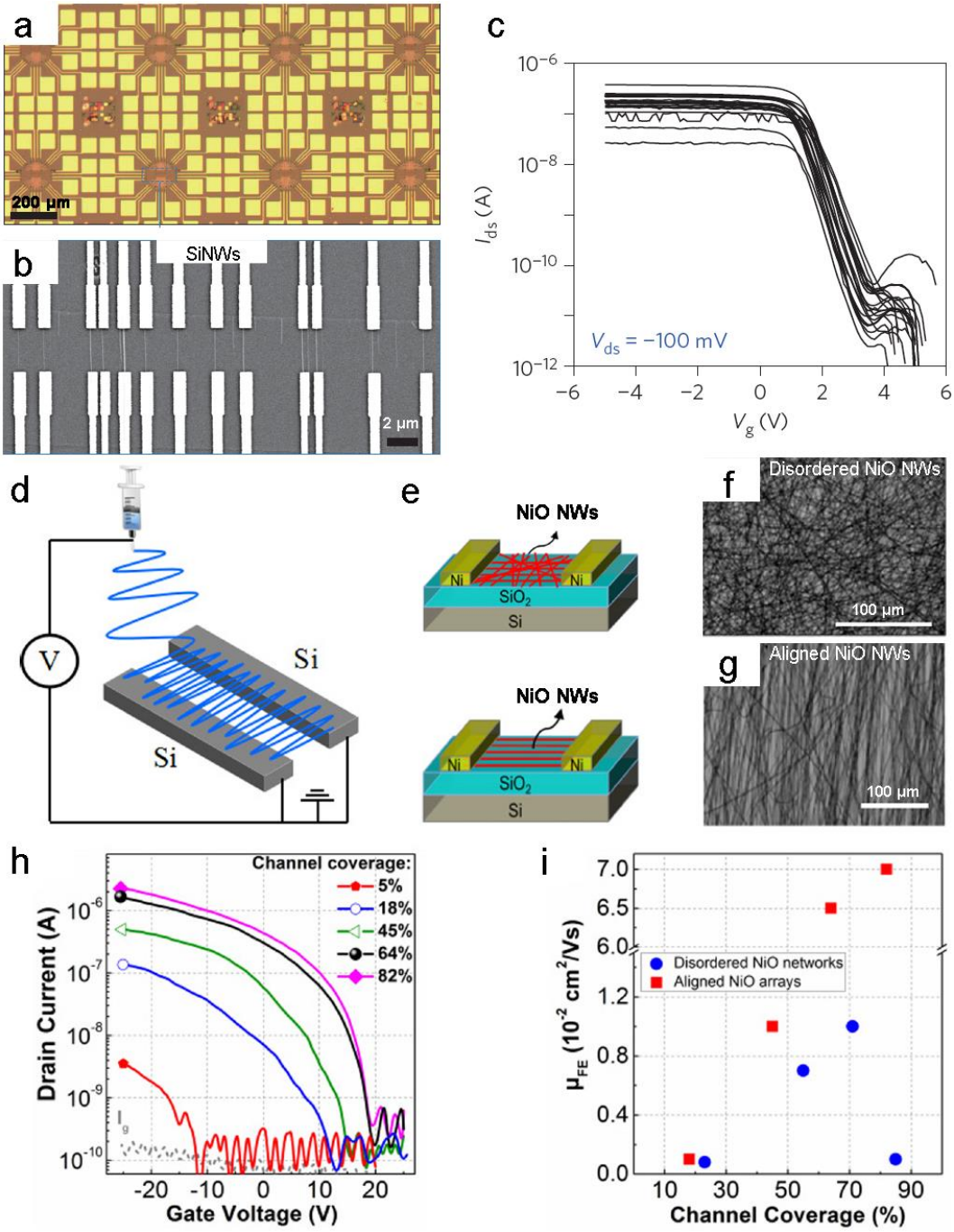

Fig. 22 (a) Optical image of the NW device arrays connecting to electrode arrays. (b) SEM image of the device arrays. (c) I_{ds}-V_g characteristics (V_{ds} = 0.1 V) from 20 top-gated Ge/Si core-shell NW devices oriented by nanocombing. Reproduced with permission from ref. 176. Copyright 2013 Nature. (d) Schematic of the aligned electrospinning process. (e) The FET structure with disordered NiO NWs (upper) and aligned NiO NWs (lower). (f-g) Optical microscopy image of disordered (f) and aligned NiO NWs network (g). (h) The transfer characteristics of the FETs based on aligned NiO NWs with different channel coverages (V_{DS} = 20 V). (i) The variation of μ_{FE} values for the FETs based on disordered and aligned NiO NWs with different channel coverage. Reproduced with permission from ref. 197. Copyright 2018 American Chemical Society.

leaving AgNW networks with controllable pitch. These flexible and transparent electrodes showed an averaged transparency of up to 97.3% and sheet resistance as low as 2.7 Ω sq^{-1}, while maintaining high conductivity after more than 3000 bending cycles (Fig. 21c) or even after they were twisted in water or ethanol.[261] Duan *et al.* prepared hierarchically oriented AgNW electrodes with a water-bath assisted assembly.[260] The electrodes based on 2 orthogonal layers of AgNWs had a sheet resistance of 11.4 Ω/sq and an optical transparency of 89.9% at 550 nm.[260] Long and co-workers fabricated the highly stretchable transparent electrodes based on the cross-aligned AgNWs (Fabrication part presented in section 3.10).[235] Contrary to most other reports, such devices showed higher conductivity at the stretched state compared to the released state as the alignment was done during the stretched state (Fig. 21d). After 100 stretch-release cycles, the conductivity of the electrode remained almost the same at the released state, and the sheet

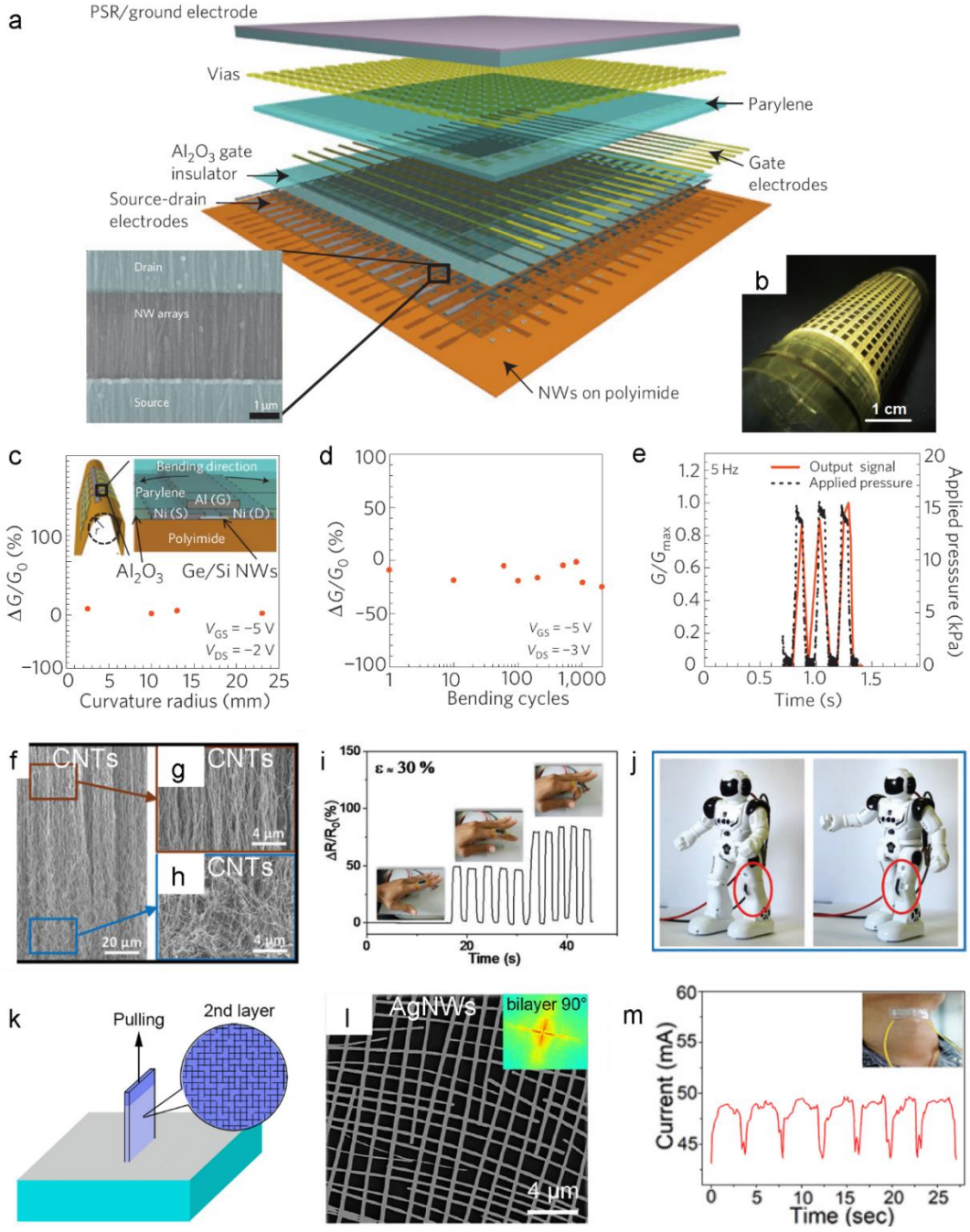

Fig. 23 (a) Schematic of the passive and active layers of NW e-skin (insert: SEM of a NW array). (b) Optical photographs of an e-skin device under rolling condition. (c-d) Mechanical testing of integrated pressure-sensor devices. (c) The normalized conductance change, $\Delta G/G_o$, of a representative pixel at different curvature radii, The insets illustrate the device structure and bending orientation used in the experiments. (d) $\Delta G/G_o$ as a function of mechanical bending cycles, demonstrating the mechanical robustness of the device with minimal performance degradation even after 2,000 bending cycles of bending and relaxing. (e) Time-resolved measurements of the output signal for an applied pressure frequency of 5 Hz. Reproduced with permission from ref. 262. Copyright 2010 Nature. (f) SEM image of gradient CNTs. (g) SEM image of anisotropic part of gradient CNTs. (h) SEM image of isotropic part of the gradient CNTs. (i) The relative resistance change of CNTs strain sensors under different finger motions. (j) Photograph of CNTs strain sensors mounted on the "knee" of a robot. Reproduced from ref. 263 with permission from Royal Society of Chemistry. (k) Schematic illustration of fabrication of sensitive and transparent sensor by the dip-coating technique. (l) SEM of cross-aligned AgNWs. (m) Repeatability testing and application of the transparent sensor for swallowing detection. Reproduced with permission from ref. 264. Copyright 2019 Nature.

resistance at the stretched state increased slightly (Fig. 21e). Such electrodes exhibited a significantly lower sheet resistance, higher or comparable transparency and stretchability than other materials systems such as CNT, graphene, Au, CuZr etc summarized in Fig. 21f.[235]

4.1.2 FETs. FETs are one group of electronic devices for which the assembly of NWs is explored. Lieber *et al.* fabricated single-NW FETs with the nanocombing technique (Fabrication part presented in section 3.4).[176] Photolithography was used to define a periodic array of electrodes around each block of oriented NWs (Fig. 22a), and the

individual NWs were then connected by electron-beam lithography (Fig. 22b). A large number of individual NW devices were available within each block, which was achieved thanks to the excellent NW orientation and end-to-end registration. Using such approach, single-NW FETs can be fabricated from core-shell Ge/Si NWs with a high yield of ~ 90% and with a very high reproducibility. Fig. 22c shows the drain current (I_{ds}) versus gate-voltage (V_g) data from 20 representative devices which demonstrated that the individual nanowire FETs have reproducible behavior as the I_{ds}-V_g curves were almost the same.[176] Shan and co-workers for the first time demonstrated the low-voltage FETs based on *p*-type oxide NWs.[197] For the fabrication of aligned arrays, two parallel conducting Si strips were grounded as collector (Fig. 22d). Fig. 22e shows the models of the devices with disordered (upper) and aligned (lower) NiO NW network. Fig. 22f-g are optical microscopy images of the disordered (Fig. 22f) and aligned (Fig. 22g) NiO NWs with comparable NW coverage. To explore the charge transport properties of the obtained NiO NWs, the NW networks with different channel coverage were assembled into FETs by changing the NW collection time (NW density) during the electrospinning process.[197] Fig. 22h shows the (I_{ds}-V_g) of the aligned NiO NW FETs with different channel coverage, the electrical properties of the FETs were improved with higher channel coverage. The field-effect mobilities (μ_{FE}) of the FETs based on disordered or aligned NiO NWs with different channel coverage are shown in Fig. 22i and the integrated FETs based on oriented NWs exhibited superior electrical performance.[197] Manners and co-workers also fabricated the FETs from fiber-like micelles with controlled length assembly from π-conjugated copolymers containing regioregular P3HT core and a solubilizing regiosymmetric P3HT or PS corona.[267] The fibers were subsequently incorporated as the active layer in FETs. The resulting charge carrier mobilities were highly dependent on both the degree of polymerization of core-form block and the fiber length, and was independent of corona composition.[267]

4.1.3 E-skins and strain sensors. The assembly of 1D-nanoobjects can be helpful for making so-called "electronic skins" (E-skins) and strain sensors. Javey *et al.* demonstrated macroscale (7 × 7 cm^2) integration of parallel NW arrays as the active-matrix backplane of a flexible pressure-sensor array (18 × 19 pixels).[262] Ge/Si core/shell NW arrays were contact printed on a polyimide substrate followed by device fabrication process (Fig. 23a). Fig. 23a insert presents the SEM image of the NW array. Fig. 23b is the optical photograph of a fully fabricated e-skin device (7 × 7 cm^2 with a 19 × 18 pixel array) under rolling. This integrated sensor array can be effectively applied as an artificial electronic skin, capable of monitoring applied pressure profiles at a low operating voltage of less than 5 V and showed excellent mechanical robustness and reliability, without performance degradation on bending to small radii of curvature (2.5 mm) for more than 2,000 bending cycles (Fig. 23c-d).[262] $\Delta G/G_o$ is used as an index to test the performance, where G and G_o are the conductance for the bent and relaxed states respectively and ΔG is the difference between the two. This e-skin device demonstrated the fast and deterministic response as they are still responsive without a significant signal degradation up to 5 Hz (Fig. 23e).[262]

Gui and co-worker fabricated highly stretchable and sensitive strain sensor based on CNTs.[263] By integrating randomly oriented and well aligned CNTs, acting as sensitive and stretchable conductive elements, respectively, into a continuous changing structure (Fig. 23f-h), these strain sensors showed very high sensitivity (gauge factor (GF) = 13.5), ultra-stretchability (> 550%), fast response speed (< 33 ms) and recovery speed (< 60 ms) and lossless detection of a 8 Hz mechanical signal.[263] The gauge factor is the ratio of the relative change in electrical resistance R, to the mechanical strain ε. In addition, the gradient CNTs strain sensors also showed great durability in a dynamic test of 12 000 cycles, as well as extraordinary linearity and ultra-low working voltage (10 mV). These sensors can be mounted on knuckles to monitor the finger motions (Fig. 23i), it can even be applied to digitize every motion of robots (Fig. 23j).[263] Recently, Yin *et al*. reported the alignment of ordered AgNW array via the dip-coating technique (Fig. 23k) for fabricating of transparent sensors based on cross-aligned AgNWs (Fig. 23l).[264] These sensors

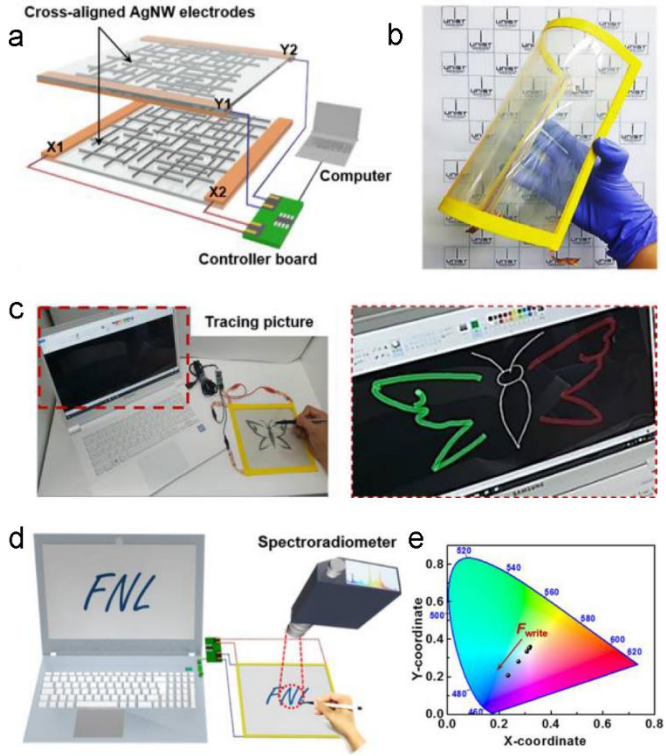

Fig. 24 (a) Schematic representation of the large-area touch screen fabricated with the cross-aligned AgNWs. (b) Photograph of the large-area touch screen. (c) Demonstration of tracing a butterfly picture located below the touch screen. (d) Schematic illustration of the mechanochromic touch screen system with the color analysis using a spectroradiometer. (e) Representation of the color coordinates on the CIE 1931 color space according to the different writing force. Reproduced with permission from ref. 265. Copyright 2017 American Chemical Society.

represented a considerable breakthrough in both sensitivity and transparency, giving maximum transmittance of 86.3% at a wavelength of 550 nm and the maximum GF as high as 84.6 at a strain of 30%. These flexible sensors have stable and reliable response to motion capture and human body signals such as swallowing detections (Fig. 23m).[264]

4.1.4 Touch screens. Ko and co-workers demonstrated a large-area, flexible, and transparent touch screen based on a four-wire resistive-

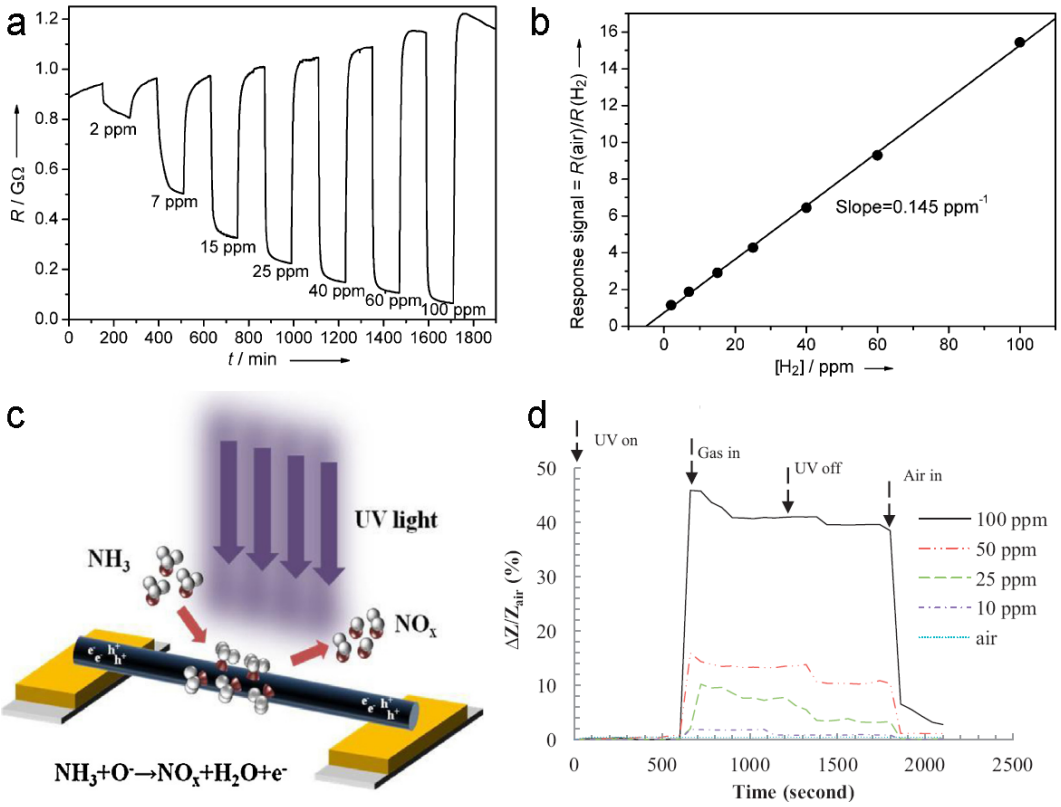

Fig. 25 (a) Changes of resistance and (b) response signal of an oriented $W_{18}O_{49}$ NW thin film (10 layers) as function of different H_2 concentrations at room temperature in synthetic air with 50% relative humidity as carrier gas. Reproduced with permission from ref. 269. Copyright 2015 Wiley-VCH. (c) Schematic illustration of the self-regenerating photocatalytic sensor based on assembled TiO_2 NWs for chemical vapor sensing. (d) Dynamic response and recovery of the sensor to NH_3 vapor with different concentrations. Reproduced with permission from ref. 202. Copyright 2014 Elsevier Inc.

type touch screen using cross-aligned AgNWs transparent conductive electrodes as the top and bottom transparent electrodes.[265] When a voltage was applied across *X* or *Y* layers between *X*1-*X*2 and *Y*1-*Y*2 busbars, the other touching layer can divide the applied voltage and the voltage change at the touch position was captured by a controller circuit board (Fig. 24a). Fig. 24b shows the flexible and transparent touch screen based on AgNWs that had an active area of 20 × 20 cm^2. This device was demonstrated to trace a picture of a butterfly below the transparent touch screen (Fig. 24c).[265] This touch screen also enabled the detection of intensity of force during writing by the change in color of mechanochromic force sensor, which was analyzed by the spectroradiometer (Fig. 24d). The degree of color change can be analyzed by standard colorimetric system CIE 1931. Fig. 24e shows the average color coordinated of letters "FNL" with different applied forces, where *X*-*Y* coordinates move to the deep blue region with increasing force.[265]

4.2 Environmental sensors

Chemical detectors (e.g. for the detection of various gases) or photodetectors (e.g. for UV or IR light) are important for numerous applications in chemical detection or environmental monitoring. Recently, metal NWs have been paid wide attention in sensing applications due to their 1D geometry, high surface to volume ratio and high crystallinity.[268] Compared to sensors made of single NWs or randomly oriented NWs, sensors composed of oriented NWs have shown a higher sensitivity, reproducibility and mechanical stability.

For example, Niederberger *et al.* oriented high aspect ratio Tungsten Oxide ($W_{18}O_{49}$) NWs with the LB technique (section 3.1) onto metallic electrodes and used these patterned substrates as devices for sensing H_2.[269] The performance of the device was investigated by measuring the resistance changes of the thin films composed of different layers of oriented $W_{18}O_{49}$ upon exposure to different concentrations of H_2 at ambient conditions. It was found that the devices should have at least 3 layers of $W_{18}O_{49}$ thin films; otherwise, there was no sensitivity for detecting H_2. Moreover, the sensor with the highest sensitivity and the best baseline stability was composed of 10 oriented $W_{18}0_{49}$ NW layers, with which the signal (resistance) increased as concentration in H_2 increased from 2 to 100 ppm (Fig. 25a) and the calculated response signal $R_{(air)}/R_{(H2)}$ gave a linear relationship with increasing H_2 concentration (Fig. 25b). The sensor also showed high repeatability over nine sensing cycles.[269]

Wang *et al.* assembled TiO_2 NWs between two electrodes for the detection of chemical vapors including NH_3, acetone and ethanol.[202] The working principle of the vapor sensors is shown in Fig. 25c. The length of the two coplanar electrodes and the distance in between were 40 µm and 10 µm, respectively. The glass substrate was firstly coated with titanium followed by gold to enhance the glass-gold bonding. The electrode pattern was fabricated by photolithography approaches.[202] When UV light was absent, the impedance of the sensor didn't exhibit any detectable change of NH_3 with concentration varying from 10-100 ppm due to the low electron and holes densities of TiO_2 NWs at room temperature. Under UV

irradiation, TiO_2 acts as a photocatalyst which can be used for detecting NH_3 in a sensor geometry in which TiO_2 NWs bridge two electrodes (Fig. 25c). The impedance ($\Delta Z/Z_{air}$) of assembled TiO_2 NWs increased in the presence of NH_3 (Fig. 25d) indicating the decrease of carrier density of TiO_2 NWs. However, when the air was purged into the detection chamber, the impedance of the sensor was returned to the initial value. The limit of detection (LoD) of the fabricated TiO_2 NWs sensor to ammonia gas was also investigated. As decreasing NH_3 concentration the impedance of TiO_2 NWs under UV light decreased. The plotted impedance change as a function of NH_3 concentration suggested a linear response range from 10 ppm to 100 ppm. A LoD of 10 ppm was thus deduced.[202] Note that a gas sensor based on crystalline $Cu_{2-x}Se$ NW bundles was also reported.[270]

4.3 Biological applications

As already mentioned in section 3.8, aligned AgNWs are able to act as templates for directing nanoparticle growth. Some oriented 1D-nanoobjects can even enhance the differentiation and orientation of cells, which could be interesting for engineering functional tissues with anisotropic properties. For example, in native musculoskeletal tissue, the myoblasts form aligned fibers in a highly ordered manner through the fusion into the multinucleated myotubes. The capillary flow (fabrication details in section 3.11) assembled 1D nanoobjects has been applied to guide the orientation a differentiation of C2C12 myoblasts.[240] Four kinds of oriented capillaries, TMVH, TMVL, RGDH and RGDL, were prepared for cell studies. The letter H stands for high coverage and L for low coverage of aligned 1D-nanoobjects on the

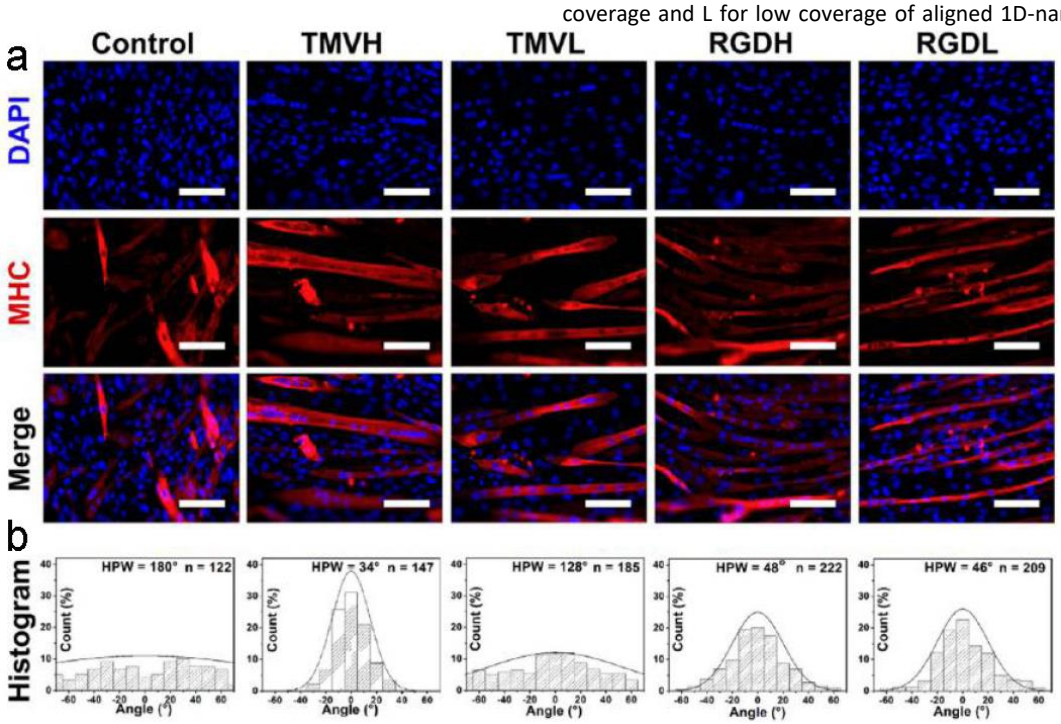

Fig. 26 (a) Fluorescent image of the C2C12 cells with the induction of differentiation for 7 days on the tubes with different nanoobjects TMVH, TMVL, RGDH and RGDL (scale bar: 100 μm). (b) Histograms of the angular distribution of myotubes. Reproduced with permission from ref. 240. Copyright 2013 American Chemical Society

The aligned NWs assemblies can be applied to detect the light. Shen *et al.* aligned Zn_3P_2 NW arrays on both rigid SiO_2/Si substrates and flexible PET substrates by contact printing (section 3.4).[165] For both the rigid substrates and flexible substrates, the oriented NWs showed an intense response to the visible and ultraviolet light with different wavelength. The photocurrent decreased with decreased light intensities.[165] Song and co-workers oriented organolead iodide perovskite (OIP) NWs by evaporation-induced assembly (section 3.3). The resulting NW arrays could be used as photodetectors.[271] These devices absorbed more than 90% of the light from UV to the whole visible region, and they showed an excellent photodetector performance. The current changed reversibly and quickly when alternating dark and illuminated states and the ratio I_{light}/I_{dark} can be as high as 23.[271] Furthermore, the detectivity and the response speed can reach 2.5×10^{12} Jones and 0.3 ms.[271] In addition, nondestructive transparent photosensors,[272] UV light detectors[273, 274] and near-infrared photodetectors[275] were also reported.

functionalized capillary tubes, and random capillary tubes were used as the control. RGD is the mutant TMV with inserted sequence GRGDSPG which can enhance cell attachment and stimulate osteogenic differentiation. There was no obvious difference in the cells attachment to substrates observed overnight.[240] Fig. 26a presents the fluorescence images of the cells with myosin heavy chain (MHC) (red) and DAPI (blue) staining on different substrates after 7 days cultured in differentiation medium (DM). The appearance of MHC staining indicated the formation of the myotubes in all groups. The TMVH showed the best alignment, and the RGDH and RGDL showed the moderate alignment; RGDH was a little higher than RGDL. The TMVL seldom displayed alignment, while there was no alignment in the random TMV coated surface as analyzed by the histograms of angular distributions of myotubes (Fig. 26b). The low degree of the alignment in TMVL mainly due to low density of TMV which was insufficient to guide the C2C12 cells. However, the low density of RGD was still able to guide the

orientation of cells due to the strong binding motifs, RGD peptides, for C2C12 cells.[240]

4.4 Plasmonic applications

Recently, Fontana *et al.* fabricated dynamic plasmonic pixels for controlling light by the electric-field-induced alignment of plasmonic NRs in organic solvents.[67] The pixel was composed of a suspension of NRs orientable by electric fields (Fig. 27d-e). Backlit by a white light

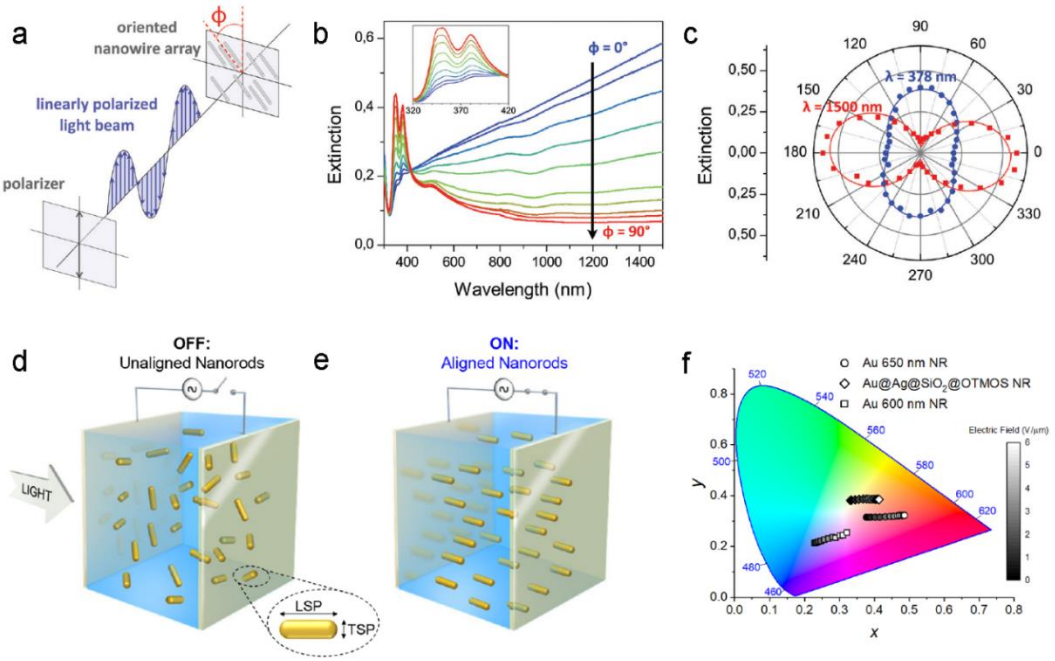

Fig. 27 (a) Schematic illustration of the polarized UV-Vis-NIR measurement. (b) UV-Vis-NIR spectra of the aligned AgNW thin film measured at different polarization angles with respect to the NW orientation. (c) Polar plot of the extinction at 378 nm and 1500 nm of an aligned AgNW thin film as a function of the polarization angle. Reproduced from ref. 231 with permission from the Royal Society of Chemistry. (d-e) Schematic depiction of the dynamic plasmonic pixel when the applied electric field is OFF (unaligned) and ON (aligned). (f) CIE 1931 *x,y* chromaticity coordinates for three different NR suspensions. Reproduced with permission from ref. 67. Copyright 2019 American Chemical Society.

Well-oriented metallic NW thin films can show interesting optical properties because of their anisotropic characteristic and the strong electromagnetic fields arising between adjacent NWs upon excitation of the plasmon modes. Such oriented plasmonic thin films could find applications in nanoplasmonics or polarizers.[276] The GIS oriented AgNW thin films showed that the UV-Vis-NIR extinction spectra of the film were dependent on the angle between the polarization direction of the incident light and the alignment direction (Fabrication part presented in section 3.9) (Fig. 27a), which highlighted their macroscopic anisotropic optical properties.[231] When the polarization is parallel to the long axis of the NWs, the longitudinal surface plasmon (LSP) is excited; whereas the transverse surface plasmon (TSP) is excited when the polarization is perpendicular to the long axis (Fig. 27b). The transmittance of light through aligned AgNW thin films is thus highly polarization- and wavelength-dependent (Fig. 27c), and such thin films can thus be used as wavelength-dependent polarizers. Multilayered AgNWs thin films being oriented in the same direction exhibited similar optical properties. The polarization efficiency increased dramatically with the number of AgNW layers. For monolayered AgNW thin film, the polarization efficiencies were 31% at 347 nm and -57% at 1500 nm, while for 4-layered sample, the polarization efficiency can reach to 92% and -97% in the UV and near IR region, respectively.[231] Wrinkle-assisted aligned AuNRs also showed similar anisotropic optical properties.[91]

illuminant, each nanorod suspension transmitted a different distribution of visible light wavelengths. The light modulation crossed a significant portion of visible and infrared spectrum (600-2400 nm) can be achieved by tuning the geometry and composition (Au and Au@Ag) of the nanorods. The AuNRs were labeled according to their LSPs: for example, the LSPs of “Au 650 nm NR” and “Au 600 nm NR” were at 650 nm and 600 nm, respectively. The Au@Ag@SiO_2@OTMOS NR meant the AuNRs coated with Ag, SiO_2, and functionalized with OTMOS. When the NRs were aligned, the resulting modulation of the spectrum was manifested as a distinct change in the observed color and brightness of the light passing through the NR suspension.[67] Fig. 27f presents the color rendering properties of the NRs that quantified according to colorimetric system CIE 1931. In each case, when the LSP mode was suppressed upon alignment, more red light was transmitted through the NR suspensions, and the chromaticity moved toward the red region of the diagram. The greater transmission of light was further exhibited as an increase in luminance.[67]

4.5 Surface-Enhanced Raman Scattering (SERS)

Raman scattering is a common analysis tool based on inelastic light scattering due to the excitation of vibrational modes but it is an inherently extremely inefficient process. The Raman scattering cross-section can be strongly enhanced when the analytic molecules are located near a nanostructured metal surface, thereby many efforts

have been dedicated to the design of substrates with engineered nanostructures to increase the sensitivity of Raman scattering, leading to a technique named Surface-Enhanced Raman Scattering (SERS).[277] In particular, the density and nature of the so-called "hot spots" that appear in the gap between two adjacent plasmonic nanoparticles can be conveniently engineered in thin films of oriented 1D-nanoobjects. Such NW SERS substrates have several advantages: highly reproducible fabrication, wide range of compounds to be detected and flexible working environments either in solution or in atmosphere.

acid (4-MBA) and R6G, which demonstrated that it could be served as a versatile platform to probe mixture pollutions (Fig. 28c).[244] Jiang *et al.* developed a simple method for fabricating SERS substrates with designed enhancement mechanisms.[278] The LB assembled AgNW thin films were further modified with a galvanic replacement reaction (GRR). As the GRR can reduce the noise produced by the PVP coating, these SERS substrates were more sensitive to non-fluorescent probe molecules as well as more selective to molecules with a strong binding affinity to AgNWs. The GRR LB substrates showed very high SERS sensitivity in the detection of 4-

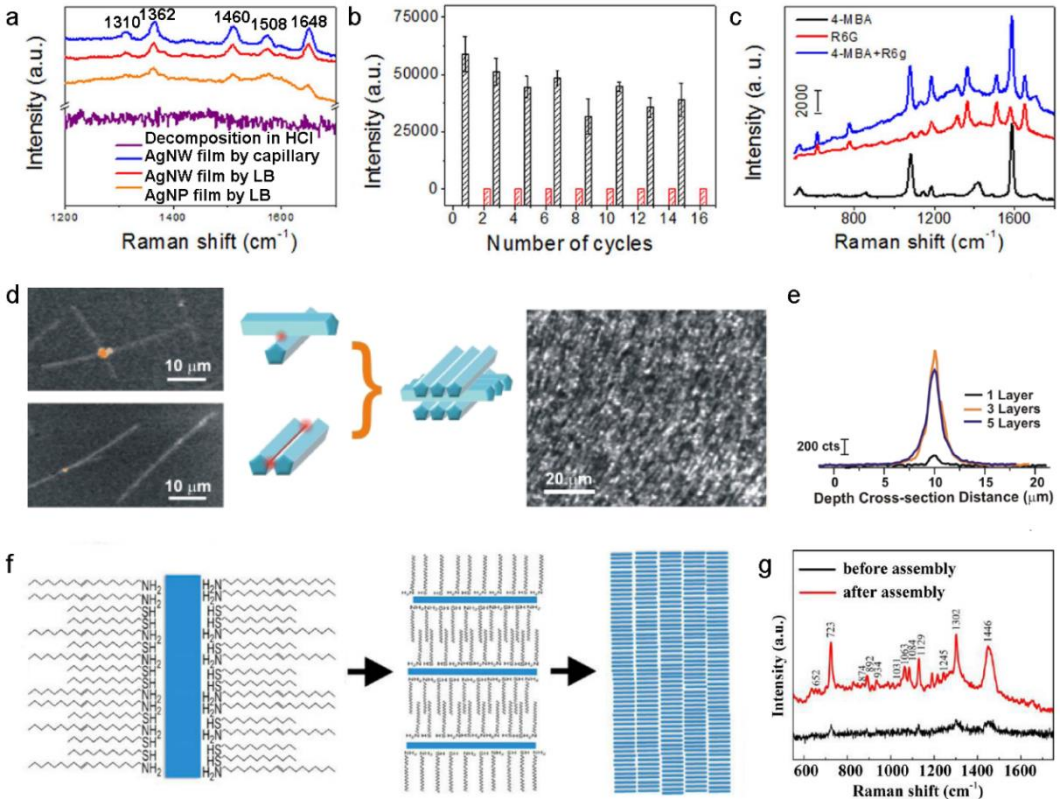

Fig. 28 (a) SERS spectra of thin films with NPs/NWs assembled by different techniques. (b) Cyclic measurement of the reusable capillary SERS substrate before (black bar) and after (red bar) dispersed into the concentrated HCl solution. (c) SERS spectra of the substrate adsorbed R6G, 4-MBA, and a mixture of R6G and 4-MBA. Reproduced with permission from ref. 244. Copyright 2012 Nature. (d) Scheme of crossed and parallel AgNWs structures for high density "hot spots" (e) Depth intensity profile of AgNWs from 1 layer to 5 layers. Reproduced with permission from ref. 280. Copyright 2013 American Chemical Society. (f) Schematic assembly mechanism of Cu_7Te_5 NRs. (g) SERS spectra of Cu_7Te_5 NRs (before assembly) and the superstructures (after assembly). Reproduced with permission from ref. 281. Copyright 2016 American Chemical Society.

Yang *et al.* prepared oriented AgNWs thin films by the Langmuir-Blodgett method, which can be used as excellent SERS substrates for sensing thiol-2,4-dinitrotoluene and Rhodamine 6G (R6G) with large enhancement factors.[126] Liu *et al.* fabricated SERS substrates by aligning AgNWs with glass capillary or LB technique and AgNPs were used as a reference.[244] This SERS sensor can be used cyclically by simply immersing it in the concentrated hydrogen chloride (HCl) acid to remove the residual R6G. It was found that both AgNW showed higher Raman enhancement than AgNPs while the capillary oriented AgNW thin film outperformed the LB technique device (Fig. 28a). The detection limit of capillary oriented AgNW thin film for sensing the R6G can be as low as 5×10^{-9} M. Fig. 28b shows that the cycle test of SERS substrate after repetitive washing in HCl. Moreover, the AgNW thin film can be used to detect the mixture of 4-Mercaptobenzoic

aminothiophenol with a detection limit as low as 8 nM, which may attribute to the strong chemical binding between the probe molecules and SERS substrate.[278] Wang *et al.* prepared SERS substrates based on assembled AgNWs for sensing the toxic arsenic (As) in drinking water with single digit ppb sensitivity.[279]

Besides the monolayer NW thin films, multilayered assembled NW films can also be used as SERS substrates. For example, Ling *et al.* fabricated 3D woodpile-like structures containing a high density of "hot spots".[280] In order to obtain a SERS substrate with a homogeneous intensity distribution, the electromagnetic coupling between alternating perpendicular layers of AgNW in the 3D woodpile structure was optimized to reach a high density of hot spots arising from the vertical and lateral gaps in the woodpile layers

(Fig. 28d).[280] The SERS enhancement factor increased with the number of assembled Ag NW layers from 1 layer to 3 layers but decreased when the number reached to 5 (Fig. 28e). In addition, these 3D structures were not sensitive to sample orientation and laser illumination, making them versatile for various applications.[280] Recently, Zheng *et al.* reported superstructure assemblies composed of Cu_7Te_5 NRs for SERS application.[281] The oleylamine (OLA)/n-dodecanethiol (DDT) mixture as a binary capping agent was a prerequisite for the hierarchical self-assembly of Cu_7Te_5 NRs. The Cu_7Te_5 NRs were first side-by-side assembled into 1D NWs perpendicular to the longitude axis of the NR because of the synergistic capping of OLA and DDT, which were then side-by-side aligned parallel to the NR longitude direction into two-dimensional (2D) NW bundles (Fig. 28f). These NW bundles were further rolled up to 3D superstructures. These Cu_7Te_5 superstructures exhibited much stronger SERS enhancement compared to the individual Cu_7Te_5 NRs, which may be due to the enhanced local electromagnetic field in the well-aligned architectures (Fig. 28g).[281]

4.6 Application in energy saving and generation devices

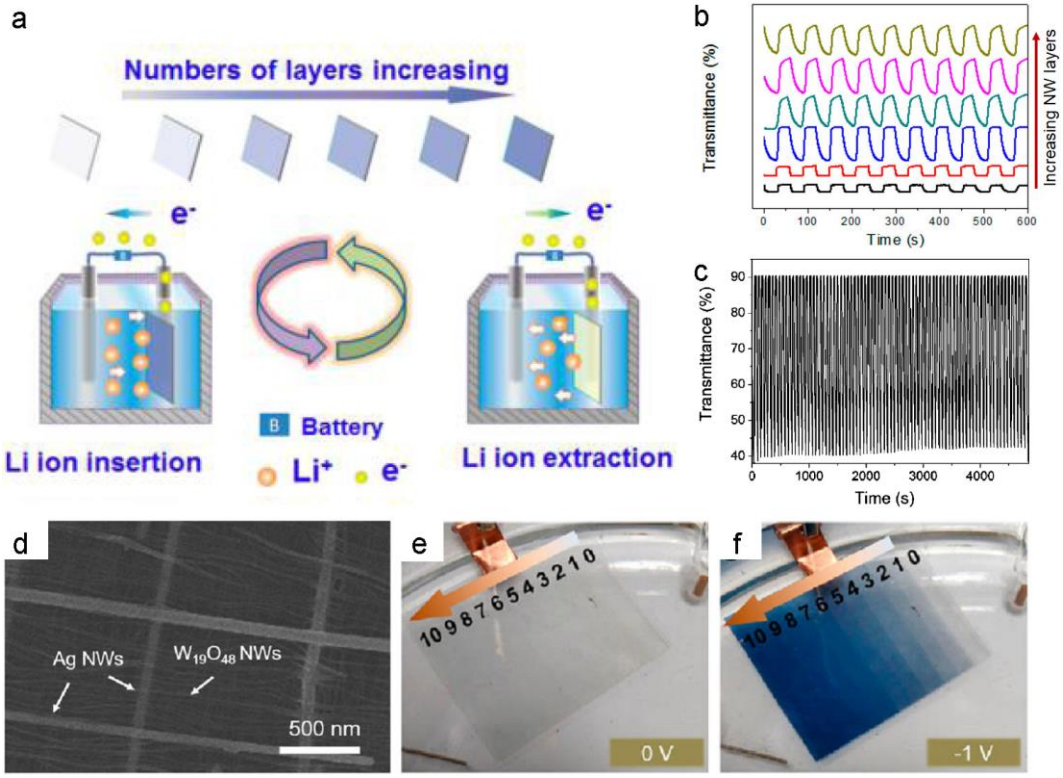

Fig. 29 (a) Schematic illustration of reversible electrochromic $W_{18}O_{49}$ NWs thin film devices. (b) Electrochromic switching of the different layers of aligned $W_{18}O_{49}$ NWs thin film devices, the transmittance change of the devices increase with the film thickness (NW layers). (c) Stability of electrochromic switching of the $W_{18}O_{49}$ NWs thin films. Reproduced with permission from ref. 286. Copyright 2013 American Chemical Society. (d) SEM image of the co-assembled Ag/$W_{18}O_{49}$ NWs networks on the PET substrate. (e-f) Optical graphs of the thin film device prior and after applied with an external voltage. Reproduced with permission from ref. 287. Copyright 2017 American Chemical Society.

4.6.1 Smart windows. Windows are the least energy efficient parts of a building and smart windows are considered the most effective way to improve the energy balance in the housing sector.[282] Thermochromic[283, 284] and electrochromic windows are considered as two promising technologies for reducing the cost of energy for heating or cooling. Electrochromism[285] is a color change induced by a reversible electrochemical process, here tungsten oxide has attracted attention due to its interesting electrochromic properties.[285]

Yu *et al.* fabricated ordered $W_{18}O_{49}$ NW thin films with the LB technique (section 3.1), the well oriented $W_{18}O_{49}$ NWs, with periodic structure can be readily used as electrochromic smart windows and exhibit reversibly switchable electrochromism when applying negative or positive voltage.[286] The electrochromic mechanism of $W_{18}O_{49}$ in $LiClO_4$ aqueous solution as the electrolyte can be expressed as $W_{18}O_{49} + xe^- + xLi^+ \rightleftharpoons Li_xW_{18}O_{49}$. This coloration or bleaching of the $W_{18}O_{49}$ NW thin films is due to the insertion or extraction of the Li ions and electrons (Fig. 29a). Fig. 29b shows the in-situ coloration/bleaching characteristics of the NW thin films, the electrochromic properties of the $W_{18}O_{49}$ NW thin films exhibited significant relationship with their thickness. This kind of devices displayed good stability up to about 1000 cycles (Fig. 29c).[286] The same group also co-assembled AgNW and $W_{18}O_{49}$ NWs into multilayered aligned NW networks on PET substrate with tunable transparency and conductivity for fabrication of transparent flexible smart windows (Fig. 29d).[287] These devices showed similar results as their previous work, the transmittance changing between the transparent state and the colored state became more obvious and stable when the number of $W_{18}O_{49}$ NW layers was increased (Fig. 29e-f).[287]

4.6.2 Piezoelectric nanogenerator. Lightweight flexible and/or wearable generators of energy are required for driving any self-

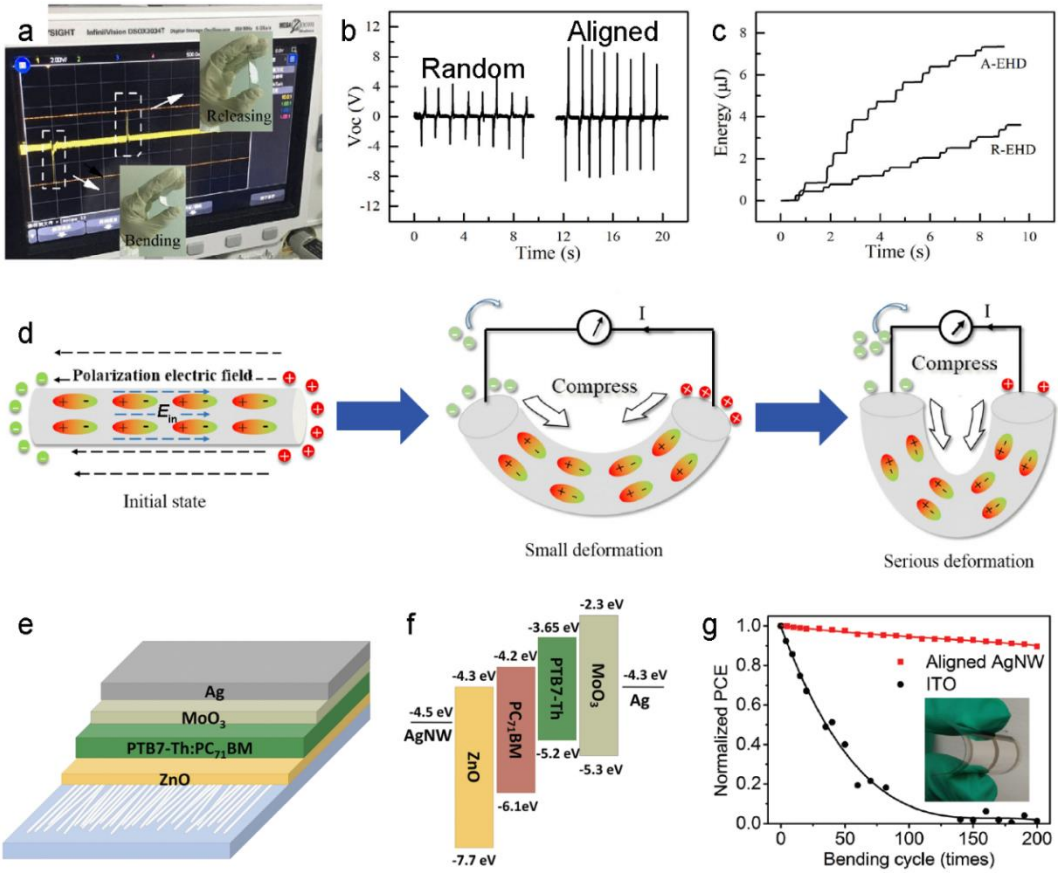

Fig. 30 (a) The photograph of the EH at releasing and bending conditions. (b) The output V_{oc} of R-EH (left) and A-EH (right) under periodic bending. (c) The output energy of R-EH and A-EH calculated from the output V_{oc}. (d) The mechanism of generating electric signals by the EH. Reproduced with permission from ref. 293. Copyright 2018 Elsevier Inc. (e) Structure illustration and (f) energy band diagram of devices based on aligned AgNW electrodes. (g) Normalized PCEs of a flexible device based on aligned AgNWs and ITO on PET substrates as a function of the number of bending cycles. Reproduced from ref. 238 with permission from the Royal Society of Chemistry.

powered portable or personal device. So-called "Energy harvesters" (EHs), make use of piezoelectric effects, and can harvest kinetic energy such as arising from small movements (e.g. from vibration, breathing, breezing and tapping).[288-293] Wang and co-workers fabricated EHs containing $(Ba_{0.85}Ca_{0.15})(Ti_{0.9}Zr_{0.1})O_3$ NWs (BCTZ NWs), both aligned (A-BCTZ NWs) and random (R-BCTZ NWs) by electrospinning where an electric field between parallel electrodes is orienting the NWs.[293] Fig. 30a displays the output signal of the EH in the bent (downward pulse signal) and in the relaxed state (upward pulse signal). The maximum output V_{oc} for aligned EH (A-EH) is higher than random EH (R-EH) (Fig. 30b).[293] The average power during the measurement period was calculated to be ~0.95 μW and ~2 μW for R-EH and A-EH respectively (Fig. 30c).[293] Fig. 30d illustrates the mechanism of generating electric signals. Under an external electric field, the separation between positive and negative charges of the internal electric dipoles was elongated. An inner electric field (E_{in}) along the opposite direction of polarization electric field was built up, resulting in equivalent opposite space charges absorbed on its surface to keep the charge balance (Fig. 30d left). Bending of EH will result in decreasing E_{in} and escape of space charge from the surface, leading to the generation of an electric signal (Fig. 30d middle and right). In contrast, releasing of EH will lead to the restoration of E_{in} to its original state and the space charges will be attracted to the surface again. The intensity of electric signal depended on the bending extent of the EH.[293]

4.6.3 Solar cells. Yang *et al.* reported a solution process based on "capillary-assisted fluidic assembly" technique for the alignment of AgNWs (Section 3.11).[238] It was found that well-aligned AgNWs networks can remarkably improve the performance in terms of transparency and sheet resistance (T = 92.7%, R_s = 16.6 Ω sq^{-1}). Polymer solar cells (PSCs) with an active area of 1.0 cm^2 can be fabricated with the device architecture of glass/AgNWs/ZnO/photoactive layer/MoO_3/Ag (Fig. 30e). Poly[4,8-bis(5-(2-ethylhexyl)thiophen-2-yl)benzo[1,2-*b*;4,5-*b'*]dithiophene-2-(carboxylate-2-6-diyl)] (PTB7-Th) and [6,6]-phenyl-C_{71}-butyric acid methyl ester ($PC_{71}BM$) were used as materials of the photoactive layer, Fig. 30f presents all the energy band diagram including all the layers of the devices. The aligned AgNW networks also exhibited significantly better mechanical stability than the brittle ITO films, about 89% of the initial power conversion efficiency (PCE) can be retained even after 200 bending cycles , whereas PCE of the ITO based device sharply decreased only after 50 cycles (Fig. 30g).[238]

5. Summary and Perspectives

Over the past 20 years, significant progress has been achieved to

develop macroscopic scaled arrays composed of aligned 1D-nanoobjects and to integrate these ordered arrays in functional devices. In this review, the main strategies for the oriented assembly of 1D-nanoobjects have been summarized, including methods that lead to monolayered arrays assembled with in-plane anisotropy at an interface and methods that can be repeated to form more complex multilayered architectures.

The in-plane alignment of NRs, NWs and NFs is one prerequisite for fabricating composite materials with macroscopic anisotropy in which the 1D-nanoobjects are confined to a slab or stratum or film with a given thickness (section 2). If this thickness is on the order of the diameter of the 1D-nanoobject in question, one could consider this to be a "monolayer". The thicker this layer is the more one will approach anisotropic "bulk" composites.

In contrast, some techniques allow to prepare layered anisotropic materials with much more complex anisotropies for the design of next generation composites (section 3). In these approaches one is free to choose the chemical nature of the respective 1D-nanoobject and its alignment direction in each individual monolayer slab and strata with individually different layers can be placed above each other. This opens systematic pathways to complex anisotropies in which either the alignment direction can be defined at will (for example criss-cross alignment) or the multilayer sequence of chemically different nanoobjects can be defined at will or both.

The methods for alignment of 1D-nanoobjects described in this review can also be categorized based on the driving force governing the oriented assembly (Table 1). Ideally, one could dream of an approach able to generate well-controlled large-area oriented 1D-nanoobjects assemblies of any type of 1D-nanoobject on any substrate with a high alignment quality and with a complex architecture and which only requires very simple equipment. Obviously, there is no existing approach that fulfills all these requirements, and each method has its own advantages and limits which are outlined in Table 1. As an example, capillary flows can align 1D-nanoobjects very efficiently, but it is difficult to scale-up this approach to large areas and it is impossible to construct complex architectures with different orientations in each layer. Another example is Grazing-Incidence Spraying (GIS) which can be used to align 1D-nanoobjects on very large scales, but which presently does not work well for aligning NRs with low aspect ratios.[231, 232] Such limitations also apply to other approaches in which the alignment is brought about by liquid shear. Template assisted alignment, on the other hand, could facilitate the alignment of low aspect ratio nanoobjects, but is severely limited by the requirement of patterned surfaces. Understanding the advantages and limitations of each method can help choosing the approach which is best suited for the requirements of each specific application. Sometimes, two or more assembly techniques need to be combined in order to fabricate functional devices based on aligned 1D-nanoobjects.[233]

Aligned 1D-nanoobjects assemblies have already proven to be useful for a wide range of applications (section 4). However, most of the studies present proof-of-concept prototypes of nanodevices and a lot of efforts are still necessary to reach the requirements for making them commercially available at a reasonable cost. For instance, the durability of the functional devices is a very important parameter and it is a challenge for various applications that should not be ignored. The encapsulation of the 1D-nanoobjects either before or after the assembly may be a good way to address this issue, as it has been for example demonstrated for AgNWs encapsulated with a protective, oxidation-resistant iongel.[294]

It was shown in this review that the performance of various nanodevices was enhanced by using oriented 1D-nanoobjects arrays, but there are certainly other fields that could benefit from such nanostructures and that still need to be explored. We hope this review will facilitate the application of aligned 1D-nanoobjects in new domains to efficiently make use of their unique properties, and that it will motivate researchers in the field to keep on improving the quality of the assembly and the degree of complexity that can be achieved as well as to explore new approaches and new applications.

Acknowledgements

The Principal Investigator of this project (Y.L.) wishes to thank Sino-Singapore International Joint Research Institute for funding support. This research is supported by the Singapore Ministry of Education (MOE) Academic Research Fund Tier one RG200/17, and the National Research Foundation, Prime Minister's Office, Singapore under its Campus for Research Excellence and Technological Enterprise (CREATE) programme.

Table 1 Existing aligning approaches in literatures

Driving forces	Aligning methods	Advantages	Disadvantages	Materials	Comments	Ref.
External field	Magnetic-field	1. Good alignment 2. Different 1D-nanoobjects	1. Special setup	Ni, Co, modified Ag NWs etc	1. It might be improved and form complex architectures	42-50
	Electric-field	1. Good alignment 2. Different 1D-nanoobjects	1. Special setup	Si, PbSe, GaN, CdSe NWs, PFS micelles etc	1. It might be improved and form complex architectures	51-69
Mechanical force	Rubbing	1. Large areas 2. Simple setup 3. Positional control	1. Moderate alignment 2. Specific 1D-nanoobjects	CNTs, SiNWs	1. The quality of the final in-plane alignment is related to the quality of the original vertical alignment	71, 72
	Stretching the substrate	1. Large areas 2. Simple setup 3. Different 1D-nanoobjects	1. Moderate alignment	Ag, Si, ZnO NWs	1. It might be improved and form complex architectures	104-107
	Contact printing	1. Large areas 2. Different 1D-nanoobjects 3. Positional control 4. Complex architectures	1. Special setup 2. Specific substrates	Si, Ge, GaAs, ZnO, Zn_2GeO_4, $In_2Ge_2O_7$, Zn_3P_2, CdS_xSe_{1-x}, Ge/Si core/shell NWs etc	1. The quality of the final in-plane alignment is related to the quality of the original vertical alignment	157-176
External field etc	Electrospinning	1. Large areas 2. Positional control 3. Complex architectures	1. Specific 1D-nanoobjects 2. Special setup	Polymer NFs		188, 194, 195, 199-212

Shear force	Shear coating	1. Large areas 2. Different substrates 3. Different 1D-nanoobjects	1. Moderate alignment	Polymer NFs, CNTs, AgNWs etc	1. It might be improved and form complex architectures	73-75, 87
	Langmuir-Blodgett Method	1. Good alignment 2. Large areas 3. Different 1D-nanoobjects 4. Complex architectures	1. Special setup	Ge, Ag, Te, Si, VO_2 NWs, ZnO NRs, CNTs, Au microwires etc	1. Suitable for aligning 1D-nanoobjects with different aspect ratios	117, 121-129, 131, 133, 134
	Bubble-blowing	1. Large areas 2. Simple setup 3. Different 1D-nanoobjects 4. Complex architectures	1. Specific substrates	SiNWs, CNTs, nanosprings, GNT@CuNB nanoobjects		135-138
	Dip-coating	1. Large areas 2. Simple setup 3. Different substrates 4. Different 1D-nanoobjects 5. Complex architectures	1. Moderate alignment	Ag, AsAg, $V_2O_5.nH_2O$ NWs, CNCs	1. The alignment is highly dependent on the aspect ratio of the 1D-nanoobjects	177-179
	Brush coating	1. Large areas 2. Simple setup 3. Different substrates 4. Different 1D-nanoobjects 5. Complex architectures	1. Moderate alignment	Polymers, AgNWs	1. The only method allowing alignment in continuous multi-directions by a single step	217, 218
	Spray-assisted Layer-by-Layer assembly	1. Large areas 2. Different substrates 3. Different 1D-nanoobjects 4. Complex architectures	1. Special setup	Cellulose nanofibrils, AgNWs, AuNRs	1. The alignment is highly dependent on the aspect ratio of the 1D-nanoobjects	230-233

	Agitation-assisted Layer-by-Layer alignment	1. Large areas 2. Simple setup 3. Different substrates 4. Different 1D-nanoobjects 5. Complex architectures	1. Moderate Alignment	AgNWs	1. The alignment is highly dependent on the aspect ratio of the 1D-nanoobjects	234, 235
	Fluidic flow	1. Different 1D-nanoobjects 2. Complex architectures	1. Small areas	AuNRs, TMV, bacteriophage M13, cellulose nanofibrils, DNA molecules, GaP, InP, Ag, Si, CdS, V_2O_5 NWs etc	1. The alignment is highly dependent on the aspect ratio of the 1D-nanoobjects	236-252
Template	Wrinkled substrates	1. Large areas 2. Different 1D-nanoobjects 3. Positional control	1. Specific substrates	SiNWs, AuNRs, CdSe NRs, 1D oligopeptides etc	1. Suitable for aligning 1D-nanoobjects with different aspect ratios 2. It might be improved and form complex architectures	88-99
	Liquid crystals	1. Good alignment 2. Simple setup	1. Specific 1D-nanoobjects	Polymer NFs, CdS NWs		109, 110
	Interconnecting patterned surface with 1D-nanoobjects	1. Large areas 2. Positional control	1. Specific substrates 2. Specific 1D-nanoobjects	DNA origami, CNTs, Au-tipped CdS NRs	1. The alignment of the 1D-nanoobjects is highly dependent on geometry of the binding sites	111-114
	Liquid bridge induced assembly	1. Good alignment 2. Large areas 3. Positional control	1. Specific substrates	Polymer NFs		115, 116

Please do not adjust margins

Interface	Evaporation induced assembly	1. Large areas 2. Simple setup 3. Different substrates 4. Different 1D-nanoobjects 5. Complex architectures	1. Moderate alignment	Au, Ag, Organic NWs, polymers, DNA, halloysite NTs etc		139-156
	Liquid-liquid interface	1. Large areas 2. Simple setup 3. Different substrates 4. Different 1D-nanoobjects 5. Complex architectures	1. Moderate alignment	CdSe NRs, Ag NWs etc		180-184
Interactions	Interactions between NWs	1. Good alignment 2. Simple setup 3. Different kinds of arrays	1. Specific 1D-nanoobjects	CoP NWs		100
	Co-assembly with other nanoobjects	1. Good alignment 2. Simple setup	1. Specific 1D-nanoobjects	$Na_{0.44}MnO_2$ NWs, AuNWs, CNTs, π-conjugated polymers	1. Special interactions between different kinds of nanoobjects is a prerequisite for the alignment	101-103

References

1 Y. Cui and C. M. Lieber, *Science*, 2001, **291**, 851-853.
2 R. Beckman, E. Johnston-Halperin, Y. Luo, J. E. Green and J. R. Heath, *Science*, 2005, **310**, 465-468.
3 D. Wang, B. A. Sheriff and J. R. Heath, *Nano Lett.*, 2006, **6**, 1096-1100.
4 X. Jiang, Q. Xiong, S. Nam, F. Qian, Y. Li and C. M. Lieber, *Nano Lett.*, 2007, **7**, 3214-3218.
5 J.-p. Colinge, C.-w. Lee, A. Afzalian, N. D. Akhavan, R. Yan, I. Ferain, P. Razavi, B. O'Neill, A. Blake, M. White, A.-m. Kelleher, B. McCarthy and R. Murphy, *Nat. Nanotechnol.*, 2010, **5**, 225-229.
6 C. K. Chan, H. Peng, G. Liu, K. McIlwrath, X. F. Zhang, R. A. Huggins and Y. Cui, *Nat. Nanotechnol.*, 2007, **3**, 31.
7 H. Wu, G. Chan, J. W. Choi, I. Ryu, Y. Yao, M. T. McDowell, S. W. Lee, A. Jackson, Y. Yang, L. Hu and Y. Cui, *Nat. Nanotechnol.*, 2012, **7**, 310.
8 Z. L. Wang and W. Wu, *Angew. Chem., Int. Ed.*, 2012, **51**, 11700-11721.
9 M. Law, J. Goldberger and P. Yang, *Annu. Rev. Mater. Res.*, 2004, **34**, 83-122.
10 C. Pan, L. Dong, G. Zhu, S. Niu, R. Yu, Q. Yang, Y. Liu and Z. L. Wang, *Nat. Photonics*, 2013, **7**, 752.
11 E. Stern, A. Vacic, N. K. Rajan, J. M. Criscione, J. Park, B. R. Ilic, D. J. Mooney, M. A. Reed and T. M. Fahmy, *Nat. Nanotechnol.*, 2010, **5**, 138-142.
12 R. Yan, J.-H. Park, Y. Choi, C.-J. Heo, S.-M. Yang, L. P. Lee and P. Yang, *Nat. Nanotechnol.*, 2011, **7**, 191.
13 G. Lu, H. De Keersmaecker, L. Su, B. Kenens, S. Rocha, E. Fron, C. Chen, P. Van Dorpe, H. Mizuno, J. Hofkens, J. A. Hutchison and H. Uji-i, *Adv. Mater.*, 2014, **26**, 5124-5128.
14 M. Kwiat, R. Elnathan, M. Kwak, J. W. de Vries, A. Pevzner, Y. Engel, L. Burstein, A. Khatchtourints, A. Lichtenstein, E. Flaxer, A. Herrmann and F. Patolsky, *J. Am. Chem. Soc.*, 2012, **134**, 280-292.
15 H. Peretz-Soroka, A. Pevzner, G. Davidi, V. Naddaka, R. Tirosh, E. Flaxer and F. Patolsky, *Nano Lett.*, 2013, **13**, 3157-3168.
16 Y. Weizmann, F. Patolsky, I. Popov and I. Willner, *Nano Lett.*, 2004, **4**, 787-792.
17 Y. Xia, P. Yang, Y. Sun, Y. Wu, B. Mayers, B. Gates, Y. Yin, F. Kim and H. Yan, *Adv. Mater.*, 2003, **15**, 353-389.
18 N. P. Dasgupta, J. Sun, C. Liu, S. Brittman, S. C. Andrews, J. Lim, H. Gao, R. Yan and P. Yang, *Adv. Mater.*, 2014, **26**, 2137-2184.
19 Z. Liu, J. Xu, D. Chen and G. Shen, *Chem. Soc. Rev.*, 2015, **44**, 161-192.
20 M. Hasegawa and M. Iyoda, *Chem. Soc. Rev.*, 2010, **39**, 2420-2427.
21 S. Mann, *Nat. Mater.*, 2009, **8**, 781.
22 B. Wiley, Y. Sun and Y. Xia, *Acc. Chem. Res.*, 2007, **40**, 1067-1076.
23 Q. Tang, H. Li, Y. Song, W. Xu, W. Hu, L. Jiang, Y. Liu, X. Wang and D. Zhu, *Adv. Mater.*, 2006, **18**, 3010-3014.
24 X. Zhang, X. Zhang, W. Shi, X. Meng, C. Lee and S. Lee, *Angew. Chem., Int. Ed.*, 2007, **46**, 1525-1528.
25 Z. Fan, D. Wang, P.-C. Chang, W.-Y. Tseng and J. G. Lu, *Appl. Phys. Lett.*, 2004, **85**, 5923-5925.
26 Z. Fan and J. G. Lu, *Appl. Phys. Lett.*, 2005, **86**, 032111.
27 L. Jiang, H. Dong and W. Hu, *Soft Matter*, 2011, **7**, 1615-1630.
28 T. Ackermann, R. Neuhaus and S. Roth, *Sci. Rep.*, 2016, **6**, 34289.
29 M. Jagota and N. Tansu, *Sci. Rep.*, 2015, **5**, 10219.
30 O. Trotsenko, A. Tokarev, A. Gruzd, T. Enright and S. Minko, *Nanoscale*, 2015, **7**, 7155-7161.
31 J.-W. Liu, H.-W. Liang and S.-H. Yu, *Chem. Rev.*, 2012, **112**, 4770-4799.
32 X. Liu, Y.-Z. Long, L. Liao, X. Duan and Z. Fan, *ACS Nano*, 2012, **6**, 1888-1900.
33 K. J. Ziegler, B. Polyakov, J. S. Kulkarni, T. A. Crowley, K. M. Ryan, M. A. Morris, D. Erts and J. D. Holmes, *J. Mater. Chem.*, 2004, **14**, 585-589.
34 Y.-Z. Long, M. Yu, B. Sun, C.-Z. Gu and Z. Fan, *Chem. Soc. Rev.*, 2012, **41**, 4560-4580.
35 S.-Y. Zhang, M. D. Regulacio and M.-Y. Han, *Chem. Soc. Rev.*, 2014, **43**, 2301-2323.
36 B. Nikoobakht, C. A. Michaels, S. J. Stranick and M. D. Vaudin, *Appl. Phys. Lett.*, 2004, **85**, 3244-3246.
37 S. A. Fortuna, J. Wen, I. S. Chun and X. Li, *Nano Lett.*, 2008, **8**, 4421-4427.
38 D. Tsivion, M. Schvartzman, R. Popovitz-Biro, P. von Huth and E. Joselevich, *Science*, 2011, **333**, 1003-1007.
39 M. Schvartzman, D. Tsivion, D. Mahalu, O. Raslin and E. Joselevich, *Proc. Natl. Acad. Sci. U. S. A.*, 2013, **110**, 15195-15200.
40 B. Su, Y. Wu and L. Jiang, *Chem. Soc. Rev.*, 2012, **41**, 7832-7856.
41 M. Kwiat, S. Cohen, A. Pevzner and F. Patolsky, *Nano Today*, 2013, **8**, 677-694.
42 D. Fragouli, R. Buonsanti, G. Bertoni, C. Sangregorio, C. Innocenti, A. Falqui, D. Gatteschi, P. D. Cozzoli, A. Athanassiou and R. Cingolani, *ACS Nano*, 2010, **4**, 1873-1878.
43 C. M. Hangarter and N. V. Myung, *Chem. Mater.*, 2005, **17**, 1320-1324.
44 Y. Lalatonne, L. Motte, V. Russier, A. T. Ngo, P. Bonville and M. P. Pileni, *J. Phys. Chem. B*, 2004, **108**, 1848-1854.
45 S.-W. Lee, M.-C. Jeong, J.-M. Myoung, G.-S. Chae and I.-J. Chung, *Appl. Phys. Lett.*, 2007, **90**, 133115.
46 B. Wang, Y. Ma, N. Li, Y. Wu, F. Li and Y. Chen, *Adv. Mater.*, 2010, **22**, 3067-3070.
47 J. Yuan, H. Gao, F. Schacher, Y. Xu, R. Richter, W. Tremel and A. H. E. Müller, *ACS Nano*, 2009, **3**, 1441-1450.
48 N. Li, G.-W. Huang, X.-J. Shen, H.-M. Xiao and S.-Y. Fu, *J. Mater. Chem. C*, 2013, **1**, 4879-4884.
49 M. S. Sultan, B. Das, K. Mandal and D. Atkinson, *J. Appl. Phys.*, 2012, **112**, 013910.
50 S. R. Darmakkolla, M. Ghobadi, L. Lampert, A. F. Pareira, A. Jenike, M. Tahir and S. B. Rananavare, *Nanoscale*, 2019, **11**, 2679-2686.
51 P. A. Smith, C. D. Nordquist, T. N. Jackson, T. S. Mayer, B. R. Martin, J. Mbindyo and T. E. Mallouk, *Appl. Phys. Lett.*, 2000, **77**, 1399-1401.
52 L. Dong, J. Bush, V. Chirayos, R. Solanki, J. Jiao, Y. Ono, J. F. Conley and B. D. Ulrich, *Nano Lett.*, 2005, **5**, 2112-2115.
53 O. Englander, D. Christensen, J. Kim, L. Lin and S. J. S. Morris, *Nano Lett.*, 2005, **5**, 705-708.
54 K. M. Ryan, A. Mastroianni, K. A. Stancil, H. Liu and A. P. Alivisatos, *Nano Lett.*, 2006, **6**, 1479-1482.
55 Y. Cao, W. Liu, J. Sun, Y. Han, J. Zhang, S. Liu, H. Sun and J. Guo, *Nanotechnology*, 2006, **17**, 2378.
56 T. H. Kim, S. Y. Lee, N. K. Cho, H. K. Seong, H. J. Choi, S. W. Jung and S. K. Lee, *Nanotechnology*, 2006, **17**, 3394.
57 D. V. Talapin, C. T. Black, C. R. Kagan, E. V. Shevchenko, A. Afzali and C. B. Murray, *J. Phys. Chem. C*, 2007, **111**, 13244-13249.
58 S. Raychaudhuri, S. A. Dayeh, D. Wang and E. T. Yu, *Nano Lett.*, 2009, **9**, 2260-2266.
59 E. M. Freer, O. Grachev, X. Duan, S. Martin and D. P. Stumbo, *Nat. Nanotechnol.*, 2010, **5**, 525.
60 C. H. Lee, D. R. Kim and X. Zheng, *Nano Lett.*, 2010, **10**,

5116-5122.
61 J. Puigmartí-Luis, D. Schaffhauser, B. R. Burg and P. S. Dittrich, *Adv. Mater.*, 2010, **22**, 2255-2259.
62 M. Duchamp, K. Lee, B. Dwir, J. W. Seo, E. Kapon, L. Forró and A. Magrez, *ACS Nano*, 2010, **4**, 279-284.
63 J. K. Kawasaki and C. B. Arnold, *Nano Lett.*, 2011, **11**, 781-785.
64 A. W. Maijenburg, M. G. Maas, E. J. B. Rodijk, W. Ahmed, E. S. Kooij, E. T. Carlen, D. H. A. Blank and J. E. ten Elshof, *J. Colloid Interface Sci.*, 2011, **355**, 486-493.
65 N. Petchsang, M. P. McDonald, L. E. Sinks and M. Kuno, *Adv. Mater.*, 2013, **25**, 601-605.
66 P. P. Donahue, C. Zhang, N. Nye, J. Miller, C.-Y. Wang, R. Tang, D. Christodoulides, C. D. Keating and Z. Liu, *ACS Nano*, 2018, **12**, 7343-7351.
67 N. J. Greybush, K. Charipar, J. A. Geldmeier, S. J. Bauman, P. Johns, J. Naciri, N. Charipar, K. Park, R. A. Vaia and J. Fontana, *ACS Nano*, 2019, **13**, 3875-3883.
68 J. B. Gilroy, T. Gädt, G. R. Whittell, L. Chabanne, J. M. Mitchels, R. M. Richardson, M. A. Winnik and I. Manners, *Nat. Chem.*, 2010, **2**, 566-570.
69 J. B. Gilroy, P. A. Rupar, G. R. Whittell, L. Chabanne, N. J. Terrill, M. A. Winnik, I. Manners and R. M. Richardson, *J. Am. Chem. Soc.*, 2011, **133**, 17056-17062.
70 S. Kinge, M. Crego-Calama and D. N. Reinhoudt, *ChemPhysChem*, 2008, **9**, 20-42.
71 W. A. deHeer, W. S. Bacsa, A. Châtelain, T. Gerfin, R. Humphrey-Baker, L. Forro and D. Ugarte, *Science*, 1995, **268**, 845-847.
72 A. Pevzner, Y. Engel, R. Elnathan, T. Ducobni, M. Ben-Ishai, K. Reddy, N. Shpaisman, A. Tsukernik, M. Oksman and F. Patolsky, *Nano Lett.*, 2010, **10**, 1202-1208.
73 M. Chang, D. Choi and E. Egap, *ACS Appl. Mater. Interfaces*, 2016, **8**, 13484-13491.
74 M. Chang, Z. Su and E. Egap, *Macromolecules*, 2016, **49**, 9449-9456.
75 S. Park, G. Pitner, G. Giri, J. H. Koo, J. Park, K. Kim, H. Wang, R. Sinclair, H.-S. P. Wong and Z. Bao, *Adv. Mater.*, 2015, **27**, 2656-2662.
76 Y. Diao, B. C. K. Tee, G. Giri, J. Xu, D. H. Kim, H. A. Becerril, R. M. Stoltenberg, T. H. Lee, G. Xue, S. C. B. Mannsfeld and Z. Bao, *Nat. Mater.*, 2013, **12**, 665.
77 B. Dörling, V. Vohra, T. T. Dao, M. Garriga, H. Murata and M. Campoy-Quiles, *J. Mater. Chem. C*, 2014, **2**, 3303-3310.
78 G. Giri, D. M. DeLongchamp, J. Reinspach, D. A. Fischer, L. J. Richter, J. Xu, S. Benight, A. Ayzner, M. He, L. Fang, G. Xue, M. F. Toney and Z. Bao, *Chem. Mater.*, 2015, **27**, 2350-2359.
79 J. A. Reinspach, Y. Diao, G. Giri, T. Sachse, K. England, Y. Zhou, C. Tassone, B. J. Worfolk, M. Presselt, M. F. Toney, S. Mannsfeld and Z. Bao, *ACS Appl. Mater. Interfaces*, 2016, **8**, 1742-1751.
80 B. J. Worfolk, S. C. Andrews, S. Park, J. Reinspach, N. Liu, M. F. Toney, S. C. B. Mannsfeld and Z. Bao, *Proc. Natl. Acad. Sci. U. S. A.*, 2015, **112**, 14138-14143.
81 Y. Diao, L. Shaw, Z. Bao and S. C. B. Mannsfeld, *Energy Environ. Sci.*, 2014, **7**, 2145-2159.
82 J. Lee, A. R. Han, J. Kim, Y. Kim, J. H. Oh and C. Yang, *J. Am. Chem. Soc.*, 2012, **134**, 20713-20721.
83 J. Lee, A. R. Han, H. Yu, T. J. Shin, C. Yang and J. H. Oh, *J. Am. Chem. Soc.*, 2013, **135**, 9540-9547.
84 S. Schott, E. Gann, L. Thomsen, S.-H. Jung, J.-K. Lee, C. R. McNeill and H. Sirringhaus, *Adv. Mater.*, 2015, **27**, 7356-7364.
85 J. Kim, J. Peretti, K. Lahlil, J.-P. Boilot and T. Gacoin, *Adv. Mater.*, 2013, **25**, 3295-3300.
86 X. Liu, G. Qi, A. M. G. Park, A. Rodriguez-Gonzalez, A. Enotiadis, W. Pan, V. Kosma, G. D. Fuchs, B. J. Kirby and E. P. Giannelis, *Small*, 2019, **15**, 1901666.
87 A. Takemoto, T. Araki, Y. Noda, T. Uemura, S. Yoshimoto, R. Abbel, C. Rentrop, J. van den Brand and T. Sekitani, *Nanotechnology*, 2019, **30**, 37LT03.
88 S. Liu, J. B.-H. Tok, J. Locklin and Z. Bao, *Small*, 2006, **2**, 1448-1453.
89 Q. Zhang, S. Gupta, T. Emrick and T. P. Russell, *J. Am. Chem. Soc.*, 2006, **128**, 3898-3899.
90 Y. Yu, C. Ng, T. A. F. König and A. Fery, *Langmuir*, 2019, **35**, 8629-8645.
91 M. Tebbe, M. Mayer, B. A. Glatz, C. Hanske, P. T. Probst, M. B. Müller, M. Karg, M. Chanana, T. A. F. König, C. Kuttner and A. Fery, *Faraday Discuss.*, 2015, **181**, 243-260.
92 C. Hanske, M. Tebbe, C. Kuttner, V. Bieber, V. V. Tsukruk, M. Chanana, T. A. F. König and A. Fery, *Nano Lett.*, 2014, **14**, 6863-6871.
93 S. G. Lee, H. Kim, H. H. Choi, H. Bong, Y. D. Park, W. H. Lee and K. Cho, *Adv. Mater.*, 2013, **25**, 2162-2166.
94 X. Zhou, Y. Zhou, J. C. Ku, C. Zhang and C. A. Mirkin, *ACS Nano*, 2014, **8**, 1511-1516.
95 R. Ashkar, M. J. A. Hore, X. Ye, B. Natarajan, N. J. Greybush, T. Lam, C. R. Kagan and C. B. Murray, *ACS Appl. Mater. Interfaces*, 2017, **9**, 25513-25521.
96 V. Flauraud, M. Mastrangeli, G. D. Bernasconi, J. Butet, D. T. L. Alexander, E. Shahrabi, O. J. F. Martin and J. Brugger, *Nat. Nanotechnol.*, 2017, **12**, 73.
97 B. Li, L. R. Valverde, F. Zhang, Y. Zhou, S. Li, Y. Diao, W. L. Wilson and C. M. Schroeder, *ACS Appl. Mater. Interfaces*, 2017, **9**, 41586-41593.
98 B. Teshome, S. Facsko and A. Keller, *Nanoscale*, 2014, **6**, 1790-1796.
99 B. Teschome, S. Facsko, K. V. Gothelf and A. Keller, *Langmuir*, 2015, **31**, 12823-12829.
100 S.-Y. Zhang, E. Ye, S. Liu, S. H. Lim, S. Y. Tee, Z. Dong and M.-Y. Han, *Adv. Mater.*, 2012, **24**, 4369-4375.
101 Y. Li and Y. Wu, *J. Am. Chem. Soc.*, 2009, **131**, 5851-5857.
102 W. W. Leow and W. Hwang, *Langmuir*, 2011, **27**, 10907-10913.
103 W. Yang, L. Qu, R. Zheng, Z. Liu, K. R. Ratinac, L. Shen, D. Yu, L. Yang, C. J. Barrow, S. P. Ringer, L. Dai and F. Braet, *Chem. Mater.*, 2011, **23**, 2760-2765.
104 G.-W. Hsieh, J. Wang, K. Ogata, J. Robertson, S. Hofmann and W. I. Milne, *J. Phys. Chem. C*, 2012, **116**, 7118-7125.
105 H. Tang, Y. Lin and H. A. Sodano, *Adv. Energy Mater.*, 2012, **2**, 469-476.
106 F. Xu, J. W. Durham, B. J. Wiley and Y. Zhu, *ACS Nano*, 2011, **5**, 1556-1563.
107 J. W. Durham and Y. Zhu, *ACS Appl. Mater. Interfaces*, 2013, **5**, 256-261.
108 J. Bang, J. Choi, F. Xia, S. S. Kwon, A. Ashraf, W. I. Park and S. Nam, *Nano Lett.*, 2014, **14**, 3304-3308.
109 S. Samitsu, Y. Takanishi and J. Yamamoto, *Macromolecules*, 2009, **42**, 4366-4368.
110 K. Pal, M. L. N. M. Mohan and S. Thomas, *Org. Electron.*, 2016, **39**, 25-37.
111 B. Ding, H. Wu, W. Xu, Z. Zhao, Y. Liu, H. Yu and H. Yan, *Nano Lett.*, 2010, **10**, 5065-5069.
112 A. C. Pearson, E. Pound, A. T. Woolley, M. R. Linford, J. N. Harb and R. C. Davis, *Nano Lett.*, 2011, **11**, 1981-1987.
113 E. Penzo, M. Palma, R. Wang, H. Cai, M. Zheng and S. J. Wind, *Nano Lett.*, 2015, **15**, 6547-6552.
114 A. Marcovici, G. Le Saux, V. Bhingardive, P. Rukenstein, K. Flomin, K. Shreteh, R. Golan, T. Mokari and M. Schvartzman, *ACS Nano*, 2018, **12**, 10016-10023.
115 C. Yan, B. Su, Y. Shi and L. Jiang, *Nano Today*, 2019, **25**, 13-26.
116 B. Su, S. Wang, J. Ma, Y. Wu, X. Chen, Y. Song and L. Jiang, *Adv. Mater.*, 2012, **24**, 559-564.
117 A. R. Tao, J. Huang and P. Yang, *Acc. Chem. Res.*, 2008, **41**,

1662-1673.
118 Q. Guo, X. Teng, S. Rahman and H. Yang, *J. Am. Chem. Soc.*, 2003, **125**, 630-631.
119 S. Chen, *Langmuir*, 2001, **17**, 2878-2884.
120 H. Song, F. Kim, S. Connor, G. A. Somorjai and P. Yang, *J. Phys. Chem. B*, 2005, **109**, 188-193.
121 P. Yang and F. Kim, *ChemPhysChem*, 2002, **3**, 503-506.
122 F. Kim, S. Kwan, J. Akana and P. Yang, *J. Am. Chem. Soc.*, 2001, **123**, 4360-4361.
123 S. Jin, D. Whang, M. C. McAlpine, R. S. Friedman, Y. Wu and C. M. Lieber, *Nano Lett.*, 2004, **4**, 915-919.
124 J.-W. Liu, J.-H. Zhu, C.-L. Zhang, H.-W. Liang and S.-H. Yu, *J. Am. Chem. Soc.*, 2010, **132**, 8945-8952.
125 L. Mai, Y. Gu, C. Han, B. Hu, W. Chen, P. Zhang, L. Xu, W. Guo and Y. Dai, *Nano Lett.*, 2009, **9**, 826-830.
126 A. Tao, F. Kim, C. Hess, J. Goldberger, R. He, Y. Sun, Y. Xia and P. Yang, *Nano Lett.*, 2003, **3**, 1229-1233.
127 D. Wang, Y.-L. Chang, Z. Liu and H. Dai, *J. Am. Chem. Soc.*, 2005, **127**, 11871-11875.
128 D. Whang, S. Jin, Y. Wu and C. M. Lieber, *Nano Lett.*, 2003, **3**, 1255-1259.
129 H. Jiang, T. P. Vinod and R. Jelinek, *Adv. Mater. Interfaces*, 2014, **1**.
130 Y. Yang, J.-L. Wang, L. Liu, Z.-H. Wang, J.-W. Liu and S.-H. Yu, *Nanoscale*, 2017, **9**, 52-55.
131 X. Li, L. Zhang, X. Wang, I. Shimoyama, X. Sun, W.-S. Seo and H. Dai, *J. Am. Chem. Soc.*, 2007, **129**, 4890-4891.
132 L. J. Cote, F. Kim and J. Huang, *J. Am. Chem. Soc.*, 2009, **131**, 1043-1049.
133 P. Yang, *Nature*, 2003, **425**, 243.
134 R. Zhu, Y. Lai, V. Nguyen and R. Yang, *Nanoscale*, 2014, **6**, 11976-11980.
135 G. Yu, A. Cao and C. M. Lieber, *Nat. Nanotechnol.*, 2007, **2**, 372.
136 S. Wu, K. Huang, E. Shi, W. Xu, Y. Fang, Y. Yang and A. Cao, *ACS Nano*, 2014, **8**, 3522-3530.
137 S. Wu, L. Yang, M. Zou, Y. Yang, M. Du, W. Xu, L. Yang, Y. Fang and A. Cao, *Nano Lett.*, 2016, **16**, 4917-4924.
138 S. Wu, D. Chen, Y. Yuan and A. Cao, *Nanotechnology*, 2018, **29**, 395601.
139 A. Bensimon, A. Simon, A. Chiffaudel, V. Croquette, F. Heslot and D. Bensimon, *Science*, 1994, **265**, 2096-2098.
140 Y.-P. Du, Y.-W. Zhang, Z.-G. Yan, L.-D. Sun and C.-H. Yan, *J. Am. Chem. Soc.*, 2009, **131**, 16364-16365.
141 N. R. Jana, *Angew. Chem., Int. Ed.*, 2004, **43**, 1536-1540.
142 T. P. J. Knowles, T. W. Oppenheim, A. K. Buell, D. Y. Chirgadze and M. E. Welland, *Nat. Nanotechnol.*, 2010, **5**, 204.
143 C. Liu, X. Liu, Y. Xu, H. Sun, Y. Li, Y. Shi, M. V. Lee, T. Yamada, T. Hasegawa, Y.-Y. Noh and T. Minari, *Mater. Horiz.*, 2017, **4**, 259-267.
144 H. Nakao, T. Taguchi, H. Shiigi and K. Miki, *Chem. Commun.*, 2009, DOI: 10.1039/B821988E, 1858-1860.
145 T. K. Sau and C. J. Murphy, *Langmuir*, 2005, **21**, 2923-2929.
146 W. Xu, R. Leeladhar, Y.-T. Tsai, E.-H. Yang and C.-H. Choi, *Appl. Phys. Lett.*, 2011, **98**, 073101.
147 C. Zhang, X. Zhang, X. Zhang, X. Fan, J. Jie, J. C. Chang, C.-S. Lee, W. Zhang and S.-T. Lee, *Adv. Mater.*, 2008, **20**, 1716-1720.
148 C. Zhang, X. Zhang, X. Zhang, X. Ou, W. Zhang, J. Jie, J. C. Chang, C.-S. Lee and S.-T. Lee, *Adv. Mater.*, 2009, **21**, 4172-4175.
149 Z. Wang, R. Bao, X. Zhang, X. Ou, C.-S. Lee, J. C. Chang and X. Zhang, *Angew. Chem., Int. Ed.*, 2011, **50**, 2811-2815.
150 J.-H. Li, Y. Xi, L. D. Pozzo, J.-T. Xu and C. K. Luscombe, *J. Mater. Chem. C*, 2017, **5**, 5128-5134.
151 H. Dai, R. Ding, M. Li, J. Huang, Y. Li and M. Trevor, *Sci. Rep.*, 2014, **4**, 6742.
152 Y. Zhao, G. Cavallaro and Y. Lvov, *J. Colloid Interface Sci.*, 2015, **440**, 68-77.
153 A. Sánchez-Iglesias, B. Rivas-Murias, M. Grzelczak, J. Pérez-Juste, L. M. Liz-Marzán, F. Rivadulla and M. A. Correa-Duarte, *Nano Lett.*, 2012, **12**, 6066-6070.
154 D. Kim, W. K. Bae, S.-H. Kim and D. C. Lee, *Nano Lett.*, 2019, **19**, 963-970.
155 Y. Rong, L. Song, P. Si, L. Zhang, X. Lu, J. Zhang, Z. Nie, Y. Huang and T. Chen, *Langmuir*, 2017, **33**, 13867-13873.
156 I. Ahmad, H. P. Jansen, H. J. W. Zandvliet and E. S. Kooij, *Nanotechnology*, 2015, **27**, 025301.
157 A. Javey, Nam, R. S. Friedman, H. Yan and C. M. Lieber, *Nano Lett.*, 2007, **7**, 773-777.
158 Z. Fan, J. C. Ho, Z. A. Jacobson, R. Yerushalmi, R. L. Alley, H. Razavi and A. Javey, *Nano Lett.*, 2008, **8**, 20-25.
159 Z. Fan, J. C. Ho, T. Takahashi, R. Yerushalmi, K. Takei, A. C. Ford, Y.-L. Chueh and A. Javey, *Adv. Mater.*, 2009, **21**, 3730-3743.
160 T. Takahashi, K. Takei, J. C. Ho, Y.-L. Chueh, Z. Fan and A. Javey, *J. Am. Chem. Soc.*, 2009, **131**, 2102-2103.
161 T. I. Lee, W. J. Choi, J. P. Kar, Y. H. Kang, J. H. Jeon, J. H. Park, Y. S. Kim, H. K. Baik and J. M. Myoung, *Nano Lett.*, 2010, **10**, 3517-3523.
162 S.-S. Yoon and D.-Y. Khang, *J. Mater. Chem.*, 2012, **22**, 10625-10630.
163 T. Toshitake, N. Patricia, T. Kuniharu, C. F. Alexandra, J. Arash, C. W. Ming, C. Z. Ning and J. Ali, *Nanotechnology*, 2012, **23**, 045201.
164 Z. Liu, B. Liang, G. Chen, G. Yu, Z. Xie, L. Gao, D. Chen and G. Shen, *J. Mater. Chem. C*, 2013, **1**, 131-137.
165 G. Yu, B. Liang, H. Huang, G. Chen, Z. Liu, D. Chen and G. Shen, *Nanotechnology*, 2013, **24**, 095703.
166 D. Roßkopf and S. Strehle, *Nanotechnology*, 2016, **27**, 185301.
167 Y.-K. Kim, P. S. Kang, D.-I. Kim, G. Shin, G. T. Kim and J. S. Ha, *Small*, 2009, **5**, 727-734.
168 W. S. Lee, S. Won, J. Park, J. Lee and I. Park, *Nanoscale*, 2012, **4**, 3444-3449.
169 W. S. Lee, J.-h. Choi, I. Park and J. Lee, *Langmuir*, 2012, **28**, 17851-17858.
170 R. Yerushalmi, Z. A. Jacobson, J. C. Ho, Z. Fan and A. Javey, *Appl. Phys. Lett.*, 2007, **91**, 203104.
171 N. Han, Z.-x. Yang, F. Wang, G. Dong, S. Yip, X. Liang, T. F. Hung, Y. Chen and J. C. Ho, *ACS Appl. Mater. Interfaces*, 2015, **7**, 20454-20459.
172 Y. Wang, Z. Yang, X. Wu, N. Han, H. Liu, S. Wang, J. Li, W. Tse, S. Yip, Y. Chen and J. C. Ho, *Nanoscale Res. Lett.*, 2016, **11**, 191.
173 N. Han, Z.-x. Yang, F. Wang, S. Yip, D. Li, T. F. Hung, Y. Chen and J. C. Ho, *ACS Nano*, 2016, **10**, 6283-6290.
174 G. Chen, B. Liang, Z. Liu, G. Yu, X. Xie, T. Luo, Z. Xie, D. Chen, M.-Q. Zhu and G. Shen, *J. Mater. Chem. C*, 2014, **2**, 1270-1277.
175 C. García Núñez, F. Liu, W. T. Navaraj, A. Christou, D. Shakthivel and R. Dahiya, *Microsystems & Nanoengineering*, 2018, **4**, 22.
176 J. Yao, H. Yan and C. M. Lieber, *Nat. Nanotechnol.*, 2013, **8**, 329-335.
177 J. Huang, R. Fan, S. Connor and P. Yang, *Angew. Chem., Int. Ed.*, 2007, **46**, 2414-2417.
178 J. Feng, H. Xia, F. You, H. Mao, X. Ma, H. Tao, X. Zhao and M.-C. Wang, *J. Alloy. Compd.*, 2018, **735**, 607-612.
179 X. Qi, Z. Lu, E.-M. You, Y. He, Q.-e. Zhang, H.-J. Yi, D. Li, S.-Y. Ding, Y. Jiang, X. Xiong, J. Xu, D. Ge, X. Y. Liu and H. Bai, *ACS Nano*, 2018, **12**, 12701-12712.
180 J. He, Q. Zhang, S. Gupta, T. Emrick, T. P. Russell and P. Thiyagarajan, *Small*, 2007, **3**, 1214-1217.
181 J. K. Lim, B. Y. Lee, M. L. Pedano, A. J. Senesi, J.-W. Jang, W. Shim, S. Hong and C. A. Mirkin, *Small*, 2010, **6**, 1736-1740.

182 J.-W. Liu, S.-Y. Zhang, H. Qi, W.-C. Wen and S.-H. Yu, *Small*, 2012, **8**, 2412-2420.
183 H.-Y. Shi, B. Hu, X.-C. Yu, R.-L. Zhao, X.-F. Ren, S.-L. Liu, J.-W. Liu, M. Feng, A.-W. Xu and S.-H. Yu, *Adv. Funct. Mater.*, 2010, **20**, 958-964.
184 S.-Y. Zhang, J.-W. Liu, C.-L. Zhang and S.-H. Yu, *Nanoscale*, 2013, **5**, 4223-4229.
185 X. Lu, C. Wang and Y. Wei, *Small*, 2009, **5**, 2349-2370.
186 D. Li, Y. Wang and Y. Xia, *Nano Lett.*, 2003, **3**, 1167-1171.
187 D. Li and Y. Xia, *Nano Lett.*, 2004, **4**, 933-938.
188 D. Li, G. Ouyang, J. T. McCann and Y. Xia, *Nano Lett.*, 2005, **5**, 913-916.
189 A. Greiner and J. H. Wendorff, *Angew. Chem., Int. Ed.*, 2007, **46**, 5670-5703.
190 D. He, B. Hu, Q.-F. Yao, K. Wang and S.-H. Yu, *ACS Nano*, 2009, **3**, 3993-4002.
191 K. E. Roskov, K. A. Kozek, W.-C. Wu, R. K. Chhetri, A. L. Oldenburg, R. J. Spontak and J. B. Tracy, *Langmuir*, 2011, **27**, 13965-13969.
192 Y. Lee, S.-Y. Min and T.-W. Lee, *Macromol. Mater. Eng.*, 2017, **302**, 1600507.
193 Y. J. Yun, W. G. Hong, N.-J. Choi, H. J. Park, S. E. Moon, B. H. Kim, K.-B. Song, Y. Jun and H.-K. Lee, *Nanoscale*, 2014, **6**, 6511-6514.
194 D. Li, Y. Wang and Y. Xia, *Adv. Mater.*, 2004, **16**, 361-366.
195 G. Tuğrul, T. Gökhan, S. Umut, G. Aziz, T. Servet, S. Emre and M. D. Mustafa, *Nanotechnology*, 2018, **29**, 135202.
196 G. Cadafalch Gazquez, S. Lei, A. George, H. Gullapalli, B. A. Boukamp, P. M. Ajayan and J. E. ten Elshof, *ACS Appl. Mater. Interfaces*, 2016, **8**, 13466-13471.
197 A. Liu, Y. Meng, H. Zhu, Y.-Y. Noh, G. Liu and F. Shan, *ACS Appl. Mater. Interfaces*, 2018, **10**, 25841-25849.
198 D. H. Kang, N. K. Kim and H. W. Kang, *Nanotechnology*, 2019, **30**, 365303.
199 M. V. Kakade, S. Givens, K. Gardner, K. H. Lee, D. B. Chase and J. F. Rabolt, *J. Am. Chem. Soc.*, 2007, **129**, 2777-2782.
200 D. Zhang and J. Chang, *Nano Lett.*, 2008, **8**, 3283-3287.
201 G. S. Bisht, G. Canton, A. Mirsepassi, L. Kulinsky, S. Oh, D. Dunn-Rankin and M. J. Madou, *Nano Lett.*, 2011, **11**, 1831-1837.
202 S. Wang, Z.-X. Lin, W.-H. Wang, C. L. Kuo, K. C. Hwang and C.-C. Hong, *Sens. Actuators, B*, 2014, **194**, 1-9.
203 C.-L. Zhang, K.-P. Lv, N.-Y. Hu, L. Yu, X.-F. Ren, S.-L. Liu and S.-H. Yu, *Small*, 2012, **8**, 2936-2940.
204 Y. F. Yao, Z.-Z. Gu, J. Z. Zhang, C. Pan, Y. Y. Zhang and H. M. Wei, *Adv. Mater.*, 2007, **19**, 3707-3711.
205 D. Yang, B. Lu, Y. Zhao and X. Jiang, *Adv. Mater.*, 2007, **19**, 3702-3706.
206 Y. Liu, X. Zhang, Y. Xia and H. Yang, *Adv. Mater.*, 2010, **22**, 2454-2457.
207 T. Tamura and H. Kawakami, *Nano Lett.*, 2010, **10**, 1324-1328.
208 D. J. Lipomi, R. C. Chiechi, M. D. Dickey and G. M. Whitesides, *Nano Lett.*, 2008, **8**, 2100-2105.
209 A. Attout, S. Yunus and P. Bertrand, *Polym. Eng. Sci.*, 2008, **48**, 1661-1666.
210 R. Dersch, T. Liu, A. K. Schaper, A. Greiner and J. H. Wendorff, *J. Polym. Sci., Part A: Polym. Chem.*, 2003, **41**, 545-553.
211 P. Katta, M. Alessandro, R. D. Ramsier and G. G. Chase, *Nano Lett.*, 2004, **4**, 2215-2218.
212 X. Bai, S. Liao, Y. Huang, J. Song, Z. Liu, M. Fang, C. Xu, Y. Cui and H. Wu, *Nano Lett.*, 2017, **17**, 1883-1891.
213 Q. Wang, B. Su, H. Liu and L. Jiang, *Adv. Mater.*, 2014, **26**, 4889-4894.
214 Q. Wang, Q. Meng, P. Wang, H. Liu and L. Jiang, *ACS Nano*, 2015, **9**, 4362-4370.
215 T. Yamamoto, Q. Meng, H. Liu, L. Jiang and M. Doi, *Langmuir*, 2016, **32**, 3262-3268.
216 T. Yamamoto, Q. a. Meng, Q. Wang, H. Liu, L. Jiang and M. Doi, *NPG Asia. Mater.*, 2016, **8**, e241.
217 F.-J. Lin, C. Guo, W.-T. Chuang, C.-L. Wang, Q. Wang, H. Liu, C.-S. Hsu and L. Jiang, *Adv. Mater.*, 2017, **29**, 1606987.
218 L. Meng, R. Bian, C. Guo, B. Xu, H. Liu and L. Jiang, *Adv. Mater.*, 2018, **30**, 1706938.
219 G. Decher, *Science*, 1997, **277**, 1232-1237.
220 G. Decher and J.-D. Hong, *Makromol. Chem., Macromol. Symp.*, 1991, **46**, 321-327.
221 G. Decher, J. D. Hong and J. Schmitt, *Thin Solid Films*, 1992, **210-211**, 831-835.
222 J. J. Richardson, J. Cui, M. Björnmalm, J. A. Braunger, H. Ejima and F. Caruso, *Chem. Rev.*, 2016, **116**, 14828-14867.
223 S. Srivastava and N. A. Kotov, *Acc. Chem. Res.*, 2008, **41**, 1831-1841.
224 S. Zhao, F. Caruso, L. Dähne, G. Decher, B. G. De Geest, J. Fan, N. Feliu, Y. Gogotsi, P. T. Hammond, M. C. Hersam, A. Khademhosseini, N. Kotov, S. Leporatti, Y. Li, F. Lisdat, L. M. Liz-Marzán, S. Moya, P. Mulvaney, A. L. Rogach, S. Roy, D. G. Shchukin, A. G. Skirtach, M. M. Stevens, G. B. Sukhorukov, P. S. Weiss, Z. Yue, D. Zhu and W. J. Parak, *ACS Nano*, 2019, **13**, 6151-6169.
225 A. Izquierdo, S. S. Ono, J. C. Voegel, P. Schaaf and G. Decher, *Langmuir*, 2005, **21**, 7558-7567.
226 J. Cho and F. Caruso, *Chem. Mater.*, 2005, **17**, 4547-4553.
227 S. S. Qureshi, Z. Zheng, M. I. Sarwar, O. Félix and G. Decher, *ACS Nano*, 2013, **7**, 9336-9344.
228 S. Vial, I. Pastoriza-Santos, J. Pérez-Juste and L. M. Liz-Marzán, *Langmuir*, 2007, **23**, 4606-4611.
229 Y. Wang, Z. Tang, P. Podsiadlo, Y. Elkasabi, J. Lahann and N. A. Kotov, *Adv. Mater.*, 2006, **18**, 518-522.
230 R. Blell, X. Lin, T. Lindström, M. Ankerfors, M. Pauly, O. Felix and G. Decher, *ACS Nano*, 2017, **11**, 84-94.
231 H. Hu, M. Pauly, O. Felix and G. Decher, *Nanoscale*, 2017, **9**, 1307-1314.
232 S. Sekar, V. Lemaire, H. Hu, G. Decher and M. Pauly, *Faraday Discuss.*, 2016, **191**, 373-389.
233 P. T. Probst, S. Sekar, T. A. F. König, P. Formanek, G. Decher, A. Fery and M. Pauly, *ACS Appl. Mater. Interfaces*, 2018, **10**, 3046-3057.
234 W.-Z. Li, W. Wei, J.-Y. Chen, J.-X. He, S.-N. Xue, J. Zhang, X. Liu, X. Li, Y. Fu, Y.-H. Jiao, K. Zhang, F. Liu and E.-H. Han, *Nanotechnology*, 2013, **24**, 105302.
235 H. Hu, S. Wang, S. Wang, G. Liu, T. Cao and Y. Long, *Adv. Funct. Mater.*, 2019, **29**, 1902922.
236 Y. Huang, X. Duan, Q. Wei and C. M. Lieber, *Science*, 2001, **291**, 630-633.
237 B.-R. Yang, W. Cao, G.-S. Liu, H.-J. Chen, Y.-Y. Noh, T. Minari, H.-C. Hsiao, C.-Y. Lee, H.-P. D. Shieh and C. Liu, *ACS Appl. Mater. Interfaces*, 2015, **7**, 21433-21441.
238 F. Wu, Z. Li, F. Ye, X. Zhao, T. Zhang and X. Yang, *J. Mater. Chem. C*, 2016, **4**, 11074-11080.
239 Y. Lin, E. Balizan, L. A. Lee, Z. Niu and Q. Wang, *Angew. Chem., Int. Ed.*, 2010, **49**, 868-872.
240 X. Zan, S. Feng, E. Balizan, Y. Lin and Q. Wang, *ACS Nano*, 2013, **7**, 8385-8396.
241 S. Kang, T. Kim, S. Cho, Y. Lee, A. Choe, B. Walker, S.-J. Ko, J. Y. Kim and H. Ko, *Nano Lett.*, 2015, **15**, 7933-7942.
242 K. M. O. Håkansson, A. B. Fall, F. Lundell, S. Yu, C. Krywka, S. V. Roth, G. Santoro, M. Kvick, L. Prahl Wittberg, L. Wågberg and L. D. Söderberg, *Nat. Commun.*, 2014, **5**, 4018.
243 M. J. Gordon and D. Peyrade, *Appl. Phys. Lett.*, 2006, **89**, 053112.
244 J.-W. Liu, J.-L. Wang, W.-R. Huang, L. Yu, X.-F. Ren, W.-C. Wen and S.-H. Yu, *Sci. Rep.*, 2012, **2**, 987.
245 H. Lee, B. Seong, J. Kim, Y. Jang and D. Byun, *Small*, 2014, **10**, 3918-3922.
246 S. Yan, L. Lu, H. Meng, N. Huang and Z. Xiao,

Nanotechnology, 2010, **21**, 095303.
247 S. Nagashima, H. D. Ha, D. H. Kim, A. Košmrlj, H. A. Stone and M.-W. Moon, *Proc. Natl. Acad. Sci. U. S. A.*, 2017, **114**, 6233-6237.
248 H. Zhou, P. Heyer, H.-J. Kim, J.-H. Song, L. Piao and S.-H. Kim, *Chem. Mater.*, 2011, **23**, 3622-3627.
249 S. Murali, T. Xu, B. D. Marshall, M. J. Kayatin, K. Pizarro, V. K. Radhakrishnan, D. Nepal and V. A. Davis, *Langmuir*, 2010, **26**, 11176-11183.
250 Y.-K. Kim, S. J. Park, J. P. Koo, G. T. Kim, S. Hong and J. S. Ha, *Nanotechnology*, 2007, **18**, 015304.
251 M. Liu, Y. Chen, Q. Guo, R. Li, X. Sun and J. Yang, *Nanotechnology*, 2011, **22**, 125302.
252 B. Park, I.-G. Bae and Y. H. Huh, *Sci. Rep.*, 2016, **6**, 19485.
253 T. Rueckes, K. Kim, E. Joselevich, G. Y. Tseng, C.-L. Cheung and C. M. Lieber, *Science*, 2000, **289**, 94-97.
254 Y. Cui and C. M. Lieber, *Science*, 2001, **291**, 851-853.
255 Z. Zhong, D. Wang, Y. Cui, M. W. Bockrath and C. M. Lieber, *Science*, 2003, **302**, 1377-1379.
256 L. Liao, Y.-C. Lin, M. Bao, R. Cheng, J. Bai, Y. Liu, Y. Qu, K. L. Wang, Y. Huang and X. Duan, *Nature*, 2010, **467**, 305.
257 H. Yan, H. S. Choe, S. Nam, Y. Hu, S. Das, J. F. Klemic, J. C. Ellenbogen and C. M. Lieber, *Nature*, 2011, **470**, 240.
258 T. I. Lee, W. J. Choi, K. J. Moon, J. H. Choi, J. P. Kar, S. N. Das, Y. S. Kim, H. K. Baik and J. M. Myoung, *Nano Lett.*, 2010, **10**, 1016-1021.
259 M. C. McAlpine, H. Ahmad, D. Wang and J. R. Heath, *Nat. Mater.*, 2007, **6**, 379.
260 S.-k. Duan, Q.-l. Niu, J.-f. Wei, J.-b. He, Y.-a. Yin and Y. Zhang, *Phys. Chem. Chem. Phys.*, 2015, **17**, 8106-8112.
261 J.-W. Liu, J.-L. Wang, Z.-H. Wang, W.-R. Huang and S.-H. Yu, *Angew. Chem., Int. Ed.*, 2014, **53**, 13477-13482.
262 K. Takei, T. Takahashi, J. C. Ho, H. Ko, A. G. Gillies, P. W. Leu, R. S. Fearing and A. Javey, *Nat. Mater.*, 2010, **9**, 821.
263 B. Liang, Z. Lin, W. Chen, Z. He, J. Zhong, H. Zhu, Z. Tang and X. Gui, *Nanoscale*, 2018, **10**, 13599-13606.
264 F. Yin, H. Lu, H. Pan, H. Ji, S. Pei, H. Liu, J. Huang, J. Gu, M. Li and J. Wei, *Sci. Rep.*, 2019, **9**, 2403.
265 S. Cho, S. Kang, A. Pandya, R. Shanker, Z. Khan, Y. Lee, J. Park, S. L. Craig and H. Ko, *ACS Nano*, 2017, **11**, 4346-4357.
266 J.-L. Wang, M. Hassan, J.-W. Liu and S.-H. Yu, *Adv. Mater.*, 2018, **30**, 1803430.
267 X. Li, P. J. Wolanin, L. R. MacFarlane, R. L. Harniman, J. Qian, O. E. C. Gould, T. G. Dane, J. Rudin, M. J. Cryan, T. Schmaltz, H. Frauenrath, M. A. Winnik, C. F. J. Faul and I. Manners, *Nat. Commun.*, 2017, **8**, 15909.
268 E. Comini and G. Sberveglieri, *Mater. Today*, 2010, **13**, 36-44.
269 W. Cheng, Y. Ju, P. Payamyar, D. Primc, J. Rao, C. Willa, D. Koziej and M. Niederberger, *Angew. Chem., Int. Ed.*, 2015, **54**, 340-344.
270 J. Xu, W. Zhang, Z. Yang, S. Ding, C. Zeng, L. Chen, Q. Wang and S. Yang, *Adv. Funct. Mater.*, 2009, **19**, 1759-1766.
271 H. Deng, D. Dong, K. Qiao, L. Bu, B. Li, D. Yang, H.-E. Wang, Y. Cheng, Z. Zhao, J. Tang and H. Song, *Nanoscale*, 2015, **7**, 4163-4170.
272 Y. Wang, M. Shahid, J. Cheng, H. Nishijima and W. Pan, *Nanotechnology*, 2017, **28**, 155202.
273 W. Cheng and M. Niederberger, *Langmuir*, 2016, **32**, 2474-2481.
274 Y. Ning, Z. Zhang, F. Teng and X. Fang, *Small*, 2018, **14**, 1703754.
275 Y.-Y. Wang, Y.-D. Wu, W. Peng, Y.-H. Song, B. Wang, C.-Y. Wu and Y. Lu, *Nanoscale*, 2018, **10**, 18502-18509.
276 M. Mayer, M. J. Schnepf, T. A. F. König and A. Fery, *Adv. Opt. Mater.*, 2019, **7**, 1800564.
277 J. Reguera, J. Langer, D. Jiménez de Aberasturi and L. M. Liz-Marzán, *Chem. Soc. Rev.*, 2017, **46**, 3866-3885.
278 N. L. Netzer, Z. Tanaka, B. Chen and C. Jiang, *J. Phys. Chem. C*, 2013, **117**, 16187-16194.
279 C. Chen, J. Hao, L. Zhu, Y. Yao, X. Meng, W. Weimer and Q. K. Wang, *J. Mater. Chem. A*, 2013, **1**, 13496-13501.
280 M. Chen, I. Y. Phang, M. R. Lee, J. K. W. Yang and X. Y. Ling, *Langmuir*, 2013, **29**, 7061-7069.
281 J. Zheng, B. Dai, J. Liu, J. Liu, m. Ji, J. Liu, Y. Zhou, M. Xu and J. Zhang, *ACS Appl. Mater. Interfaces*, 2016, **8**, 35426-35434.
282 Y. Ke, C. Zhou, Y. Zhou, S. Wang, S. H. Chan and Y. Long, *Adv. Funct. Mater.*, 2018, **28**, 1800113.
283 Y. Zhou, M. Layani, S. Wang, P. Hu, Y. Ke, S. Magdassi and Y. Long, *Adv. Funct. Mater.*, 2018, **28**, 1705365.
284 Y. Ke, Y. Yin, Q. Zhang, Y. Tan, P. Hu, S. Wang, Y. Tang, Y. Zhou, X. Wen, S. Wu, T. J. White, J. Yin, J. Peng, Q. Xiong, D. Zhao and Y. Long, *Joule*, 2019, **3**, 858-871.
285 C.-G. Granqvist, *Nat. Mater.*, 2006, **5**, 89-90.
286 J.-W. Liu, J. Zheng, J.-L. Wang, J. Xu, H.-H. Li and S.-H. Yu, *Nano Lett.*, 2013, **13**, 3589-3593.
287 J.-L. Wang, Y.-R. Lu, H.-H. Li, J.-W. Liu and S.-H. Yu, *J. Am. Chem. Soc.*, 2017, **139**, 9921-9926.
288 H. Fang, X. Wang, Q. Li, D. Peng, Q. Yan and C. Pan, *Adv. Energy Mater.*, 2016, **6**, 1600829.
289 J. Liu, N. Cui, L. Gu, X. Chen, S. Bai, Y. Zheng, C. Hu and Y. Qin, *Nanoscale*, 2016, **8**, 4938-4944.
290 C. C. Jin, H. H. Fan, Y. Wang, H. L. Hwang, Y. F. Zhang and Q. Wang, *Ceram. Int.*, 2017, **43**, 14476-14480.
291 Q.-L. Zhao, G.-P. He, J.-J. Di, W.-L. Song, Z.-L. Hou, P.-P. Tan, D.-W. Wang and M.-S. Cao, *ACS Appl. Mater. Interfaces*, 2017, **9**, 24696-24703.
292 C. C. Jin, X. C. Liu, C. H. Liu, H. L. Hwang and Q. Wang, *Appl. Surf. Sci.*, 2018, **447**, 430-436.
293 C. C. Jin, X. C. Liu, C. H. Liu, Y. Wang, H. L. Hwang and Q. Wang, *Mater. Design*, 2018, **144**, 55-63.
294 W. Xiong, H. Liu, Y. Chen, M. Zheng, Y. Zhao, X. Kong, Y. Wang, X. Zhang, X. Kong, P. Wang and L. Jiang, *Adv. Mater.*, 2016, **28**, 7167-7172.

